Control of Turning Behaviors by Spinal Projection Neurons in the Larval Zebrafish

Advisor: Florian Engert

Author: Kuo-Hua Huang

Control of Turning Behaviors by Spinal Projection Neurons in the Larval Zebrafish

Abstract

This thesis aims to examine how hindbrain spinal projection neurons (SPNs), namely RoV3, MiV1 and MiV2 control tail undulations during turning behaviors. I find that phototaxic turns differ from forward swims by an increased tail bend and a prolonged cycle period during the first undulation, while the later undulations are largely identical. Interestingly, laser ablation of RoV3, MiV1 and MiV2 neurons specifically affects the first undulation cycle by reducing the tail bend and the cycle period. Thus fish without the SPNs mainly perform forward swims in response to the turn-inducing phototaxic cues. These results suggest that the descending motor command that generates turns in larval zebrafish are composed of two pathways: one generates symmetric tail undulations, and the other, mediated by RoV3, MiV1 and MiV2 neurons, provides a brief and biased effect that modulates the first cycle of tail movement. Furthermore, fish whose unilateral SPNs are ablated are unable to perform turns toward the ablated side during the phototaxis, the optomotor response, the dark-flash response, and spontaneous swims, indicating the universal role of the SPNs in controlling visually-induced and spontaneous turns.

Simultaneous two-photon calcium imaging and motor nerve recording in paralyzed fish show that RoV3, MiV2 and most MiV1 neurons on the turning side are active during turns, and that these activities are linearly correlated to the vigor of the intended turns. However, some

MiV1 neurons are broadly tuned for all swimming directions. Computer simulations suggest that unilateral descending innervations to a specific type of spinal interneurons, namely commissural inhibitory interneurons, can generate a two-fold increase in the spinal network's cycle period. This suggests that the SPNs could potentially innervate two types of spinal interneurons, namely $CoBL_{gly}$ and CoLo, in order to control the rhythm during turns.

An additional chapter of this thesis examines the ontogeny of operant and classical learning behaviors in zebrafish. Using strategically positioned visual cues paired with electroshocks, I find that both learning behaviors are expressed reliably around week 3, and reach adult performance levels at week 6. These memories are behaviorally expressed in adults for 6 hours and retrievable for 12 hours.

Table of Contents

List of Figures and Tables

Acknowledgements

Graduate school has been a wonderful time in my life. Florian, my advisor, has been the most generous person ever in providing encouragement, advice and free beer. Thanks to all the Engert lab members. Without you, I wouldn't have so much fun in playing foosball, volleyball and poker, as well as skiing and stair running during these years in the lab.

Many thanks to the Program in Neuroscience in providing superb caring in the past six years. It is amazing how much attention the program has paid to each graduate student.

Thanks to my dissertation advisory committee members: Bence Olveczky (Chair), Markus Meister, Alex Schier, as well as my exam committee members: Venki Murthy, Nao Uchida, and Donald O'Malley in providing valuable inputs to my thesis. In addition, I would like to thank Misha Ahrens, Ruben Portugues, Kris Severi and Tim Dunn in reading and commenting on this thesis.

Finally, endless thanks to my parents. Although I often missed your weekly phone calls from Taiwan, knowing that you are constantly thinking of me really provides me the strength to move forward.

Dedicated to my parents,

Mei-Chiao Chen and Ta-Yuan Huang

CHAPTER 1
General Introduction

Overview

The ultimate goal of the central nervous system is to produce and control appropriate motor outputs. Spinal projection neurons in the brainstem and the cortex of mammals innervate motor neurons or pre-motor interneurons in the spinal cord to generate behaviors. These projection neurons thus serve as the last relay in the brain before descending motor commands reach the spinal cord. Despite the apparent significance of the spinal projection neurons in descending motor control, little is known about the exact ways by which these neurons generate and modulate behaviors.

Studies of the role of spinal projection neurons have been focused on basic, rhythmic locomotor behaviors using swimming vertebrates such as lampreys and *Xenopus* tadpoles[1]. The initiation, modulation and termination of rhythmic body movements have been studied using pharmacology, electrophysiolocal recordings, behavioral analysis and computer modeling. In the past couple of decades, the larval zebrafish (*Danio rerio*) has been used in neuroscience as a vertebrate model organism due to its well-characterized genetics and transparent body that allow for optical imaging of the activity of hundreds of neurons at single cell resolution[2]. The functional organization of the ~200 spinal projection neurons in larval zebrafish is undergoing extensive research[3–6].

Neural networks in the spinal cord possess a high degree of autonomy in generating rhythmic motor outputs during locomotion. This was first demonstrated in lampreys where

isolated spinal cords were able to express rhythmic activities with left-right alternations as long as excitatory amino acids were provided in the bath solution[7,8]. Models of spinal networks that generate rhythmic locomotion were first proposed on the basis of lamprey studies, and later confirmed by mouse studies where genetic tools were used to specifically mark or manipulate subtypes of spinal interneuron. For example, removal of a subtype of commissural inhibitory spinal interneurons using toxins controlled by the expression of homeobox-containing genes results in the loss of left-right coordination during locomotion[9]. Using homeogenes to label spinal interneurons is a powerful tool now available in larval zebrafish[10,11]. The combination of optical and genetic accessibilities makes larval zebrafish an excellent animal model for studying descending control of behaviors by spinal projection neurons.

This thesis aims to demonstrate how small groups of hindbrain spinal projection neurons (SPNs), namely RoV3, MiV1and MiV2, control tail undulations during turning behaviors in larval zebrafish. By examining turns during phototaxis, the optomotor response, the dark flash response and spontaneous swims, it is found that during turns the first cycle of tail movements is slow and biased toward the turning side; later undulations are fast and symmetric. Interestingly, removal of the SPNs by laser ablation selectively reduces the amplitude and period of the first two undulation cycles, leaving subsequent symmetric undulations unaffected. In addition, the impairment of turns is accompanied by a drastic increase in the occurrence of forward swims. The results suggest that turns involve a modification of the basic motor program of forward swims, and when the brief turning command is abolished forward swims reappear. By combining two-photon microscopy and motor-nerve readouts of the direction of fictive swims, it is found that most of the RoV3, MiV1 and MiV2 neurons are active during ipsilateral turns and their calcium fluorescent responses positively correlate with the turning strength. Some MiV1 neurons,

however, are active during a wide range of turning angles. This is consistent with an activity-dependent mechanism for motor control, which differs from a recruitment mechanism that summons more neurons as the turning strength increases. Modeling studies further suggest that the observed increase in tail bend amplitude and cycle period during turns can be simulated by unilateral descending excitation of motor neurons and commissural inhibitory spinal interneurons, respectively. Given the well-characterized identities of spinal interneurons in larval zebrafish, the simulation studies provide testable hypotheses that predict the SPNs' synaptic connections in the spinal cord.

In the following introduction, I will first describe various mechanisms which may result in rhythmic activity in the spinal cord: either via intrinsic bursting cells or using reciprocal inhibition within a network. Then the neuronal types and connections in the canonical model of spinal networks will be introduced. To combine this functional framework with our knowledge of the spinal cord of larval zebrafish, I will summarize the morphologies, physiologies, neurotransmitter types and behavioral roles of spinal interneurons in larval zebrafish, and point out the neuronal types that are rhythmically active during locomotion. As locomotion involves the processes of initiation, feedback modulation and termination, I will review mechanisms that control these processes. As expected, many of these controls are mediated by spinal projection neurons. Finally, I will summarize our current understanding of the role of spinal projection neurons in larval zebrafish.

1.1 Rhythm generation in the spinal cord

To address how descending motor commands modulate spinal oscillation, it is essential to understand how spinal oscillations arise and what parameters can be modulated. There are

two hypotheses proposed to explain the origin of neural oscillations: the oscillator hypothesis and the network hypothesis. The oscillator hypothesis uses a single neuron, having special membrane properties, as the primary determinant of the pattern. Without rhythmic synaptic inputs, these neurons periodically fire a burst of spikes, and underneath the spikes is a rhythmic fluctuation of membrane potential. Among various factors that support the formation of single-cell rhythms, a portion of negative resistance in the current-to-voltage curve (I-V curve) is shown to be determinant for oscillations. Positive current is defined as positive charges leaving the cell, and steady-state current across cell membrane typically increases as the clamped voltage increases. This results in a positive slope, or resistance, in the I-V curve. It has been shown in *Aplysia* that the presence of rhythmic bursting in a neuron can be reversibly switched off and on by cooling and warming, which also vary the shape of the I-V curve; a non-bursting silence state is accompanied by a positive slope throughout the I-V curve and a rhythmic bursting state is accompanied by the presence of negative resistance[12]. The importance of a negative resistance in creating periodic activity is also demonstrated mathematically[71,72]. A portion of negative resistance introduces a cubic nullcline in the system and permits the formation of a relaxation oscillation. This cyclic process goes through phases of slow accumulation, fast accumulation, slow decrease and fast decrease, and results in the oscillation property of the membrane voltage.

Another feature of bursting cells is the fluctuation of intracellular calcium concentration during bursting[13]. It was later found that a calcium-gated potassium current plays a critical role in repolarizing the membrane potential during oscillation. As will be demonstrated in Chapter 3, a single-cell model considering voltage-gated currents and a calcium-gated potassium current can generate relaxation oscillations that simulate the voltage fluctuation of a bursting cell.

In addition to aplysia R15 neurons, the presence of intrinsically rhythmic cells has been shown in other invertebrates such as the AB neurons in lobster pyloric system, and in vertebrates such as spinal interneurons that express homeogenes Hb9 in mice[14,15].

In contrast to the oscillator hypothesis, the network hypothesis states that the synaptic connections among neurons determine the oscillating pattern; no single neuron by itself expresses rhythmic activity. Mutual inhibition or excitation between two so called half center units has been identified in almost all oscillating networks, suggesting its critical role in generating or supporting rhythmic activities[16,17]. It has been shown computationally that a pair of non-bursters that inhibit each other can produce regular alternating bursts if they also exhibit post-inhibitory rebound (PIR)[17]. A cell exhibiting PIR will become more excitable after a period of inhibition, probably due to the increase of the available pool of voltage-gated sodium channels after hyperpolarization. When biased excitation is introduced, one neuron will become dominant due to the mutual inhibition. Activated by PIR and background excitation, the suppressed cell eventually overcomes the inhibition from its counterpart, and becomes the dominant cell. The process repeats and establishes a regular alternating activity.

Mutual inhibition can also facilitate the formation of rhythmic processes by introducing a negative resistance to the I-V curve of non-bursting cells. For example, a non-bursting cell may have a linear, positive resistance throughout its I-V curve. The synaptic inhibition provides extra outward current at the hyperpolarized voltage range, and transforms the linear I-V curve into a zigzag shape that contains a region of negative resistance. Thus two non-bursters, through the connection of mutual inhibition, may become rhythmic. On the other hand, mutual excitation providing extra inward current at the depolarized voltage range may also transform non-bursters into bursters.

1.2 Canonical model of spinal central pattern generators (CPGs)

The neural networks that generate rhythmic activities are often referred to as central pattern generators (CPGs) since they usually control basic, fundamental process such as heart beats, feeding and locomotion. CPGs have been identified in lobsters, leaches, snails, tritonia and lione for controlling processes such as gut motion, heart beating, feeding and swimming[16]. In vertebrates, CPGs have been identified in the spinal cord of tadpoles, lampreys, mice and cats. In the 1980s, Grillner and colleagues used isolated spinal cord of lamprey to study the rhythmic network of the spinal CPG. They showed that ipsilaterally projecting excitatory spinal interneurons (EINs) innervate motor neurons as well as inhibitory interneurons with either ipsilateral axons (LINs) or contralateral axons (CINs)[18]. The CINs were proposed to inhibit the opposite side of the spinal cord to ensure left-right alternation during locomotion (Figure 1.1). There is evidence to suggest that some EINs are intrinsic bursters which provide rhythmicity to the network[15], while network hypothesis has also been proposed to explain the rise of spinal oscillations[17,19].

When descending or ascending inputs create a biased excitation in the spinal cord, EINs on the biased side innervate ipsilateral motor neurons and CINs, and indirectly suppress the network on the opposite side. There are several mechanisms proposed to explain how the suppressed side overcomes the contralateral suppression and becomes active. In a network that contains intrinsic bursters, the activity of the dominant side will decrease as the bursters enter their repolarizing phase. Alternatively, EINs and CINs on the suppressed side may become more excitable after a period of hyperpolarization due to PIR. Driven by background excitation, the suppressed side eventually becomes dominant. Finally, LINs have been shown to provide a delayed inhibition to the ipsilateral CINs, which reduce the suppression to the contralateral side.

As there is a high background of excitation, a biased mutual inhibition results in the activation of the previously suppressed hemicord.

The connection of mutual inhibition in spinal CPGs attracts a lot of attention, as it not only facilitates the generation of negative resistance which supports slow bursting, but also ensures left-right alternation in swimming animals and extensor-flexor alternation in walking animals. Bath application of glycine antagonists to isolated lamprey spinal cord spares the slow bursting on each side of the spinal cord, but abolishes the left-right alternation of slow bursting[20]. A complete removal of commissural innervations by sectioning the spinal cord along the midline results in similar phenotypes[21]. In addition, the burst rhythm of the hemi cord is faster than that of an intact spinal cord. These studies suggest that each half of spinal cord is capable of generating slow bursting, likely driven by intrinsic bursters, and that mutual inhibition between the two hemicords coordinates the left-right alternation and increases the oscillation period[21].

Figure 1.1: Canonical model of the spinal central pattern generator

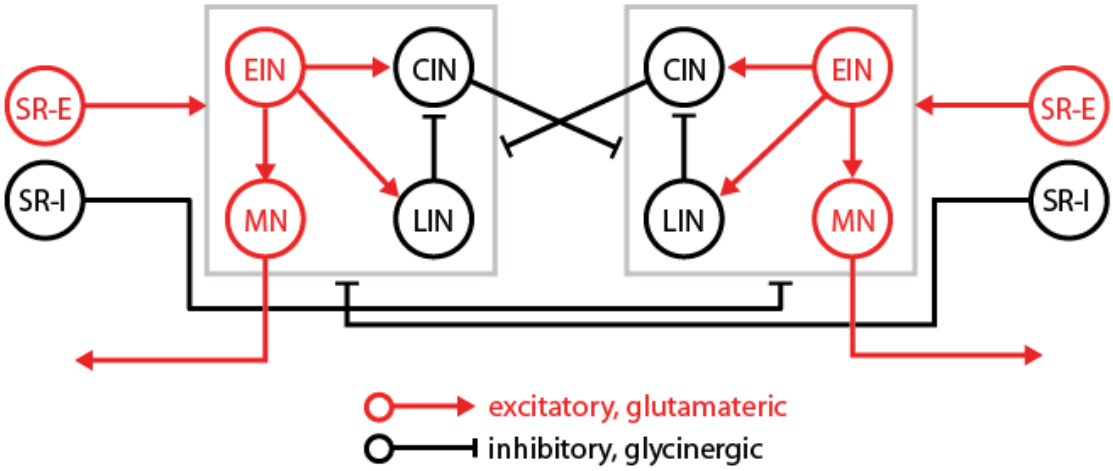

EIN, ipsilateral excitatory interneuron; **CIN**, commissural inhibitory interneuron; **LIN**, ipsilateral inhibitory interneuron; **MN**, motor neurons; **SR**: stretch receptor neuron

1.3 Genetically identified neuronal types in spinal CPGs

In the past decade, researchers have used the restricted expression of homeobox-containing genes to identify specific types of CPG neurons in mice. Since neurons of the same type can be genetically targeted, the behavioral role of the neurons can be examined by ablation experiments. It is found that, although the two species are distant in phylogeny, the spinal network of mice and lamprey appears to be largely conserved. In mice, V0 neurons are a subset of commissural inhibitory spinal interneurons that express the homeogene Dbx1[9]. Mutants lacking these neurons exhibit an increased incidence of co-bursting between left and right motor neurons. Interestingly, the alternation between flexors and extensors is intact in this mutant. Thus the V0 neurons in mice appear to serve a similar role as CINs in lamprey models. Another type of spinal inhibitory interneurons, namely V1 neurons, projects ipsilateral axons and expresses homeogenes Engrailed1[22]. Mutants without V1 neurons are unable to walk "quickly" due to significant increases in both step-cycle period and burst duration of motor neurons. This is consistent with the role of LINs in lamprey spinal cord where LINs are proposed to terminate the activity of CINs on the dominant side and allow transitions of left-right alternations. A type of excitatory spinal interneurons, namely V2a neurons, projects ipsilateral axons and expresses homeogene Chx10[23]. These neurons provide direct, excitatory drive to V0 neurons. In the absence of V2a neurons, the spinal cord fails to express consistent left-right alternations and there is a high variability in the bursting activity. This is consistent with the idea that EINs drive CINs to generate left-right alternations, and that some EINs may be intrinsic bursters that establish the rhythm of the network. As mentioned earlier, there is another type of ipsilateral excitatory interneurons that is marked by the expression of homeogene Hb9. This population of neurons has been demonstrated to be intrinsically rhythmic[14,15].

Homeogene expression has also been used to identify specific types of spinal interneurons in larval zebrafish. Homeogene Engrail1, which labels mouse spinal interneurons V1, is found to uniquely label a class of spinal interneuron, called circumferential ascending (CiA) interneurons[10] in larval zebrafish. CiA interneurons send ipsilateral inhibitions to motor neurons and sensory interneurons CoPA. Another homeogene Alx, a zebrafish homolog of mouse Chx10, labels circumferential descending (CiD) interneurons that project ipsilateral excitations to motor neurons[11]. Both CiA and CiD interneurons are found to be rhythmic during locomotion[10,11,24–27] and should be part of the CPG network. The morphology, physiology and neurotransmitter types of many spinal interneurons in larval zebrafish have been characterized using backfill labeling with fluorescent dyes, patch recordings, immunostaining, and transgenic labeling[28,29]. These findings are summarized in Table 1.1.

Table 1.1: spinal interneurons in larval zebrafish

Cell type	*Primary axon morphology*	*Neurotran-smitter type*	*Rhythmicity during locomotion*	*Synaptic connections*	*Behavior relevance*	*References*
$CoBL_{glut}$ $CoBL_{gly}$	Commissural bifurcating[1]	Glut or Gly[2]	Rhythmic[3]		Swim Escape, Struggle[7]	1: Hale 2001 (28) 2: Higashijima 2004 (29) 3: Mclean 2007 (26) 4: Gleason 2003 (30) 5: Koyama (unpublished data) 6: Satou 2009 (31) 7: Liao 2008 (32) 8: Kimura 2006 (11) 9: Higashijima (33) 10: Wyart 2009 (34)
CoLA	Commissural ascending[1]	Gly[2]	Non-rhythmic[7]		struggle[7]	
$CoSA_{glut}$ $CoSA_{gly}$	Commissural ascending [1]	Glut or Gly[2]	Non-rhythmic[7]		Swim Escape, Struggle[7]	
CoPA	Commissural ascending[1]	Glut[2]		Input: Exci. contra. Rohon Beard[4]		
MCoD	Commissural descending[1]	Glut[2]	Rhythmic[3]	Input: ipsi. MiV1[5]	Slow swims[3]	
UCoD	Commissural descending[1]	Glut[2]				
CoLo	Commissural descending[6]	Gly[6]	Non-rhythmic[7]	Output: MN[6]	Escape[6]	
CiD (Alx+)[8]	Ipsilateral descending[1]	Glut[2]	Rhythmic[3]		Swim Escape, Struggle[7]	
VeMe	Ipsilateral descending[1]	Glut[2]				
CiA (Engrail1+)[9]	Ipsilateral ascending [9]	Gly[9]	Rhythmic[3]	Output: CoPA, MN[9]	Swim[3]	
KA[10]	Ipsilateral ascending	GABA[2]		Input: central canal	Spontaneous swims	
DoLA		GABA[2]				

1.4 Initiation of locomotion

In many vertebrates, a region in the midbrain has been identified to play a key role in initiating locomotion. This area is called the mesencephalic locomotor region (MLR). When stimulated, it produces motor synergies underlying flying in geese, walking in cats, and swimming in lampreys. For example, electric stimulation of the MLR in cats generates walking behaviors on treadmills. As the simulation intensity increases, the locomotion performed by the cat changes from waking, trotting, to galloping[35]. In salamanders, stimulation of the MLR can

evoke two modes of locomotion. At subthreshold stimulation strength, rhythmic limb movement and intersegmental coordination that represent walking behavior are induced. As the stimulation strength is further increased, the frequency of stepping becomes more rapid until the limbs are eventually held back against the body wall and the swimming movements of the trunk are induced[36]. In lampreys, the MLR is found to project excitatory cholinergic inputs to reticulospinal neurons whose axons form the main descending tract to the spinal cord. It is of great interest to know how the MLR orchestrates the activation pattern of reticulospinal neurons and generates motor commands that are relayed to the spinal cord.

Spinal projection neurons clearly play a critical role in initiating locomotion. As mentioned earlier, an isolated spinal cord will start to oscillate once excitatory amino acids are provided in the bath solution. This suggests that in intact animals spinal projection neurons provide descending excitation which enables the spinal cord to oscillate during locomotion. Indeed, locomotion induced by head-touch, illumination and olfactory cues are all accompanied by the activation of spinal projection neurons[37,38]. Even for a touch stimulus applied to the tail of lampreys, the sensory afferents are sent back to the dorsal column nuclei in the caudal brainstem, which then innervate spinal projection neurons to generate locomotor behaviors[39,40]. Despite the apparent importance of descending excitation for initiating locomotion, the identity of spinal projection neurons and their connections in the spinal cord in most vertebrate animal models remains unknown. We do not know, for example, whether the descending commands for initiating locomotion and controlling turning are conveyed by the same spinal projection neurons. In chapter 2, I provide, to my knowledge, the first evidence showing the presence of independent pathways that control swim initiation and turning in vertebrates.

1.5 Termination of locomotion

Termination of locomotion may not be as simple as lack of excitatory drives at the end of each locomotor episode. In *Xenopus* tadpoles, for example, the activity of some reticulospinal neurons correlates with the stop of swimming[41]. They are silent during locomotion but become active when the tadpole stops swimming as the animal's head contacts a solid surface. Remarkably, intracellular stimulation of one of such reticulospinal neurons can terminate an ongoing motor pattern, and this effect is abolished when bicuculline is presented. The study shows that in *Xenopus* tadpoles there is a subset of spinal projection neurons that is sufficient to terminate locomotor behavior through a GABAergic inhibition. In contrast to the supraspinal mechanism, local metabolism of purinergic neurotransmitters in the spinal cord has also been shown to control the length of episodic swims in *Xenopus* tadpoles[42]. During swimming, ATP is released and activates the P2y receptors of spinal neurons to reduce voltage-gated K+ currents, thus increasing the excitability of the spinal circuit. Following its release, ATP is broken down into adenosine in the extracellular space. Adenosine binds to P1 receptors and reduces voltage-gated calcium currents, thus lowering the excitability of the spinal circuit. A gradual change in the balance of ATP and adenosine therefore seems to underlie the run-down of motor pattern for swimming in *Xenopus* tadpoles.

1.6 Sensory feedback from muscles

In addition to descending innervations, sensory feedback from the muscles also modulates spinal oscillations. In the case of cats walking on a treadmill, for example, stimulation of afferent fibers originating from extensors, which mimics an afferent signal indicating the

stretching of extensors, prolongs the extensors' bursting activity and delays the onset of flexor bursts[43]. This indicates that the stretch of a muscle group not only activates the motor neurons that innervate the same muscles, but also suppresses the motor neurons that innervate the antagonistic muscles. In lampreys, two types of stretch receptor neurons have been identified: one with ipsilaterally projecting axons that excite neurons on the same side, and the other with contralaterally projecting axons that inhibit neurons on the opposite side[44]. This suggests that during swims, sensory afferents activate the neurons on the extended side and suppress the neurons on the bent side, thus actively enhancing the expression left-right alternations. Remarkably, in an isolated spinal cord preparation, lateral movement of the caudal part of the spinal cord can entrain the CPG rhythm to deviate from its resting frequency[45,46]. This movement-induced feedback control has also been demonstrated in several other vertebrate systems and reflects a general feature of spinal networks.

1.7 Supraspinal descending motor systems in vertebrates

In mammals, supraspinal descending systems form distinct axonal tracts that project to the spinal cord. These descending tracts include the corticospinal tract, the reticulospinal tract, the vestibulospinal tract, the rubrospinal tract and the olivospinal tract. The role of the corticospinal tract in motor control is under investigation, but it does not appear to be critical for basic locomotor behaviors. Decorticated cats can still search for food, eat, and display aggressive behavior[47]. However, corticospinal projections are necessary for precise adaptation during locomotion. For example, cats with a transection of the corticospinal tract can walk normally on a treadmill, but are unable to walk on an uneven surface[48]. In all vertebrates examined,

reticulospinal neurons are considered the major descending system that controls basic locomotor behaviors. Locomotion induced by stimulating the midbrain MLR can be blocked by either reversible cooling[49] or GABA injections[50,51] in the reticular formation. Activation of neurons in the area with the cholinergic agonist, substance P, or excitatory amino acids[50–55] produces locomotion in mammals, birds and lampreys. There are very few studies, however, focusing on the synaptic connections between reticulospinal neurons and spinal interneurons. A study in adult lamprey showed that an individual reticulospinal neuron can induce monosynaptic EPSPs in all types of spinal neurons, including motor neurons, EINs, CINs and LINs[56].

Larval zebrafish express a rich repertoire of locomotor behaviors[57–59], while their supraspinal descending system is relatively simple, consisting of ~ 100 SPNs on each side of the brain. They form three clusters in the brainstem[60,61]: the midbrain nucleus of medial longitudinal fascicle (nMLF, ~30 cells/ side), the hindbrain reticular formation (~60 cells/ side) and the hindbrain vestibular nucleus (~10 cells/ side). The transparent brain and the simple descending system of larval zebrafish facilitate the functional mapping of behavioral roles of individual spinal projection neurons.

The role of the Mauthner cells, a pair of large, contralaterally projecting reticulospinal neurons, in escape behavior were first studied in goldfish[62–64]. In larval zebrafish, it was found that the tail-tap elicited escape behavior is accompanied by the activation of the Mauthner cells, while the head-tap elicited escapes are accompanied by the activation of the Mauthner cells and the two pairs of segmental homologs MiD2cm and MiD3cm[3,4]. The Mauthner cell is innervated by vestibulocochlear nerves, spiral fiber neurons and the tectal neurons, and is regulated by both feedforward and feedback inhibition[65]. The contralaterally projecting axons of the cell provide strong excitatory input to motor neurons, thus a touch on one side of the head elicits a fast tail

bend to the contralateral side. In the case of escapes induced by vibrations where Mauthner cells are activated bilaterally with a small delay, the excitatory drives from one of the Mauthner cells has to be suppressed in order to avoid bilateral muscle contractions. This appears to be mediated by a type of commissural inhibitory spinal interneurons, namely CoLo neurons, which receive electrotonic excitation from the Mauthner cell that's activated first and suppresses motor neurons on the trailing side[31]. Interestingly, in the mutant *deadly seven,* where extra Mauthner cells in the hindbrain develop, the escape behavior is largely unaffected. The extra neurons are found to divide up the spinal neurons that are normally innervated by a single Mauthner cell[66,67]. This demonstrates the plasticity of the motor system of larval zebrafish for accommodating variation in the number of spinal projection neurons.

In addition to the Mauthner cells, the behavioral roles of other spinal projection neurons have also been studied. In the midbrain nMLF, two pairs of spinal projection neurons, namely MeLc and MeLr, have shown to be important for the fish to orient its body axis before approaching prey[68]. These neurons have ipsilateral dendrites in the optic tectum, and ipsilateral axons with collaterals in each body segment untill the middle of the tail[69].

One of the innate locomotor behaviors expressed by larval zebrafish is the optomotor response (OMR), where fish swim in the direction of visual motion. It was shown that forward and lateral moving gratings can reliably elicit forward swims and turns, respectively, and these behaviors are accompanied by the activation of different sets of spinal projection neurons[6]. It was found that during forward swims, the nMLF, RoL1, RoR1, and RoM1c are strongly active, while during turns, RoM1r, RoV3, MiV1, and MiV2 are active[6]. Furthermore, laser ablation of 4~10 cells in RoV3, MiV1 and MiV2 can completely abolish the visually induced turns, establishing the causality of these spinal projection neurons in controlling visually induced

turning behaviors. Tail undulations, which provide the direct readouts of descending motor control, however, are not described in the previous study due to technical difficulties. The next chapter will address how the problem is resolved in this thesis.

1.8 Studying descending motor control using larval zebrafish

Lamprey, *Xenopus* tadpole, mouse and cat have been used as animal models for studying spinal circuitry for decades. However, it appears difficult to study supraspinal descending control in these animal models for various reasons. First, the supraspinal descending motor system in lamprey, mouse and cats is composed of many thousands of neurons. Identification of the same spinal projection neurons among individual animals is a very laborious task. A feasible solution is to use genetic markers such as the restricted expression of homeogenes to label specific types of neurons. Nevertheless, so far only mice and zebrafish are equipped with such genetic tools. Second, to study the behavioral role of subtypes of spinal projection neurons, it's advantageous and perhaps necessary to manipulate the activity of multiple neurons. Genetic ablation of neurons in mice is often confounded by developmental deficits. The development of optogenetic tools allows reversible inhibition or activation of populations of neurons, but it requires the optical accessibility of the brain. For most vertebrate models, light can only be introduced into the brain, particularly deep brain regions, by using optic fibers, which are laborious to implement and could themselves affect behavior. Due to the optical and genetic accessibility of larval zebrafish, components of spinal networks and supraspinal descending systems are well characterized. These tools and knowledge make larval zebrafish an excellent animal model for studying descending motor control. A potential drawback of studying larval zebrafish is the

organism's small size and fast speed of movement, which make the recording and analysis of behaviors a technically demanding task. But as demonstrated in this thesis, the role of small groups of spinal projection neurons in tail undulation can be precisely characterized. To better understand the dynamic nature of network oscillations during locomotion, a significant portion of this thesis involves quantitative modeling and simulation, which are indispensable tools for studying descending motor control.

Table 1.2: Spinal projection neurons in larval zebrafish

Brain region	Cell type (cells per side[1])	Axon path[1]	Caudal end of axon (myotome #)	Active during the OMR[3]	Active during touch-elicited escapes	*Reference*
Midbrain-nMLF	MeLr (1)		14[2]	Forward swims	Head tap[4]; Escape, burst swimming, struggling, slow swim, spontaneous swimming[6]	*1: Metcalf (1986)*[61] *2: Gahtan (2003)*[69] *3: Orger (2008)*[6] *4: Gahtan (2002)*[5] *5: O'Malley (1996)*[3] *6: Sankrithi (2010)*[70]
	MeLm (1)			Forward swims		
	MeLc (1)		15[2]	Forward swims		
	MeM1 (1)		11[2]	Forward swims		
	Others (~25)			Forward swims		
Hindbrain-reticular formation	Mauthner (1)	mlfDc	>25		Head tap[4], Tail Tap[5]	
	MiD2cm (1)	mlfDc	20[1], 19[2]		Head tap[4,5]	
	MiD3cm (1)	mlfDc	20[1], 18[2]		Head tap[4,5]	
	MiD2i (1)	mlfDi	8[1]			
	MiD3i (1)	mlfDi	8[1]		Head tap[4]	
	MiD2cl (1)	llfc	20[1]			
	MiD3cl (1)	llfc	20[1]			
	RoM1R (1)	mlfVi	20[1]	Turns & Forward swims		
	RoM1C (1)	mlfVi	20[1]	Forward swims	Head tap[4]	
	RoM2L (1)	mlfDi	20[1], 21[2]		Head tap[4]	
	RoM2M (1)	mlfDi	>25[1], 16[2]		Head tap[4]	
	RoM3L (1)	mlfDi	>25[1], 23[2]			
	RoM3M (2)	mlfDi	20[1]		Head tap[4]	
	MiM1 (1)	mlfDi	20[1]		Head tap[4]	
	MiR1 (1)	mlfVi	20[1]	Forward swims (weak)	Head tap[4]	
	MiR2 (1)	mlfVi	20[1]	Forward swims (weak)	Head tap[4]	
	RoV3 (~5)	mlfVi	15[1]	Turns & Forward swims	Head tap[4]	
	MiV1 (~10)	mlfVi	20[1]	Turns & Forward swims		
	MiV2 (~5)	mlfVi	20[1]	Turns & Forward swims	Head tap[4]	
	RoL1 (~12)	llfi	20[1], 10[2]	Forward swims	Head tap[4]	
	RoR1 (1)	llfc	5[1]	Forward swims		
	RoL2R (1)	llfc	15[1]			
	RoL2C (2)	llfc	5[1]			
	RoL2 (2)	llfc	8[1]			
	RoL3 (1)	llfi	15[1]			
	CaV (2)	mlfVi	15[1]			
	CaD (1)	llfc	20[1], 22[2]		Head tap[4]	
Hindbrain-vestimular nucleus	Vestibular nucleus (~10)		14[2]			

Note: mlfDc (contralateral dorsal mlf), mlfDi (ipsilateral dorsal mlf), mlfVc (contralateral ventral mlf), mlfVi (ipsilateral ventral mlf), llfc (contralateral llf), llfi (ipsilateral llf)

1.9 References

1. Deliagina, T. G., Zelenin, P. V. & Orlovsky, G. N. Encoding and decoding of reticulospinal commands. *Brain Res. Brain Res. Rev.* **40**, 166–177 (2002).
2. McLean, D. L. & Fetcho, J. R. Using imaging and genetics in zebrafish to study developing spinal circuits in vivo. *Dev Neurobiol* **68**, 817–834 (2008).
3. O'Malley, D. M., Kao, Y. H. & Fetcho, J. R. Imaging the functional organization of zebrafish hindbrain segments during escape behaviors. *Neuron* **17**, 1145–1155 (1996).
4. Liu, K. S. & Fetcho, J. R. Laser ablations reveal functional relationships of segmental hindbrain neurons in zebrafish. *Neuron* **23**, 325–335 (1999).
5. Gahtan, E., Sankrithi, N., Campos, J. B. & O'Malley, D. M. Evidence for a widespread brain stem escape network in larval zebrafish. *J. Neurophysiol.* **87**, 608–614 (2002).
6. Orger, M. B., Kampff, A. R., Severi, K. E., Bollmann, J. H. & Engert, F. Control of visually guided behavior by distinct populations of spinal projection neurons. *Nat. Neurosci.* **11**, 327–333 (2008).
7. Cohen, A. H. & Wallén, P. The neuronal correlate of locomotion in fish. 'Fictive swimming' induced in an in vitro preparation of the lamprey spinal cord. *Exp Brain Res* **41**, 11–18 (1980).

8. Brodin, L., Grillner, S. & Rovainen, C. M. N-Methyl-D-aspartate (NMDA), kainate and quisqualate receptors and the generation of fictive locomotion in the lamprey spinal cord. *Brain Res.* **325**, 302–306 (1985).
9. Lanuza, G. M., Gosgnach, S., Pierani, A., Jessell, T. M. & Goulding, M. Genetic identification of spinal interneurons that coordinate left-right locomotor activity necessary for walking movements. *Neuron* **42**, 375–386 (2004).
10. Higashijima, S., Masino, M. A., Mandel, G. & Fetcho, J. R. Engrailed-1 expression marks a primitive class of inhibitory spinal interneuron. *J. Neurosci.* **24**, 5827–5839 (2004).
11. Kimura, Y., Okamura, Y. & Higashijima, S. alx, a zebrafish homolog of Chx10, marks ipsilateral descending excitatory interneurons that participate in the regulation of spinal locomotor circuits. *J. Neurosci.* **26**, 5684–5697 (2006).
12. Wilson, W. A. & Wachtel, H. Negative resistance characteristic essential for the maintenance of slow oscillations in bursting neurons. *Science* **186**, 932–934 (1974).
13. Gorman, A. L. & Thomas, M. V. Changes in the intracellular concentration of free calcium ions in a pace-maker neurone, measured with the metallochromic indicator dye arsenazo III. *J. Physiol. (Lond.)* **275**, 357–376 (1978).
14. Wilson, J. M. *et al.* Conditional rhythmicity of ventral spinal interneurons defined by expression of the Hb9 homeodomain protein. *J. Neurosci.* **25**, 5710–5719 (2005).
15. Wilson, J. M., Cowan, A. I. & Brownstone, R. M. Heterogeneous electrotonic coupling and synchronization of rhythmic bursting activity in mouse Hb9 interneurons. *J. Neurophysiol.* **98**, 2370–2381 (2007).
16. Selverston, A. Neurophysiology. Twitching and switching. *Nature* **341**, 690–691 (1989).

17. Perkel, D. H. & Mulloney, B. Motor pattern production in reciprocally inhibitory neurons exhibiting postinhibitory rebound. *Science* **185**, 181–183 (1974).

18. Buchanan, J. T. & Grillner, S. Newly identified 'glutamate interneurons' and their role in locomotion in the lamprey spinal cord. *Science* **236**, 312–314 (1987).

19. Buchanan, J. T. Neural network simulations of coupled locomotor oscillators in the lamprey spinal cord. *Biol Cybern* **66**, 367–374 (1992).

20. Hagevik, A. & McClellan, A. D. Coupling of spinal locomotor networks in larval lamprey revealed by receptor blockers for inhibitory amino acids: neurophysiology and computer modeling. *J. Neurophysiol.* **72**, 1810–1829 (1994).

21. Cangiano, L. & Grillner, S. Fast and slow locomotor burst generation in the hemispinal cord of the lamprey. *J. Neurophysiol.* **89**, 2931–2942 (2003).

22. Gosgnach, S. *et al.* V1 spinal neurons regulate the speed of vertebrate locomotor outputs. *Nature* **440**, 215–219 (2006).

23. Crone, S. A. *et al.* Genetic ablation of V2a ipsilateral interneurons disrupts left-right locomotor coordination in mammalian spinal cord. *Neuron* **60**, 70–83 (2008).

24. Ritter, D. A., Bhatt, D. H. & Fetcho, J. R. In vivo imaging of zebrafish reveals differences in the spinal networks for escape and swimming movements. *J. Neurosci.* **21**, 8956–8965 (2001).

25. Bhatt, D. H., McLean, D. L., Hale, M. E. & Fetcho, J. R. Grading movement strength by changes in firing intensity versus recruitment of spinal interneurons. *Neuron* **53**, 91–102 (2007).

26. McLean, D. L., Fan, J., Higashijima, S., Hale, M. E. & Fetcho, J. R. A topographic map of recruitment in spinal cord. *Nature* **446**, 71–75 (2007).

27. McLean, D. L., Masino, M. A., Koh, I. Y. Y., Lindquist, W. B. & Fetcho, J. R. Continuous shifts in the active set of spinal interneurons during changes in locomotor speed. *Nat. Neurosci.* **11**, 1419–1429 (2008).

28. Hale, M. E., Ritter, D. A. & Fetcho, J. R. A confocal study of spinal interneurons in living larval zebrafish. *J. Comp. Neurol.* **437**, 1–16 (2001).

29. Higashijima, S.-I., Schaefer, M. & Fetcho, J. R. Neurotransmitter properties of spinal interneurons in embryonic and larval zebrafish. *J. Comp. Neurol.* **480**, 19–37 (2004).

30. Gleason, M. R. *et al.* Translocation of CaM kinase II to synaptic sites in vivo. *Nat. Neurosci.* **6**, 217–218 (2003).

31. Satou, C. *et al.* Functional role of a specialized class of spinal commissural inhibitory neurons during fast escapes in zebrafish. *J. Neurosci.* **29**, 6780–6793 (2009).

32. Liao, J. C. & Fetcho, J. R. Shared versus specialized glycinergic spinal interneurons in axial motor circuits of larval zebrafish. *J. Neurosci.* **28**, 12982–12992 (2008).

33. Higashijima, S.-I., Mandel, G. & Fetcho, J. R. Distribution of prospective glutamatergic, glycinergic, and GABAergic neurons in embryonic and larval zebrafish. *J. Comp. Neurol.* **480**, 1–18 (2004).

34. Wyart, C. *et al.* Optogenetic dissection of a behavioural module in the vertebrate spinal cord. *Nature* **461**, 407–410 (2009).

35. Shik, M. L., Severin, F. V. & Orlovskiĭ, G. N. [Control of walking and running by means of electric stimulation of the midbrain]. *Biofizika* **11**, 659–666 (1966).

36. Delvolvé, I., Bem, T. & Cabelguen, J. M. Epaxial and limb muscle activity during swimming and terrestrial stepping in the adult newt, Pleurodeles waltl. *J. Neurophysiol.* **78**, 638–650 (1997).

37. Ullén, F., Deliagina, T. G., Orlovsky, G. N. & Grillner, S. Visual pathways for postural control and negative phototaxis in lamprey. *J. Neurophysiol.* **78**, 960–976 (1997).

38. Dubuc, R. *et al.* Initiation of locomotion in lampreys. *Brain Res Rev* **57**, 172–182 (2008).

39. Dubuc, R., Bongianni, F., Ohta, Y. & Grillner, S. Dorsal root and dorsal column mediated synaptic inputs to reticulospinal neurons in lampreys: involvement of glutamatergic, glycinergic, and GABAergic transmission. *J. Comp. Neurol.* **327**, 251–259 (1993).

40. Dubuc, R., Bongianni, F., Ohta, Y. & Grillner, S. Anatomical and physiological study of brainstem nuclei relaying dorsal column inputs in lampreys. *J. Comp. Neurol.* **327**, 260–270 (1993).

41. Roberts, A., Li, W.-C. & Soffe, S. R. Roles for inhibition: studies on networks controlling swimming in young frog tadpoles. *J. Comp. Physiol. A Neuroethol. Sens. Neural. Behav. Physiol.* **194**, 185–193 (2008).

42. Dale, N. & Gilday, D. Regulation of rhythmic movements by purinergic neurotransmitters in frog embryos. *Nature* **383**, 259–263 (1996).

43. Whelan, P. J., Hiebert, G. W. & Pearson, K. G. Stimulation of the group I extensor afferents prolongs the stance phase in walking cats. *Exp Brain Res* **103**, 20–30 (1995).

44. Di Prisco, G. V., Wallén, P. & Grillner, S. Synaptic effects of intraspinal stretch receptor neurons mediating movement-related feedback during locomotion. *Brain Res.* **530**, 161–166 (1990).

45. Grillner, S., McClellan, A. & Perret, C. Entrainment of the spinal pattern generators for swimming by mechano-sensitive elements in the lamprey spinal cord in vitro. *Brain Res.* **217**, 380–386 (1981).

46. Andersson, O., Forssberg, H., Grillner, S. & Wallén, P. Peripheral feedback mechanisms acting on the central pattern generators for locomotion in fish and cat. *Can. J. Physiol. Pharmacol.* **59**, 713–726 (1981).

47. Bjursten, L. M., Norrsell, K. & Norrsell, U. Behavioural repertory of cats without cerebral cortex from infancy. *Exp Brain Res* **25**, 115–130 (1976).

48. LIDDELL, E. G. T. & PHILLIPS, C. G. Striatal and pyramidal lesions in the cat. *Brain* **69**, 264–279 (1946).

49. Shefchyk, S. J., Jell, R. M. & Jordan, L. M. Reversible cooling of the brainstem reveals areas required for mesencephalic locomotor region evoked treadmill locomotion. *Exp Brain Res* **56**, 257–262 (1984).

50. Garcia-Rill, E. & Skinner, R. D. The mesencephalic locomotor region. II. Projections to reticulospinal neurons. *Brain Res.* **411**, 13–20 (1987).

51. Garcia-Rill, E. & Skinner, R. D. The mesencephalic locomotor region. I. Activation of a medullary projection site. *Brain Res.* **411**, 1–12 (1987).

52. Sholomenko, G. N., Funk, G. D. & Steeves, J. D. Avian locomotion activated by brainstem infusion of neurotransmitter agonists and antagonists. II. gamma-Aminobutyric acid. *Exp Brain Res* **85**, 674–681 (1991).

53. Noga, B. R., Kettler, J. & Jordan, L. M. Locomotion produced in mesencephalic cats by injections of putative transmitter substances and antagonists into the medial reticular formation and the pontomedullary locomotor strip. *J. Neurosci.* **8**, 2074–2086 (1988).

54. Kinjo, N. *et al.* Medioventral medulla-induced locomotion. *Brain Res. Bull.* **24**, 509–516 (1990).

55. Wannier, T., Deliagina, T. G., Orlovsky, G. N. & Grillner, S. Differential effects of the reticulospinal system on locomotion in lamprey. *J. Neurophysiol.* **80**, 103–112 (1998).

56. Ohta, Y. & Grillner, S. Monosynaptic excitatory amino acid transmission from the posterior rhombencephalic reticular nucleus to spinal neurons involved in the control of locomotion in lamprey. *J. Neurophysiol.* **62**, 1079–1089 (1989).

57. Budick, S. A. & O'Malley, D. M. Locomotor repertoire of the larval zebrafish: swimming, turning and prey capture. *J. Exp. Biol.* **203**, 2565–2579 (2000).

58. Burgess, H. A. & Granato, M. Modulation of locomotor activity in larval zebrafish during light adaptation. *J. Exp. Biol.* **210**, 2526–2539 (2007).

59. Burgess, H. A., Schoch, H. & Granato, M. Distinct retinal pathways drive spatial orientation behaviors in zebrafish navigation. *Curr. Biol.* **20**, 381–386 (2010).

60. Kimmel, C. B., Powell, S. L. & Metcalfe, W. K. Brain neurons which project to the spinal cord in young larvae of the zebrafish. *J. Comp. Neurol.* **205**, 112–127 (1982).

61. Metcalfe, W. K., Mendelson, B. & Kimmel, C. B. Segmental homologies among reticulospinal neurons in the hindbrain of the zebrafish larva. *J. Comp. Neurol.* **251**, 147–159 (1986).

62. Eaton, R. C., DiDomenico, R. & Nissanov, J. Flexible body dynamics of the goldfish C-start: implications for reticulospinal command mechanisms. *J. Neurosci.* **8**, 2758–2768 (1988).

63. DiDomenico, R., Nissanov, J. & Eaton, R. C. Lateralization and adaptation of a continuously variable behavior following lesions of a reticulospinal command neuron. *Brain Res.* **473**, 15–28 (1988).

64. Nissanov, J., Eaton, R. C. & DiDomenico, R. The motor output of the Mauthner cell, a reticulospinal command neuron. *Brain Res.* **517**, 88–98 (1990).

65. Koyama, M., Kinkhabwala, A., Satou, C., Higashijima, S. & Fetcho, J. Mapping a sensory-motor network onto a structural and functional ground plan in the hindbrain. *Proc. Natl. Acad. Sci. U.S.A.* **108**, 1170–1175 (2011).

66. Gray, M., Moens, C. B., Amacher, S. L., Eisen, J. S. & Beattie, C. E. Zebrafish deadly seven functions in neurogenesis. *Dev. Biol.* **237**, 306–323 (2001).

67. Liu, K. S., Gray, M., Otto, S. J., Fetcho, J. R. & Beattie, C. E. Mutations in deadly seven/notch1a reveal developmental plasticity in the escape response circuit. *J. Neurosci.* **23**, 8159–8166 (2003).

68. Gahtan, E., Tanger, P. & Baier, H. Visual prey capture in larval zebrafish is controlled by identified reticulospinal neurons downstream of the tectum. *J. Neurosci.* **25**, 9294–9303 (2005).

69. Gahtan, E. & O'Malley, D. M. Visually guided injection of identified reticulospinal neurons in zebrafish: a survey of spinal arborization patterns. *J. Comp. Neurol.* **459**, 186–200 (2003).

70. Sankrithi, N. S. & O'Malley, D. M. Activation of a multisensory, multifunctional nucleus in the zebrafish midbrain during diverse locomotor behaviors. *Neuroscience* **166**, 970–993 (2010).

71. Strogatz, S. H. Nonlinear dynamics and chaos. Westview Press. 211-215 (2000).

72. Edelstein-Keshet, L. Mathematical models in biology. Random House Press. 330-336 (1988)

CHAPTER 2

Hindbrain RoV3, MiV1 and MiV2 neurons control turning behaviors by modulating the first cycle of symmetric tail undulations

2.1 Introduction

Zebrafish larvae perform several different types of turning behaviors, including touch-induced escape turns, turns during the optomotor response (OMR), phototaxic turns, dark-flash induced turns, the orienting behaviors during prey capture, and spontaneous turns. The OMR is an innate behavior of larval zebrafish characterized by swimming in the direction of whole-field visual motion. Turns during the OMR have been found to be mediated by small groups of hindbrain spinal projection neurons, namely RoV3, MiV1 and MiV2 neurons. These three pairs of nuclei are located ventromedially in rhombomere 3-5, respectively, and project ipsilateral axons that course as far as 2/3 of the tail (myotome 15). On the basis of their marked similarity in morphology and ventromedial position, Metcalfe et al.[1] proposed that they are segmental homologs that may serve similar functions during behaviors. Two-photon calcium imaging of spinal projection neurons in larval zebrafish shows that these three groups of ventromedial neurons express lateralized responses during OMR swims; turning to one side is accompanied by the activation of these ventromedial neurons on the turning side during the OMR[2]. Furthermore, unilateral laser ablation of RoV3, MiV1 and MIV2 results in a loss of the ability to turn toward the lesioned side[2]. Despite the clear importance of RoV3, MiV1 and MiV2 in controlling turns during the OMR, it is unknown how exactly these neurons control tail movements, partly due to the difficulty in resolving the fast movement of transparent tails in larval zebrafish.

This chapter focuses on the behavioral role of RoV3, MiV1 and MiV2 neurons in controlling rhythmic tail movement during turning behaviors. To this end, I constructed a behavioral setup to automatically record and analyze tail undulations of freely-swimming larval zebrafish. Using a newly developed phototaxic assay, turns and forward swims can be reliably induced. I find that the phototaxic turn differs from a forward swim by an increased initial tail bend amplitude, as well as an increased cycle period in the first cycle of tail undulation. The tail movement of the two behaviors becomes similar in the second undulation, and is virtually identical in the later cycles. This suggests that the descending command that controls the phototaxic turns is brief and most likely plays a role in the first cycle of tail movement. Interestingly, unilateral laser ablation of RoV3, MiV1 and MiV2 neurons specifically affects the first cycle of the tail movement. Fish without these ventromedial neurons are unable to perform the expected increase in tail bend and cannot prolong the cycle period in response to the turn-inducing phototaxic cues. Instead, they express symmetric tail undulations throughout the swim. As a result, while the ablation completely abolishes phototaxic turns, it drastically increases the occurrence of forward swims. This finding is consistent with the idea that a complete waveform of tail movement during turns is controlled by the concerted action of two descending pathways: one that generates symmetric tail movement throughout the swim and another, mediated by the RoV3, MiV1 and MiV2 neurons, that creates a brief but biased effect. In addition to the phototaxic turns, the same ablation phenotype on tail movement is observed in the OMR turns, dark-flash induced turns, and spontaneous turns, suggesting that the RoV3, MiV1 and MiV2 neurons have a universal role in controlling visually induced and spontaneous turns.

2.2 Measuring the tail undulation of freely-swimming larval zebrafish

Previous studies described swim behaviors of larval zebrafish by tracking the heading direction of the fish[2] or representing the tail with three rigid segments[3–5]. To study how spinal projection neurons modulate behaviors, however, it is necessary to precisely describe the shape of the tail and the wave propagating along it.

The main difficulty in describing the shape of a freely-swimming larval zebrafish is the poor resolution that can be achieved when imaging a small larva swimming in a large arena. In the current experimental setup, a fish is freely swimming in a 10cm-wide petri dish and recorded by a high speed camera at an image resolution of 1000-by-1000 pixels. The fish is thus represented by a limited amount of pixels, roughly 40 pixels in length and 4 pixels in width. This may seem to be plenty of pixels for representing a fish, but a standard skeletonization transformation on the image will result in undesirable results as shown in Figure 2.1C. The resulted skeleton describing the midline of the tail is either rigidly straight or unnaturally zigzagging. This is because the coordinates of the skeleton are confounded by pixel locations- that is, integer coordinates. For a tail whose width is only described by 4 pixels, it is impossible to describe a smooth curve with four available numbers.

To solve this problem, I treat each skeleton coordinate as an anchor point and move it toward the true midline of the fish. This is achieved by calculating the "center of mass" of the eight pixels surrounding the anchor point. Here the weight of each pixel is its brightness in the inverted image. In the inverted image, the pixels along the midline of the fish are usually brighter than the pixels at the edge, this calculation thus "drags" the integer coordinates toward the true midline. As shown in Figure 2.1D, the adjusted skeleton is now described by decimal

coordinates and can smoothly portray the shape of the tail. Additional steps of equal spacing of the coordinates and fitting with cubic splines give the tracking result shown in Figure 2.1E. This tracking method is strikingly robust such that a minute "J" turn performed by transparent albino mutants can be still tracked nicely. Using this algorithm, a swim can be represented by a 2D matrix that records the evolution of the tail shape (Figure 2.1G). At a recording rate of 500 frames per second, this matrix representation captures the complete tail kinematics during swims on a horizontal plane.

Figure 2.1: Measuring tail undulations of freely-swimming larval zebrafish

A-E, Extracting the midline of larval zebrafish in a digital image. **A**, A gray scale image of larval zebrafish after background subtraction. **B**, The gray scale image in A is thresholded and undergoes a skeletonization transformation. The coordinates (red dots) of the resulting skeleton form either rigid lines or unnatural zigzags. **C**, An inverted image of (**A)** overlaid by the skeleton. **D**, Each skeleton coordinate is adjusted based on the intensity of the surrounding pixels. The adjusted skeleton is much smoother and faithfully tracks the midline of the fish in the image. **E**, Using cubic splines to connect the coordinates of the adjusted skeleton. **F**, Examples of tracking results. The heading direction is labeled by the blue vector, and the tangent vectors along the tail are labeled by the orange vectors. **G**. The kinematics of a swim can be represented fully by the evolution of the tail's shape (upper panel), or represented by the undulation of heading direction (lower panel, blue trace) and the tail angle (lower panel, red trace).

Figure 2.1

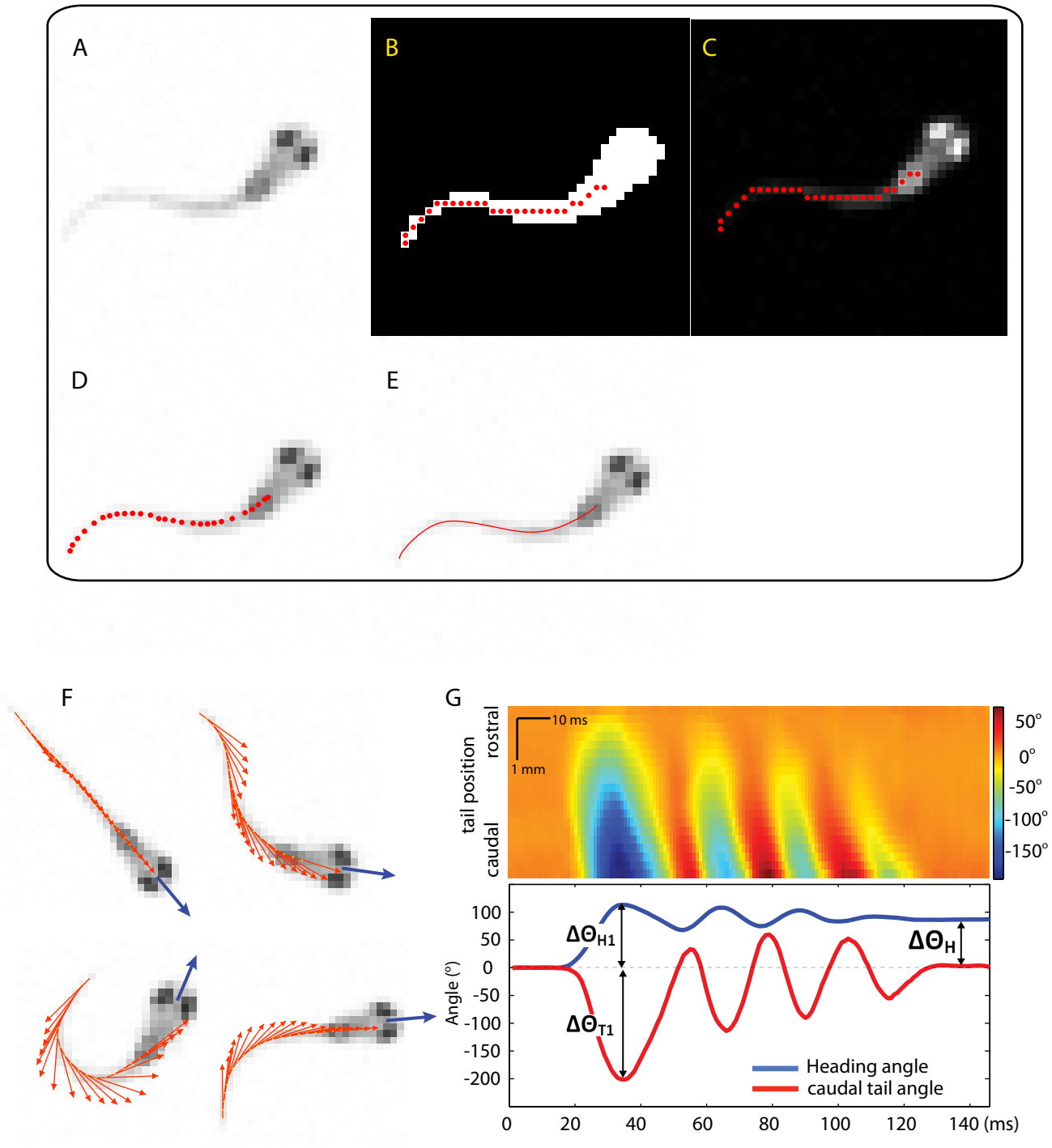
A
B
C
D
E
F
G
10 ms
1 mm
tail position
rostral
caudal
50°
0°
-50°
-100°
-150°
Angle (°)
100
50
0
-50
-100
-150
-200
ΔΘH1
ΔΘT1
ΔΘH
Heading angle
caudal tail angle
0
20
40
60
80
100
120
140 (ms)

2.3 The phototaxis behavior of larval zebrafish

Positive phototaxis is one of the innate behaviors expressed by larval zebrafish. When provided with a differentially illuminated arena, nearly all larva swim toward the brighter side and stay there for at least two minutes (Figure 2.2A). Zebrafish start to display this behavior when they locomote at 5-day post fertilization (dpf) and it starts to attenuate around 25 dpf. By 30 dpf, the behavior completely disappears (Figure 2.2D). Adult zebrafish, i.e. fish that are more than two months old and can reproduce, do not express a clear phototaxic response.

As demonstrated by Burgess et al.[6], larval zebrafish respond to localized illumination by first turning toward the light source and then swimming forward. To reliably induce phototaxic turns, here I present freely-swimming fish with a bilateral illumination contrast (Figure 2.3A), which is registered in real-time such that the black-white boundary of the contrast stimulus is always aligned along the body axis of the fish. In response to this visual environment, the fish performs consecutive turns toward the brighter side for at least 12 seconds. In comparison to the phototaxic assays developed in the previous study[6], this assay induces consecutive turns in a short period of time, which facilitates the process of data collection. In addition, since the geometry of the phototaxic cues is stabilized in relation to the fish, a stereotyped turning angle is performed whose distribution can be nicely described by a Gaussian function and be distinguished from forward swims. Finally, it is often difficult to claim for certain whether a phototaxic turn is induced by a temporal change in the luminosity, or a spatial gradient in the illumination. The result from the current assay shows that a stabilized illumination contrast in the space is sufficient to elicit robust phototaxic turns.

In this phototaxis assay, the fish swims freely in a homogenously illuminated arena for 10 seconds before the stabilized phototaxic cue is presented for 12 seconds. It takes 370ms (mode, Figure 2.3B) for the fish to perform the first turn after the onset of the visual stimulus. After that, the fish performs consecutive turns toward the illuminated side at a rate of 1.2 swims per second. In comparison to larval zebrafish's targeted turning response during phototaxis, it is interesting to note that E. Coli use a different strategy for locomotion during chemotaxis[7]. The bacteria have a higher chance of performing turns if the previous moving direction results in a decrease in sucrose concentration, and tend to swim forward if the previous move leads to an increase in the concentration. This strategy of biased random walks can also lead the E. Coli to the food source. As an organism of an intermediate complexity, C elegans appear to use both strategies in navigation[8]. It retracts if the previous crawling direction results in a decrease in the food concentration. Meanwhile, it also wiggles its head to measure the spatial gradient in order to determine the direction in which it should move forward. The later behavior is similar to zebrafish phototaxsis in that the animal measures the spatial gradient of an external cue before each movement, but is different in that zebrafish can measure light contrast instantaneously without head wiggling.

Figure 2.2: Zebrafish demonstrate phototaxis from larval to juvenile stages

A group of 15 zebrafish is tested for their phototaxis behaviors from 8 dpf to 32 dpf. The fish are put in a rectangular tank which is homogenously illuminated for 2 min (0-120 sec). Then one side of the tank becomes dark and the other side becomes bright (120-240 sec). **A**, At 8 dpf, most of the fish swim to the brighter side and stay there for 2min (120-240 sec). Here the Phototaxic Index is the number of fish on the bright side subtracted by the number on the dark side, and then divided by the total number of the fish. After the phototaxic cue is replaced by homogenous illumination (240-360 sec), the fish redistribute to both sides of the tank. The phototaxic behavior is still performed at 19 dpf (**B**) but clearly disappears at 32 dpf (**C**). In fact, a negative phototaxis appears to be weakly expressed. **D**. The phototaxis behavior is robustly expressed from 8 dpf to 24 dpf, and gradually disappears afterward. By 30 dpf, the positive phototaxis completely disappears.

Figure 2.2

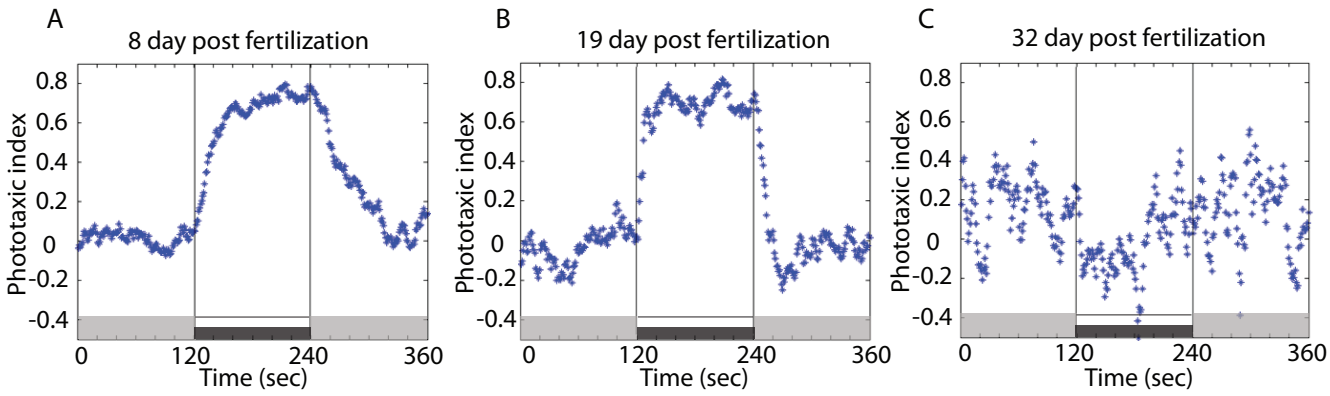
A
8 day post fertilization
B
19 day post fertilization
C
32 day post fertilization
Phototaxic index
0.8
0.6
0.4
0.2
0
-0.2
-0.4
0
120
240
360
Time (sec)

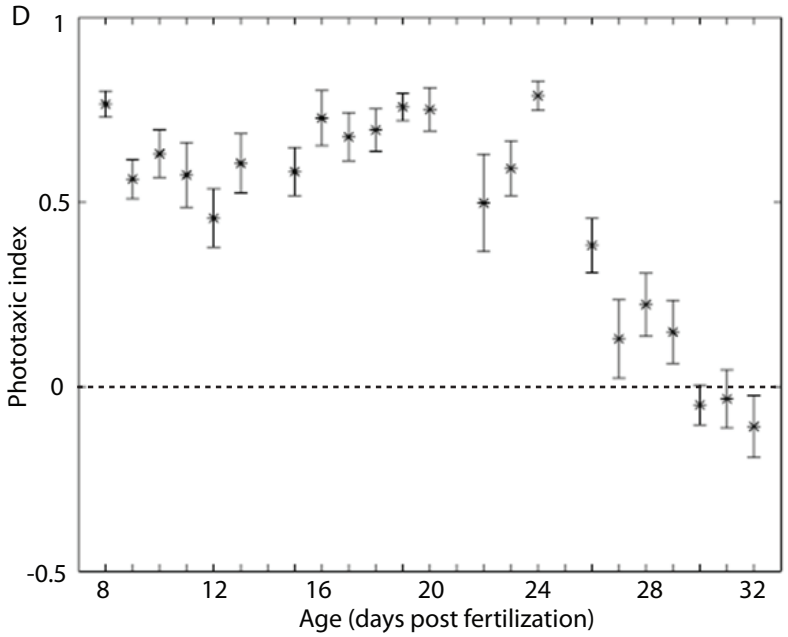
D
Phototaxic index
1
0.5
0
-0.5
8
12
16
20
24
28
32
Age (days post fertilization)

Figure2.3: Behavioral setup for phototaxis, the OMR, dark-flash response, and spontaneous swimming. A, Schematic of the behavioral setup. **B**, The response delay to the phototaxic cues.

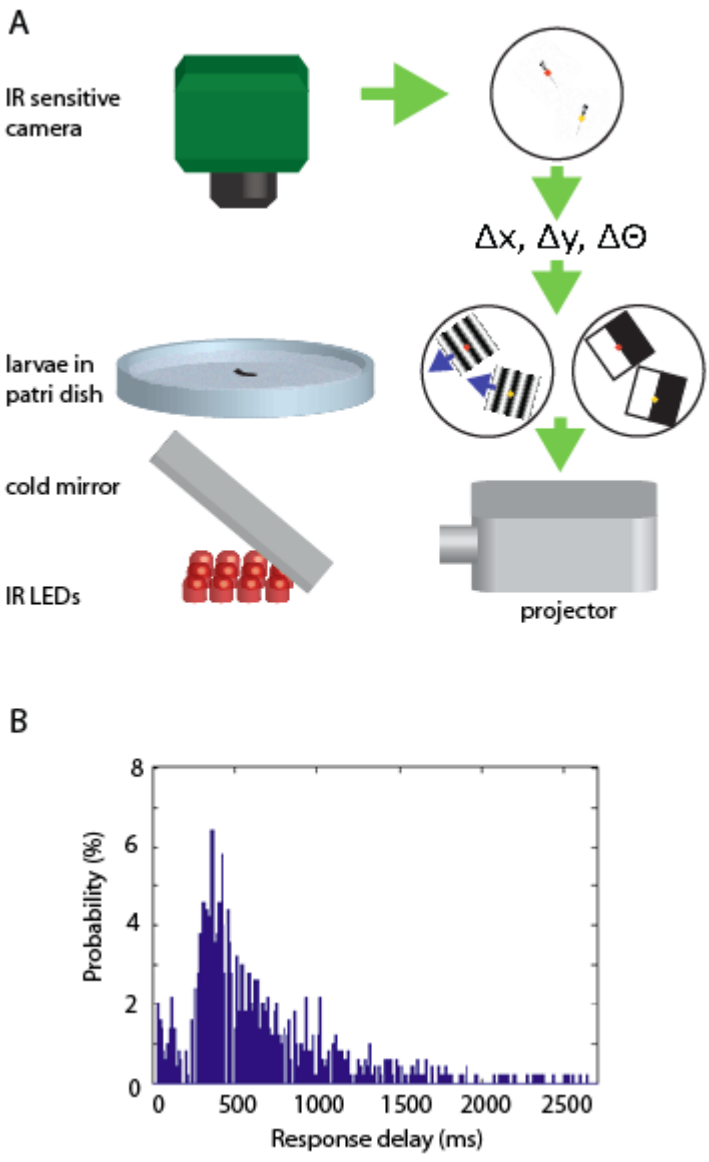

2.4 Turns differ from forward swims in the first cycle of tail undulation

To analyze turning behaviors in detail, the kinematics of head and tail movements of larval zebrafish are measured. The heading direction is the perpendicular vector that passes the midpoint between the two eyes. Since larval zebrafish perform episodic swims, a discrete change in the heading direction can be measured during each swim. In response to the phototaxic cue, the change in the heading direction ($\Delta\Theta_H$) reveals two modes of swimming behaviors; a turning mode that centers near 38° and a forward swimming mode that centers near 0° (Figure 2.4B & 2.4C). Interestingly, the forward swims are still biased in the sense that they are consistently initiated by a swing of the head toward the illuminated side (Figure 2.4D & 2.4E, red arrowheads). This bimodal characteristic of swim behaviors is also observed during the OMR when the fish is presented with laterally moving gratings (Figure 2.4F & 2.4G). Again the forward swimming mode during the OMR is initiated by a head movement following the direction of the stimuli (Figure 2.4H & 2.4I, red arrowheads).

Since tail undulations are more salient than head undulations, I measure the tail angle to examine how turns and forward swims differ during each cycle of body movement. Here the tail angle is the integral of the body curvature along the tail, or equivalently the angle difference between the heading direction and the caudal tail's tangent vector (Figure 2.5B). The finding that the phototaxic stimuli induce two modes of swimming behaviors is also manifested in the kinematics of tail movement. During the first undulation cycle, a bimodal distribution is observed in the angle of the initial tail bend (Figure 2.5C), as well as in the cycle period (Figure 2.5F). In comparison to the forward swimming mode, the turning mode is associated with an increase in the initial tail bend (142° vs. 58°) and a longer cycle period (59ms vs. 41ms). Surprisingly, the bimodal distribution almost disappears in the second undulation cycle: the

distributions of the tail bend angle and the cycle period are now nicely described by a single Gaussian function. The amplitude and rhythm of later undulations also reveal a single mode of tail movement shared by turns and forward swims (59° and 45ms, Figure 2.5E & 2.5H). Thus despite the marked difference between turns and forward swims in the first undulation cycle, later tail movement between the two behaviors is highly similar. This suggests that the descending motor command that controls turns is brief in its nature and mainly modulates the properties of the first undulation cycle during swims.

Table 2.1: *Kinematics of spontaneous swims and visually induced turns*

	Change in heading direction ($\Delta\Theta_H$) (°)	Maximal change in heading direction ($\Delta\Theta_{H1}$) (°)	Angle of 1st tail bend ($\Delta\Theta_{T1}$) (°)	Time to the first bend (ms)	1st cycle period (ΔP_{T1}) (ms)	Angle of 2nd tail bend ($\Delta\Theta_{T2}$) (°)	2nd cycle period (ΔP_{T2}) (ms)	Angle of later tail bends ($\Delta\Theta_{T3}$) (°)	Later cycle period (ΔP_{T3}) (ms)	% of swims with 3~6 undulations
Spont. forward swims (n=1385)	0.4±0.1	11.3±0.2	54.5±0.4	10.1±0.1	40.3.±0.1	69.4±0.3	39.7±0.1	56.5±0.2	43.6±0.04	97.8%
Spont. turns (n=3104)	21±0.4	39.3±0.4	116.4±0.6	17.9±0.1	52.7±0.2					
Turns in OMR (n=4458)	40.1±0.3	56.1±0.3	134.0±0.4	19.6±0.1	56.2±0.2	76.5±0.2	40.0±0.02	61.8±0.1	43.7±0.03	96.5%
Turns in phototaxis (n=3704)	38.8±0.4	61.0±0.4	142.9±0.5	20.6±0.1	59.3±0.2	73.2±0.2	40.9±0.1	58.8±0.2	44.6.0±0.03	97.7%
Turns in dark flash response (n=248)	123.0±2.7	166.2±1.9	227.4±1.5	26.4±0.4	74.5±0.8	76.4±1.2	40.6±0.3	60.7±0.8	46.7±0.1	97.7%

* See Figure 2.5A for symbol illustration.

Figure 2.4: Head movement during phototaxis and the OMR

A, A turning behavior described by the undulation of the heading direction (blue trace) and the tail angle (red trace). The fish first swings its head toward the turning side with an amplitude of $\Delta\Theta_{H1,}$ which is followed by 3-4 undulations. The final heading direction ($\Delta\Theta_H$) is markedly different from the original heading direction (0°), indicating the performance of a turn. **B** & **C**, Head movement during the phototaxis behavior. Each phototaxic cue induces two modes of behaviors: forward swims ($\Delta\Theta_H \sim 0°$) and turns ($\Delta\Theta_H \sim 38°$). **D** & **E**, The forward swim mode is consistently initiated by a head movement toward the side of a higher luminosity (red arrowheads). **F – I**, The head movement during the OMR.

Figure 2.5: Tail movement during the phototaxis and the OMR

A, The undulation of the tail movement (red trace) during a turn is divided into three cycles, and the tail bend amplitude ($\Delta\Theta_T$) and the cycle period (ΔP_T) are analyzed. **B**, The tail angle ($\Delta\Theta_T$) is the integral of the body curvature, or equivalently the angle difference between the heading direction (blue arrow) and the tangent vector at the caudal end of the tail (the orange arrow).

The two modes of the phototaxis behavior, namely forward swims and turns, are revealed in the first undulation cycle as both the tail angle (**C**) and the cycle period (**F**) show a bimodal distribution. However, starting from the second undulation cycle, there is no marked difference in the tail kinematics between the two behaviors (**D**, **E**, **G** and **H**), indicating that the two behaviors differ mainly in the first undulation cycle. **I – N**, Tail kinematics during the OMR.

Figure 2.4

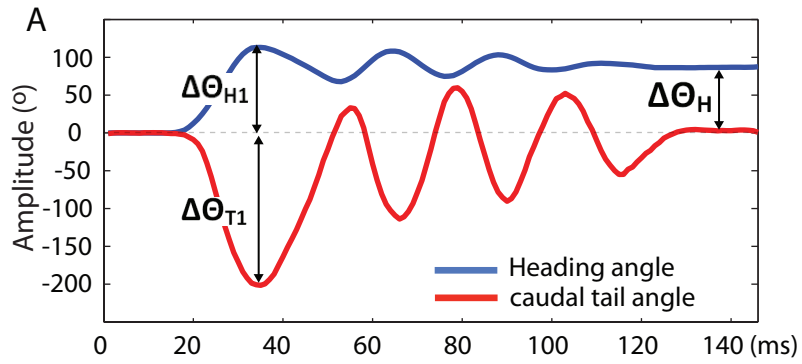

Phototaxis

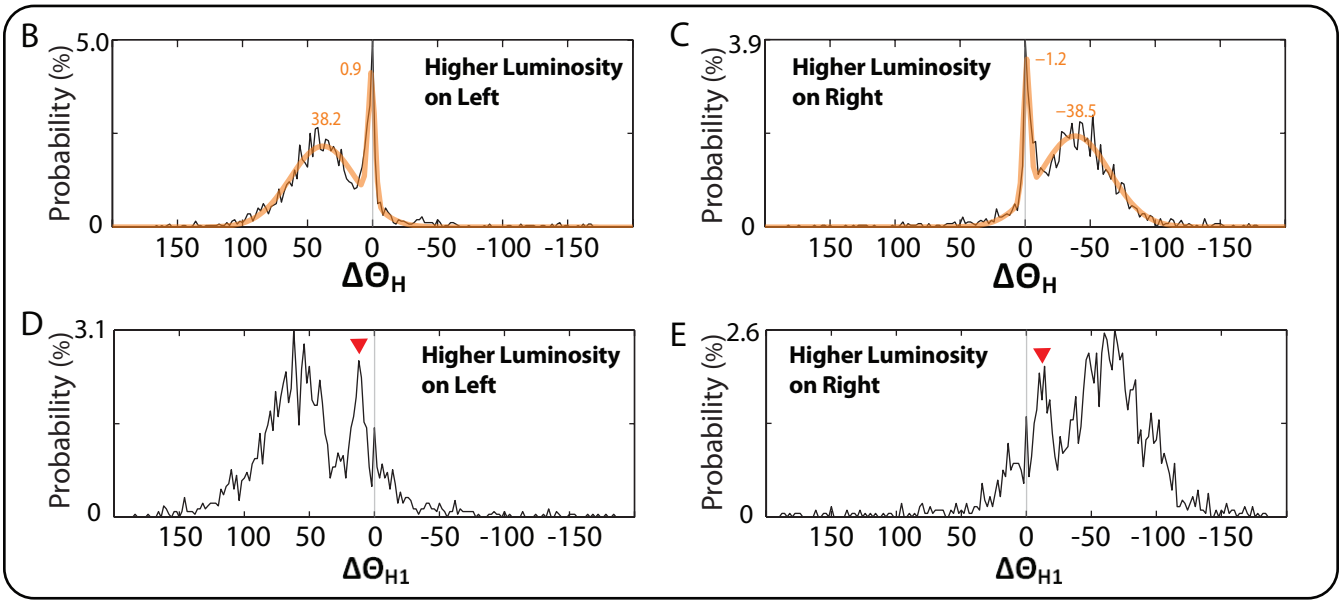

OMR

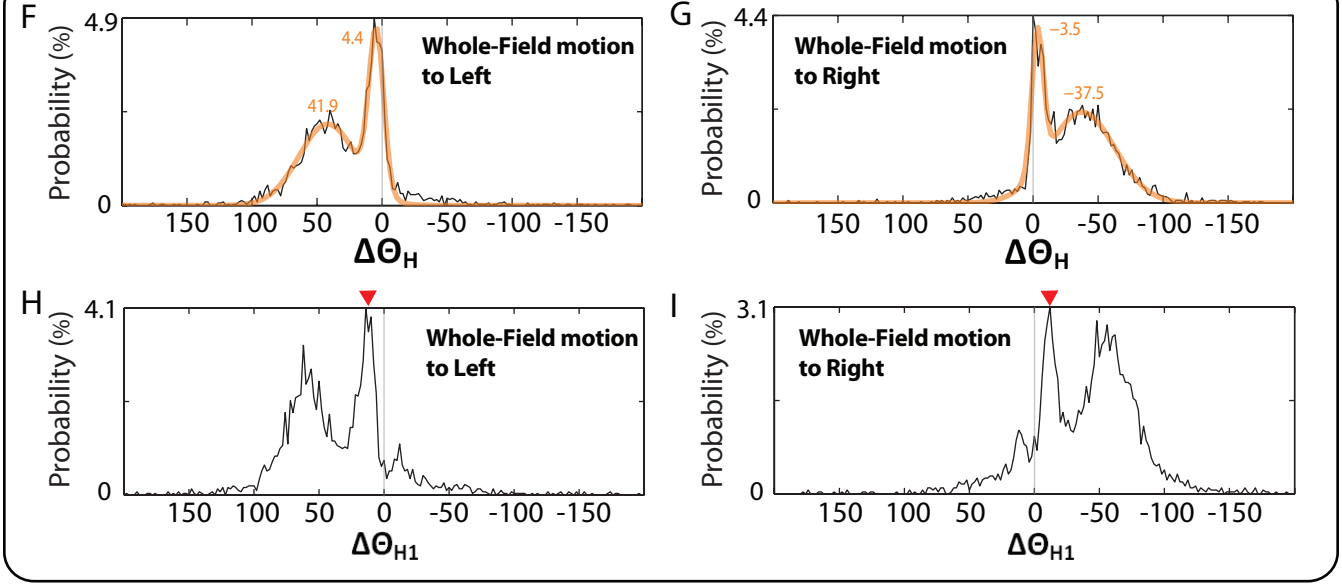

Figure 2.5

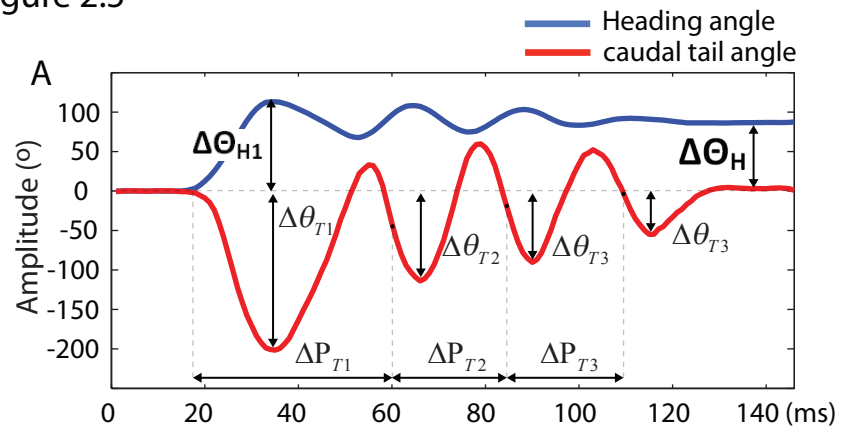

Phototaxis

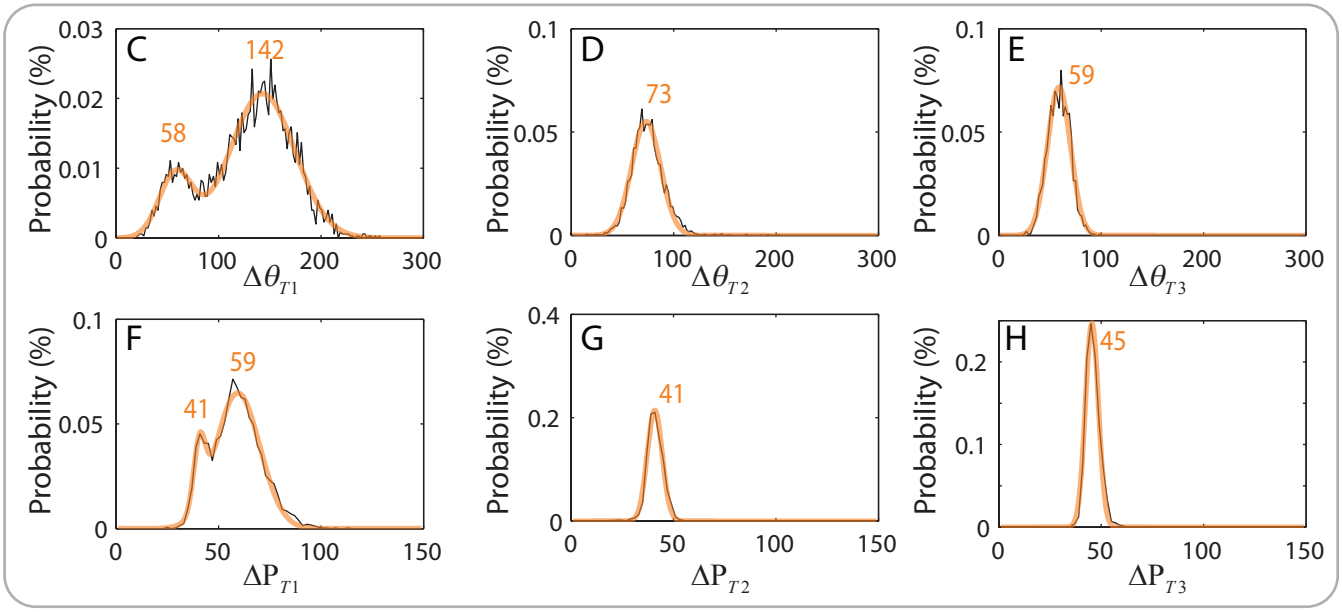

OMR

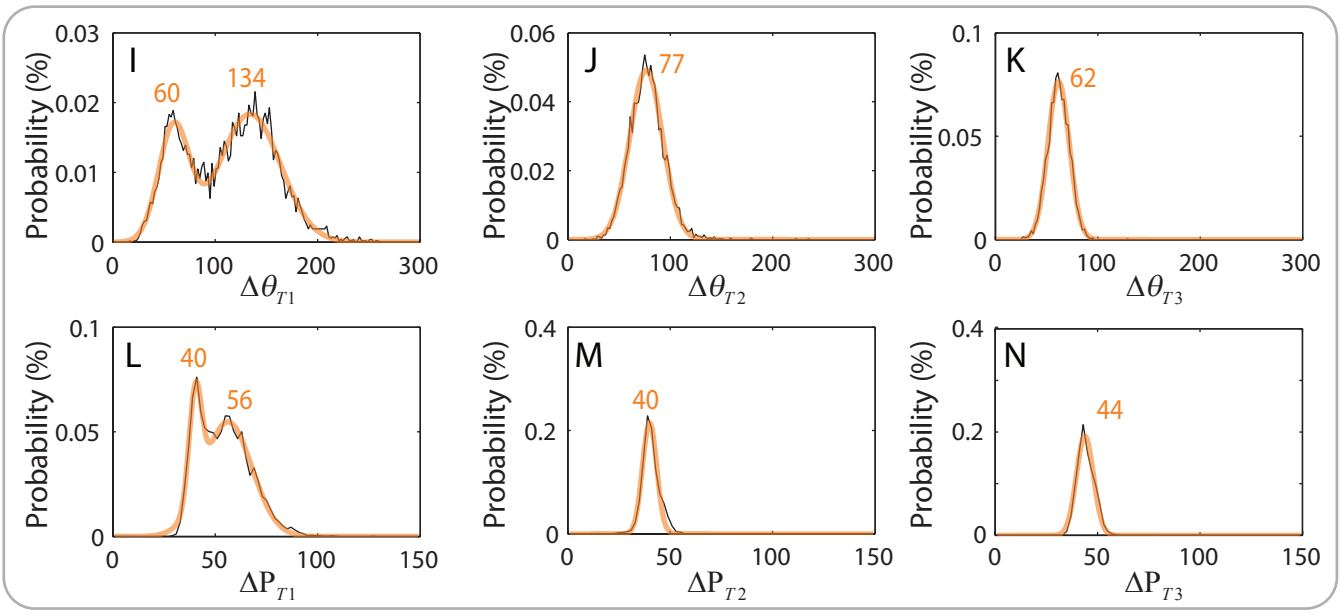

2.5 Laser ablation of hindbrain RoV3, MiV1 and MiV2 neurons affects the first cycle of tail undulation and promotes forward swims

The presence of two behaviors, namely forward swims and turns, in response to the phototaxic cues raises the question of how the two behaviors are controlled by spinal projection neurons. One potential implementation is that the two behaviors are controlled by distinct sets of spinal projection neurons. Alternatively the two behaviors share the descending pathway that generates symmetric tail undulations, but during turns an additional pathway is recruited to modulate the properties of early undulation cycles.

A previous study[2] has shown that small groups of spinal projection neurons, namely RoV3, MiV1, and MiV2, are necessary for turning during the OMR in larva zebrafish. By monitoring the location and body axis, the authors found that a unilateral removal of the spinal projection neurons abolishes the fish's ability to swim toward the ablated side in response to moving gratings, while swims to the non-ablated side are largely unaffected.

To examine the role of RoV3, MiV1 and MiV2 neurons in controlling phototaxic turns, both the phototaxis behavior and the OMR were tested in 24 larvae before and after unilateral removal of the spinal projection neurons using a two-photon laser (Figure 2.6A). Because the neurons are labeled stochastically by backfill spinal injection of dextran dyes[9], the number of ablated cells and the consequent ablation phonotype are variable. Nevertheless, fish that express a clear impairment in phototaxic turns also have a strong deficit in the OMR turns. In several cases (8 out of 24 fish), the unilateral ablation completely abolished turns toward the ablated side in response to the moving gratings or the phototaxic cues. As shown in Figure 2.6D, before the ablation the phototaxic cue induces two modes of swimming angles; the mode of small angles represents forward swims and the mode of larger angles represents phototaxic turns. Unilateral

ablation of the spinal projection neurons results in the following three observations. First, the turning mode to the ablated side is abolished. Second, the turning mode to the non-ablation side is intact. These results demonstrate the necessity of the ventromedial spinal projection neurons in controlling ipsilateral turns, but not contralateral turns, during phototaxis. The third observation is that the forward swimming mode is not impaired by the ablation. In fact, the occurrence of forward swims in response to turn-inducing phototaxic cues drastically increases after the ablation.

As mentioned earlier, forward swims and turns may be controlled by distinct sets of spinal projection neurons; each descending pathway independently generates the corresponding behavior. In such a case, ablation of RoV3, MiV1 and MiV2 should abolish turns, but have no effect on forward swims. Alternatively, forward swims and turns may share a common descending pathway that generates symmetric tail undulations. The additional turning command delivered by RoV3, MiV1 and MiV2 neurons may serve only to modulate this basic pattern in order to generate turns. In this latter case, the ablation of the neurons will not only abolish turns but also increase the occurrence of forward swims. As mentioned earlier, removal of the ventromedial spinal projection neurons results in a drastic increase in forward swims (Figure 2.6D). The percentage of swims that is associated with a change in heading direction of less than 10° dramatically increases from 20% to 95%. Analysis of the tail motion also shows the disappearance of large angle bends (mode 142°) and the increase of small angle bends (mode 54°, Figure 2.6E, red arrow), indicating that the ablation impairs turns and promotes forward swims. Interestingly, fish missing these ventromedial spinal projection neurons can perform forward swims by initiating the tail to either side of the body (Figure 2.6E, red arrowheads), suggesting

that the descending motor command for initiating forward swims excites both sides of the spinal network.

In the previous section, the analysis of tail kinematics in intact larval zebrafish suggest that descending turning commands are brief and mainly modulate the first undulation cycle. Here I examine the ablation effect on each cycle of tail undulations. After unilateral ablation of the ventromedial spinal projection neurons, the tail bend angle during the first, second and later undulations drops 61%, 6% and 3%, respectively. Similarly, the cycle period of the first, second and later undulations drops 33%, 2% and 1%, respectively. These results show that the ablation strongly affects tail movement in the first undulation cycle, weakly affects movement in the second cycle, and has nearly no effect on the later undulations. This is consistent with the idea that in intact animals the turning command conveyed by RoV3, MiV1 and MiV2 neurons is brief and mainly modulates the first undulation cycle.

The ablation study extends our understanding of descending motor control in three ways. First, it demonstrates that fish use the same set of spinal projection neurons for controlling turns in both OMR and phototaxis. As will be shown in the next section, the same fish used in this study also have an impaired turning ability during spontaneous swimming and dark-flash responses. Thus RoV3, MiV1 and MiV2 control various types of visually induced turns, as well as spontaneous turns, and may serve as the universal component in the supraspinal descending system in controlling turning behaviors. Second, the fact that the ablation mainly affects the first undulation cycle supports the notion that, in intact animals, the turning command conveyed by the spinal projection neurons is brief and mainly modulates the first undulation cycle. Finally, the drastic increase in forward swims in replacement of the disappeared turns after the ablation supports the idea that turns are generated by modulating the motor pattern of forward swims.

Figure 2.6: Laser ablation of RoV3, MiV1 and MiV2 neurons specifically affects the first undulation cycle and promotes forward swims during phototaxis and the OMR

A, Schematic of spinal projection neurons of larval zebrafish (excludes nMLF, image modified from Orger et al.,2008[6]). **B,** Two right MiV2 cells before and after laser ablation (arrows). The nearby ventral branch of the medial longitudinal fascicle (arrow head) remains intact. **C,** Example of ablation phenotypes: a visually induced right turn becomes a forward swim after ablating the spinal projection neurons on the right. The amplitude of the first tail bend is weaker and the period of the first oscillation is reduced. Turning to the non-lesion side is unaffected. **D,** Histograms of the turning angle ($\Delta\Theta_H$) before and after the ablation. Turning to the ablated side is abolished (red arrowhead) while the probability of forward swimming is drastically increased. **E,** Histograms of the tail bend angle before and after the ablation. Large-angle bends toward the lesioned side are greatly reduced (red arrows). Instead, small-angle bends on either side of the body are performed (red arrow heads). 2D histograms of tail bend angle vs. the cycle period shows that the ablation mainly affects the kinematics of the first undulation cycle (**F**) but has virtually no effect on the later cycles (**G**). In the first undulation cycle, the phototaxic cue used to induce large bend angles and prolonged cycle periods (**F**, upper right panel) can only induce tail movements with small angles and short cycle periods after the ablation (**F**, lower right panel). **H-K**, The ablation also specifically affects the first undulation cycle and promotes forward swims during the OMR.

Figure 2.6

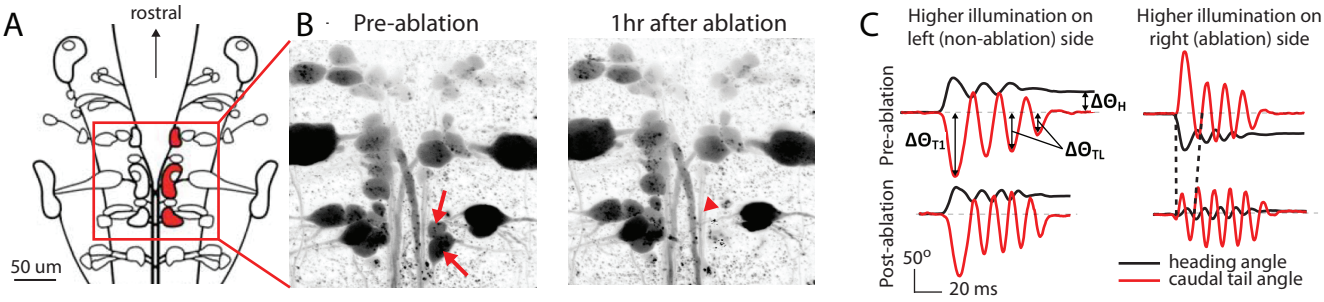

Phototaxis

D. Ablation effect on turn angle $\Delta\theta_H$

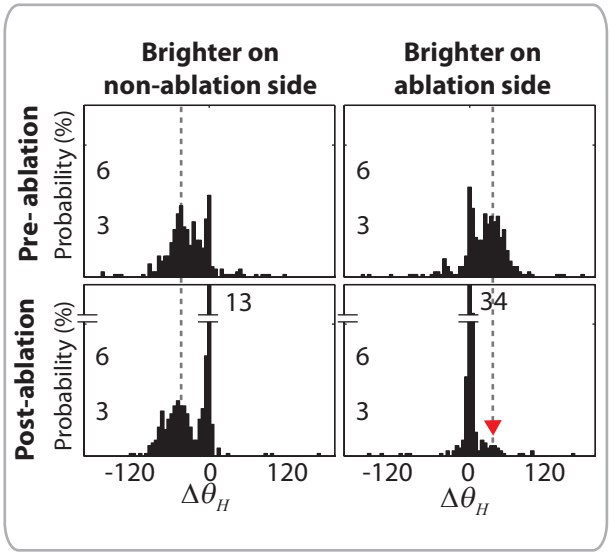

F. Ablation effect on 1st undulation $\Delta\theta_{T1}$ vs. ΔP_{T1}

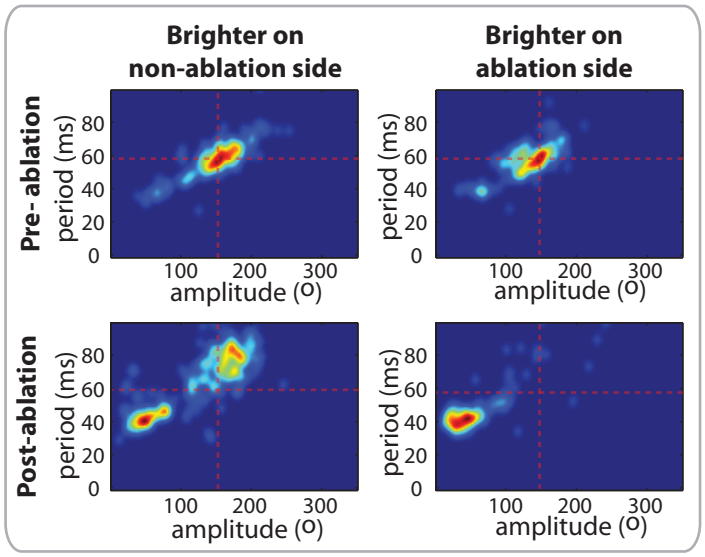

E. Ablation effect on1st tail bend $\Delta\theta_{T1}$

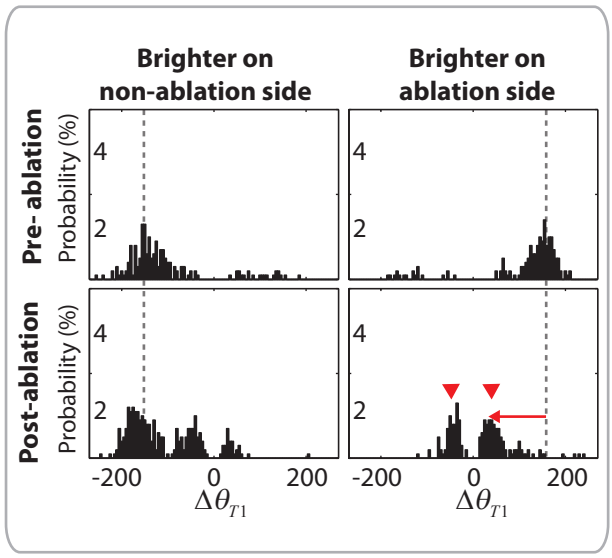

G. Ablation effect on later undulations $\Delta\theta_{T3}$ vs. ΔP_{T3}

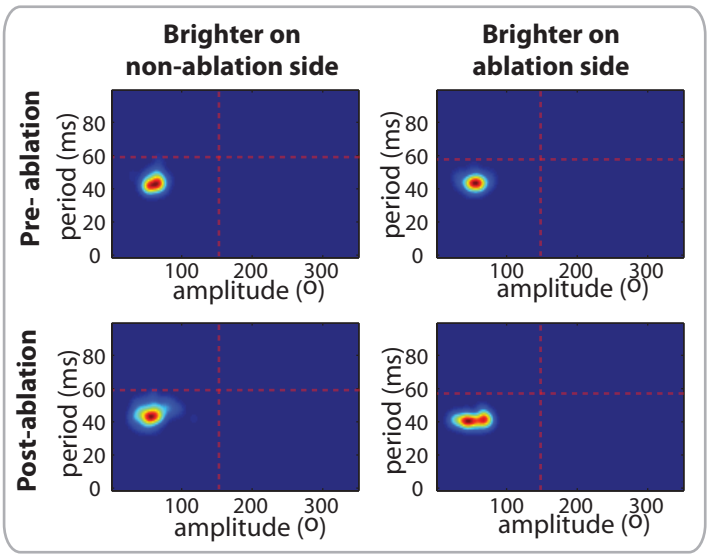

Figure 2.6 (contitued)

OMR

H. Ablation effect on turn angle $\Delta\theta_H$

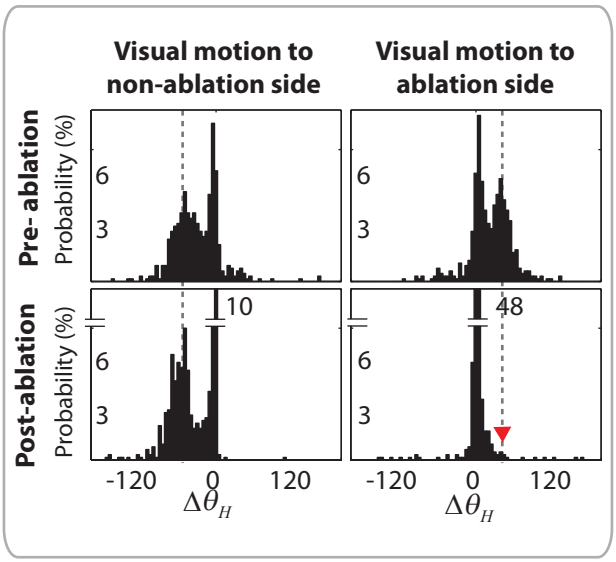

J. Ablation effect on 1st undulation $\Delta\theta_{T1}$ vs. ΔP_{T1}

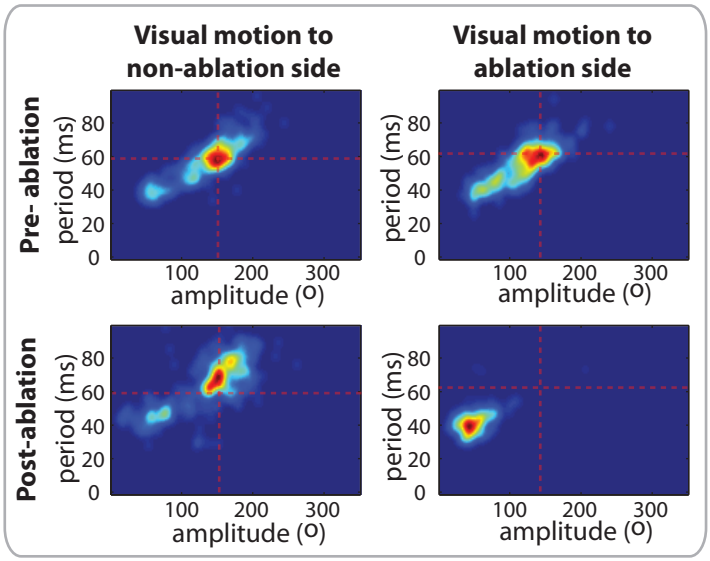

I. Ablation effect on1st tail bend $\Delta\theta_{T1}$

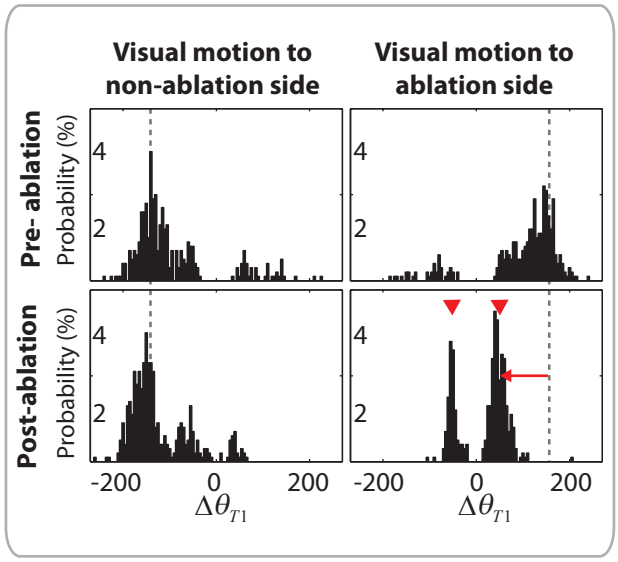

K. Ablation effect on later undulations $\Delta\theta_{T3}$ vs. ΔP_{T3}

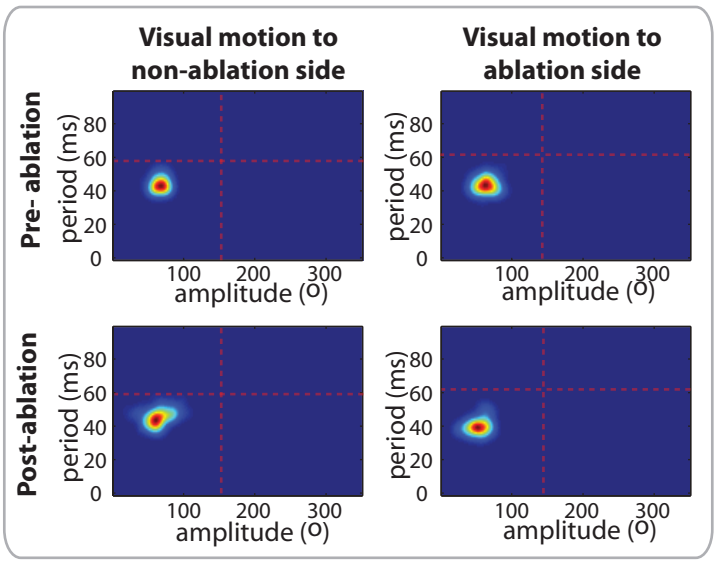

2.6 RoV3, MiV1 and MiV2 neurons are also necessary for dark flash-induced turns and spontaneous turns

In addition to controlling turns during phototaxis and the OMR, the hindbrain RoV3, MiV1 and MiV2 neurons also play a critical role in controlling spontaneous turns and the large angle turns exhibited during dark flash responses. Spontaneous swims were recorded during free swimming in ambient light without disturbances. Left and right turns occur with a similar frequency and a significant portion of the swim events are composed of forward swims (Figure 2.7B, also[3,5]). Unilateral ablation of the ventromedial spinal projection neurons decreases the occurrence of spontaneous turns toward the ablated side, and drastically increases the events of forward swims (Figure 2.7B & 2.7C). The tail bend angle and the cycle period decreases in the first undulation cycle, but the later cycles of tail movements are virtually unaffected by the ablation (Figure 2.7D & 2.7E).

In addition to touch-induced escape turns, large-angle turns can also be elicited by a sudden reduction in the illumination. Interestingly, a previous study shows that while laser ablation of Mauthner cells drastically increases the response latency of vibration induced turns, the lesion appears to have no effect on dark-flash induced turns[3]. The results in this study show that after unilateral ablation of RoV3, MiV1 and MiV2, the widely distributed turning angle expressed during the dark-flash response is abolished (Figure 2.8B & 2.8C). Again, the ablation mainly affects the first cycle of tail undulation but has no effect on the later tail undulations (Figure 2.8D & 2.8E).

Together, the ablation experiment shows that RoV3, MiV1 and MiV2 neurons have a universal role in controlling the phototaxic turns, the OMR turns, the dark-flash-induced turns, and spontaneous turns. The neurons appear to control these four types of turns in the same way -

to increase the cycle period and the initial tail bend angle in the first undulation cycle. It should be noted that these four types of turning behaviors cover a wide range of turning angles from spontaneous turns (mode: 21°), OMR turns (mode 40°), phototaxic turns (mode: 39°), to dark-flash induced turns (mode: 123°). It is likely that turns of different strength are mediated by different neurons within the RoV3, MiV1 and MiV2 nuclei. Or, alternatively, the turning strength is controlled by the same set of RoV3, MiV2 and MiV2 neurons, and the level of the neuronal activity dictates the turning strength.

Figure 2.7: Laser ablation of RoV3, MiV1 and MiV2 neurons abolishes spontaneous turns
A, Histogram of the heading-angle change ($\Delta\Theta_H$) during spontaneous swims (n = 24). The turning mode is more obvious by looking at the distribution of the initial head movement ($\Delta\Theta_{H1}$, inset). B, Histogram of the heading-angle change ($\Delta\Theta_H$) before and after the ablation (n=8, the same fish analyzed in Figure 6). Turning to the ablated side appear to be abolished (red arrowhead) while the probability of forward swimming is drastically increased. **C,** Histograms of the tail bend angle before and after the ablation. Large-angle bends toward the lesioned side are greatly reduced (red arrows). Instead, small-angle bends on either side of the body are performed (red arrow heads). 2D histograms of tail bend angle vs. the cycle period shows that the ablation mainly affects the kinematics of the first undulation cycle (**D**) but has virtually no effect on the later cycles (**E**). In the first undulation cycle, tail movements with large bend angles and prolonged cycle periods (**D**, upper panel) disappear after the ablation (**E**, lower panel).

Figure 2.7

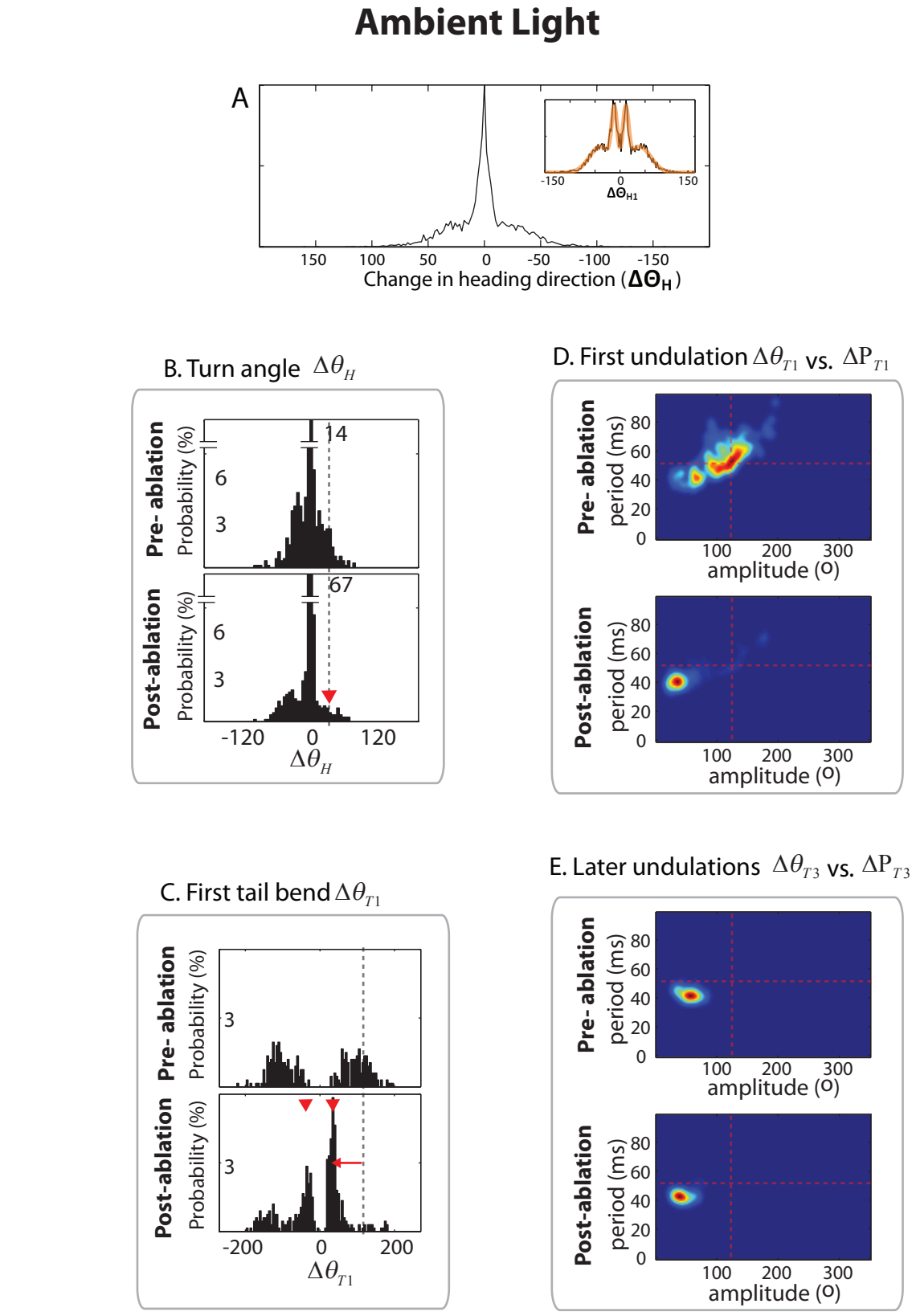
Ambient Light
A
150
100
50
0
-50
-100
-150
Change in heading direction (ΔΘH)
-150
0
150
ΔΘH1
B. Turn angle $\Delta\theta_H$
Pre- ablation
Probability (%)
14
6
3
Post-ablation
Probability (%)
67
6
3
-120
0
120
$\Delta\theta_H$
D. First undulation $\Delta\theta_{T1}$ vs. ΔP_{T1}
Pre- ablation
period (ms)
80
60
40
20
0
100
200
300
amplitude (º)
Post-ablation
period (ms)
amplitude (º)
C. First tail bend $\Delta\theta_{T1}$
Pre- ablation
Probability (%)
3
Post-ablation
Probability (%)
3
-200
0
200
$\Delta\theta_{T1}$
E. Later undulations $\Delta\theta_{T3}$ vs. ΔP_{T3}
Pre- ablation
period (ms)
amplitude (º)
Post-ablation
period (ms)
amplitude (º)

Figure 2.8: Laser ablation of RoV3, MiV1 and MiV2 neurons abolishes turns during the dark-flash response.

A, Histogram of the heading-angle change ($\Delta\Theta_H$) induced by a sudden dark flash (n = 24). Large angle turns ($\Delta\Theta_H \sim 125°$) and forward swims ($\Delta\Theta_H \sim 0°$) are often induced by the dark flash. B, Histogram of the heading-angle change ($\Delta\Theta_H$) before and after the ablation (n=8, the same fish analyzed in Figure 6). Turns to the ablated side are mostly abolished (red arrowhead) while the probability of forward swimming is increased. **C,** Histograms of the tail bend angle before and after the ablation. Large-angle bends toward the lesioned side are greatly reduced (red arrows). 2D histograms of tail bend angle vs. the cycle period shows that the ablation mainly affects the kinematics of the first undulation cycle (**D**) but has virtually no effect on the later cycles (**E**). In the first undulation cycle, tail movements with large bend angles and prolonged cycle periods (**D**, upper panel) disappear after the ablation (**E**, lower panel).

Figure 2.8

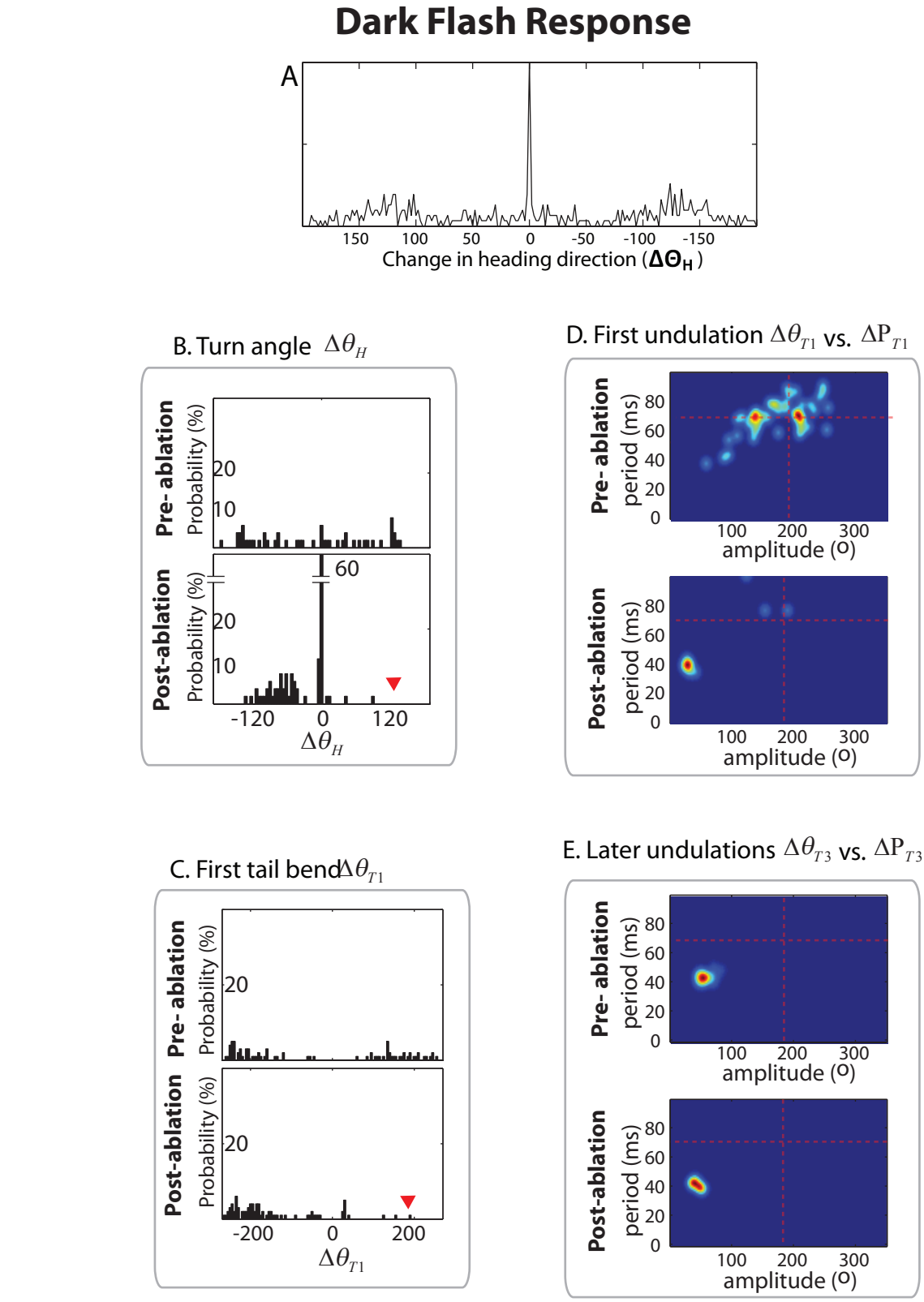
Dark Flash Response
A
150 100 50 0 -50 -100 -150
Change in heading direction (ΔΘH)
B. Turn angle $\Delta\theta_H$
Pre- ablation
Probability (%)
20
10
Post-ablation
Probability (%)
60
20
10
-120 0 120
$\Delta\theta_H$
D. First undulation $\Delta\theta_{T1}$ vs. ΔP_{T1}
Pre- ablation
period (ms)
80
60
40
20
0
100 200 300
amplitude (o)
Post-ablation
period (ms)
80
60
40
20
0
100 200 300
amplitude (o)
C. First tail bend $\Delta\theta_{T1}$
Pre- ablation
Probability (%)
20
Post-ablation
Probability (%)
20
-200 0 200
$\Delta\theta_{T1}$
E. Later undulations $\Delta\theta_{T3}$ vs. ΔP_{T3}
Pre- ablation
period (ms)
80
60
40
20
0
100 200 300
amplitude (o)
Post-ablation
period (ms)
80
60
40
20
0
100 200 300
amplitude (o)

2.7 Response of MiV1, MiV2 and RoV3 cells during different turning strength

Results from the previous section show that RoV3, MiV1 and MiV2 neurons are necessary for expression of a wide range of turning angles. By what mechanism are the animals able to perform these graded behaviors; how is the turning angle controlled at the level of the reticulospinal neurons? Three potential mechanisms could be implemented. First, the number of active neurons may increase as the strength of the behavior increases. This has been demonstrated in motor neurons where, as the load on a muscle increases, more motor neurons that innervate the muscle activated[10]. Second, the same set of neurons may simply fire at a higher frequency as the strength of the behavior increases. This activity dependent mechanism has been reported in larval zebrafish spinal cord where a subtype of spinal interneuron exhibits a graded activity as the strength of escape response increases[11]. Third, different strengths of a behavior could be controlled by different subsets of neurons. In larva zebrafish, it was found that as the swimming speed increases, there is a shift in the active set of spinal interneurons[4,12]; ventrally located interneurons tend to maintain silence during fast swims and become active during slow swims.

To examine the activation pattern of RoV3, MiV1 and MiV2 neurons during different turning strength, I employed a fictive swimming paradigm[13] (also Ahrens 2012, in press) to monitor motor output during calcium imaging. In this paralyzed preparation, spontaneous or visually elicited motor events occur at a frequency of ~1Hz. Each motor event consists of bilateral bursting activity with a left-right alternation at a frequency of ~25 Hz (Figure 2.9C & 2.9D), reminiscent of tail undulations during free swimming. When a backward lateral or lateral moving grating is presented, a burst of motor nerve activity first occurs on the side where the grating moves to (Figure 2.9 C & 2.9D). This initial burst is typically longer in duration and

higher in firing frequency than the following bursts, presumably corresponding to a strong tail bend at the beginning of a turn. To quantify the strength of bursts, we calculate the local variance, or power, of the motor nerve signal (figure 2.9 C & D, red traces). The directional bias of swims is then estimated by the power difference between left and right signals during the first 50ms of fictive swims. This measure was shown to be the most indicative of the turning direction, and was consistent with the finding that turns differ from forward swims in the first undulation cycle of tail movements (see Section 2.4).

As shown in Figure 2.9E – 2.9K, the optomotor response expressed by paralyzed, embedded fish (n=20) is not entirely identical to the response performed by freely swimming fish. Consistent with freely-swimming behaviors, paralyzed fish respond to backward lateral gratings (Figure 2.9E & 2.9K) and forward gratings (Figure 2.9H) with strong turns and forward swims, respectively. However, the fish respond to lateral gratings with a mixed response such that most swims are still biased in the grating direction but some are biased in the opposite direction (Figure 2.9F & 2.9J). The striking difference occurs when forward lateral gratings are presented: paralyzed fish consistently turn away from the direction of lateral forward gratings (Figure 2.9G & 2.9I). Not only the power of the motor nerve activity is stronger on the opposite side, but the laterality the initial burst indicates a consistent tail bend (78%) away from the grating direction. These examples demonstrate the importance of monitoring behaviors during neuronal recording, since the direction of the visual stimulus is not a perfect predictor of the animal's swimming direction.

The discrepancy between free and fictive behavior may be due to different "states" of the animal, i.e. paralyzed/embedded vs. freely swimming, or because of differences in visual stimulation, such as the reflection of the visual scene onto the microscope objective and glass

pipettes. This discrepancy, however, does not hinder my aim in correlating neuronal activity to turning strength, since the visual stimulus only serves to induce swims. The activity of a cell will be correlated to the directional bias of fictive swims, regardless what grating directions are used to induce the swims.

Armed with the ability to measure the directional bias of individual swims in paralyzed fish, I examined the activity of ventromedial cells during visually induced turns at different strength. We found that MiV2, RoV3 neurons and many of the MiV1 cells on one side of the brain were silent during contralateral turns, and their activity was elevated as the directional bias toward the ipsilateral side increased (Figure 2.9L). These cells thus express a rectifying or sigmoid activation profile in relation to the swim bias (Figure 2.9Q & 2.9R). Some of the MiV1 cells, however, are broadly turned; they are weakly active during contralateral turns and more active during weak ipsilateral turns (Figure 2.9M & 2.9V). In some cases, these two types of cells were recorded at the same optical plane during a single functional imaging experiment, excluding the possibility that the different profiles resulted from different recording conditions (Figure 2.9N & 2.9O). I did not observe neurons that were sharply tuned for large angle or small angle turns; thus no evidence supports the recruitment mechanisms mentioned in the beginning of the section.

Overall, the result suggests that the strength of turns is controlled by the activity of the same set of ventromedial spinal projection neurons, and not the number of active neurons. This conclusion is supported by the fact that ablation of subsets of the ventromedial neurons either has no effect, or impairs all turning behaviors during spontaneous swimming, phototaxis, the OMR and dark flash responses. This ablation phenotype is in line with the idea that a same set of the ventromedial spinal projection neurons control turns from small angles to large angles.

Figure 2.9: RoV3, MiV1 and MiV2 neurons show graded response during different turning strengths. **A,** Simultaneous recording of motor nerve and SPN activity in a paralyzed fish. **B**, A left MiV1 cell backfilled with a calcium sensitive dye responds strongly to left and backward left gratings and weakly to a forward right grating. Region-of-interest averaged fluorescence time series is shown in green and the deconvolved trace is in blue. Motor nerve activities are recorded bilaterally to identify fictive swims (red dots). Example fictive swims exhibiting rightward and leftward turns are magnified (**C** & **D)**. **E**–**K**, Histograms of swim bias in response to gratings moving to seven different directions. **L,** A cell's response profile in relation to the directional bias of fictive swims (the same cell as in **A**). Each point represents a swim; it indicates the fluorescent signal (ΔF/F) of the cell during a specific swim bias. The cell is silent during rightward swims and becomes progressively active as the swim bias toward the left increases. Colors indicate the direction of the moving grating during which the swim was elicited. **M,** A right MiV1 cell shows weak responses during contralateral turns and stronger responses during weak ipsilateral turns. **N** & **O,** A right MiV2 and MiV1 cell recorded on the same optic plane. **P-R,** Overlapped response profiles of MiV1, MiV2 and RoV3 neurons, respectively. Each cell's response profile, as shown in **L**, is binned by 11 intervals and represented by a black trace. The average response profile for each MiV1, MiV2, RoV3 cell type is shown in red. **S-U,** Histograms of swim bias where the maximal response is measured. The majority of the cells are most active during strong ipsilateral turns. Some MiV1 neurons, however, are most active during weak ipsilateral turns or forward swims. **V-X**, Each cell type's response during strong contralateral turns and strong ipsilateral turns. MiV2 and RoV3 neurons are active during ipsilateral turns and are highly inactive during strong contralateral turns. Several MiV1 neurons, however, are active during strong contralateral turns.

Figure 2.9

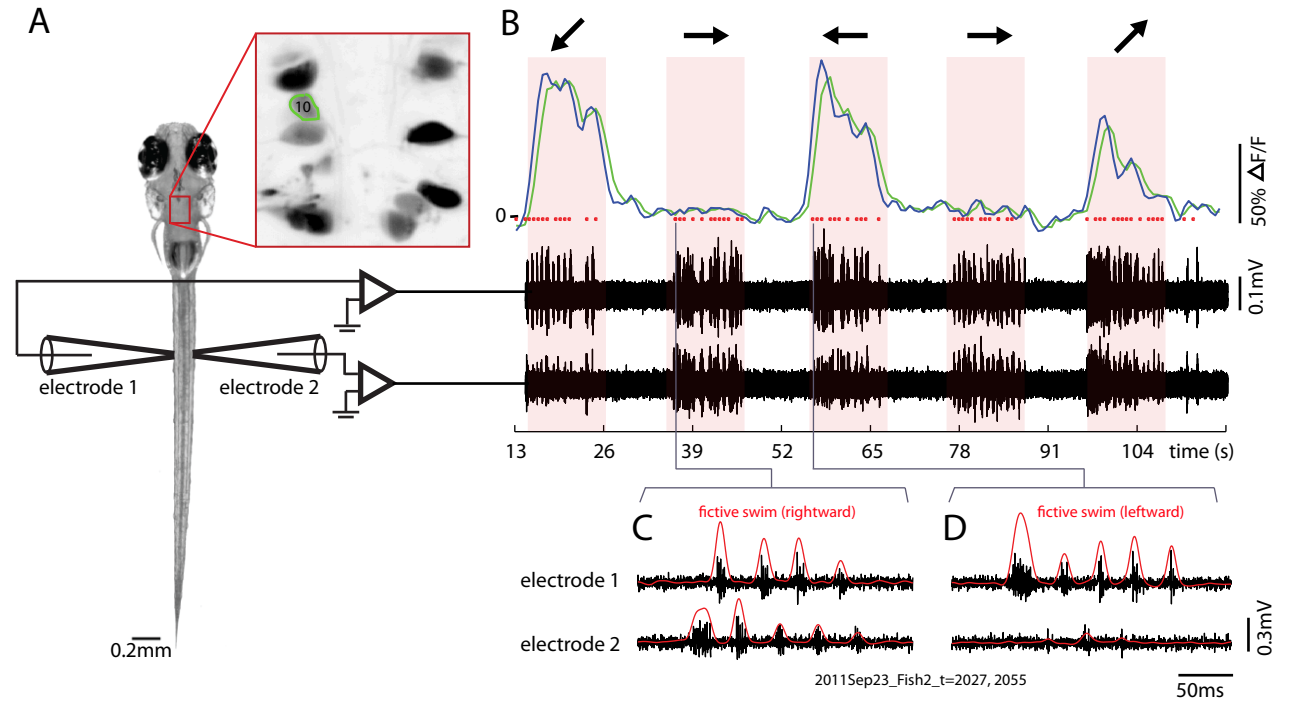
A
B
10
electrode 1
electrode 2
0.2mm
0
50% ΔF/F
0.1mV
13
26
39
52
65
78
91
104
time (s)
C
fictive swim (rightward)
D
fictive swim (leftward)
electrode 1
electrode 2
0.3mV
2011Sep23_Fish2_t=2027, 2055
50ms

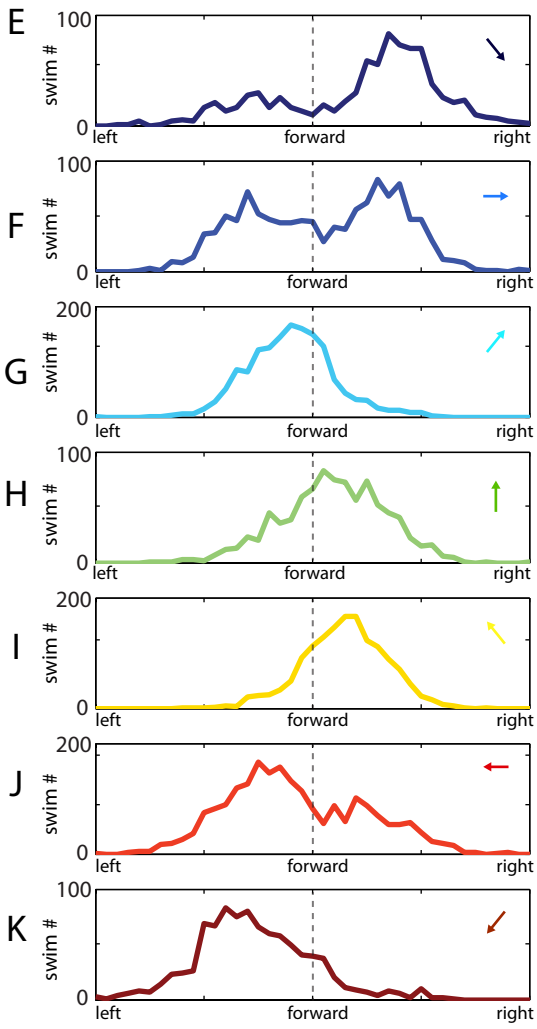
E
F
G
H
I
J
K
swim #
100
200
0
left
forward
right

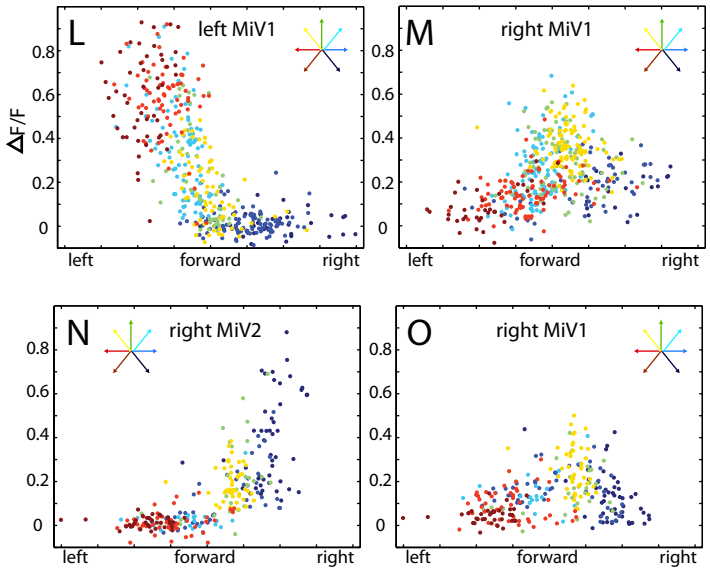
L
left MiV1
M
right MiV1
N
right MiV2
O
right MiV1
ΔF/F
0.8
0.6
0.4
0.2
0
left
forward
right

Figure 2.9 (continued)

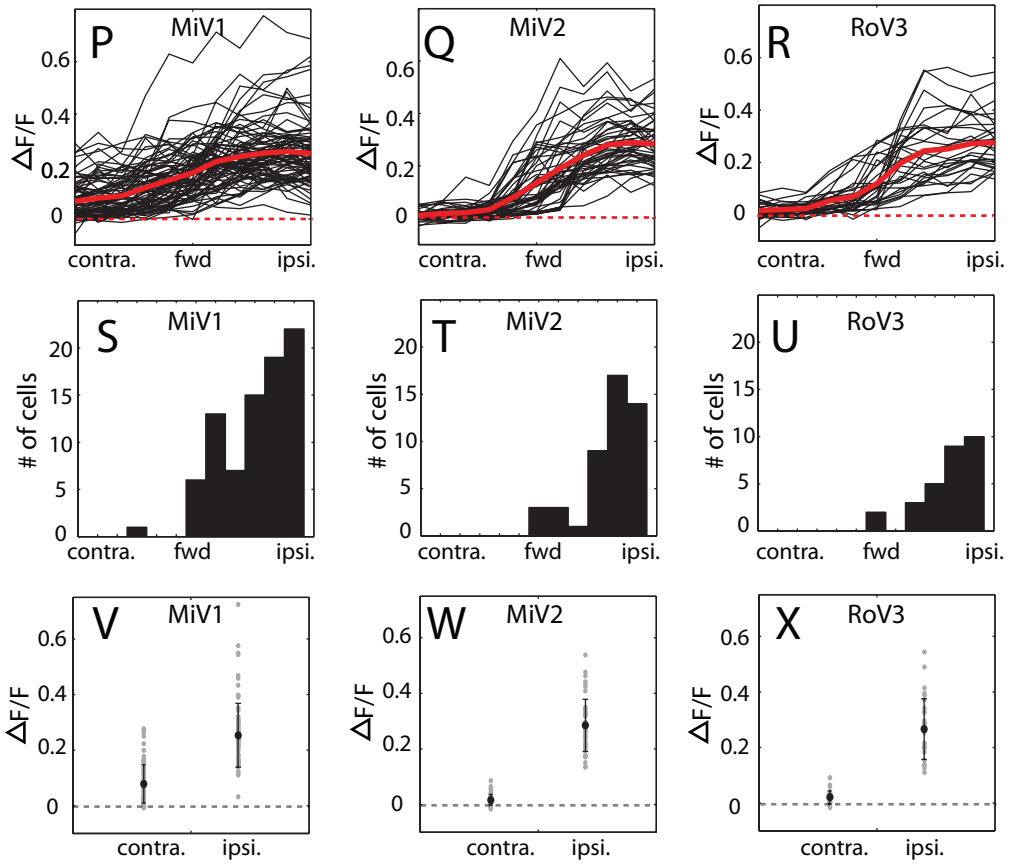

Finally, I examined whether the ventromedial cells that were active during stimulus-elicited behaviors were also active during spontaneous swims. We ranked each cell's calcium fluorescence (ΔF/F) from low to high during swims elicited by moving gratings of all directions, and used the fluorescence signal at the 90th percentile of the distribution to indicate how active the cell was during the OMR (Figure 2.10A, red bars). The same analysis was applied to the fluorescent signals acquired during spontaneous swims. We found that most ventromedial cells that were active during the OMR were also active in spontaneous swims, except for two cells in the MiV1 group (Figure 2.10C – 2.10E). Neuronal activity during the OMR was in general higher than that in spontaneous swims. Finally, the cells' activation profiles in relation to directional bias are similar in the OMR and in spontaneous swims (Figure 2.10B). This is consistent with the idea that the same subset of the ventromedial cells serves a universal role in controlling both visually elicited and spontaneous swims.

Figure 2.10: A similar set of RoV3, MiV1 and MiV2 neurons are active during spontaneous turns and OMR turns.

A, Example of the fluorescence response (ΔF/F) of a MiV1 cell during the OMR and spontaneous swims. Each dot represents a swim; it indicates the fluorescence response of the cell during a swim elicited by the grating direction marked beneath. The overall OMR response is shown in the 8th column. The response during spontaneous swims is shown in the 9th column. The 90th percentile of the overall OMR and spontaneous activity is marked with red bars, indicating how active the cell is during the two behaviors. **B,** The response profile of the MiV1 neuron during spontaneous swims showing a similar rectifying shape observed during the OMR (compare to Figure 2.9L, the same cell). **C-E,** Scatter analysis of each neuron's activity during the OMR against the activity during spontaneous swims. Each dot represents a cell; it indicates the activity the cell during the OMR and spontaneous swims. For example, the pair of red bars in panel **A** generates a dot in panel **C**. The results show that neurons that are active during the OMR are mostly active during spontaneous swims.

Figure 2.10

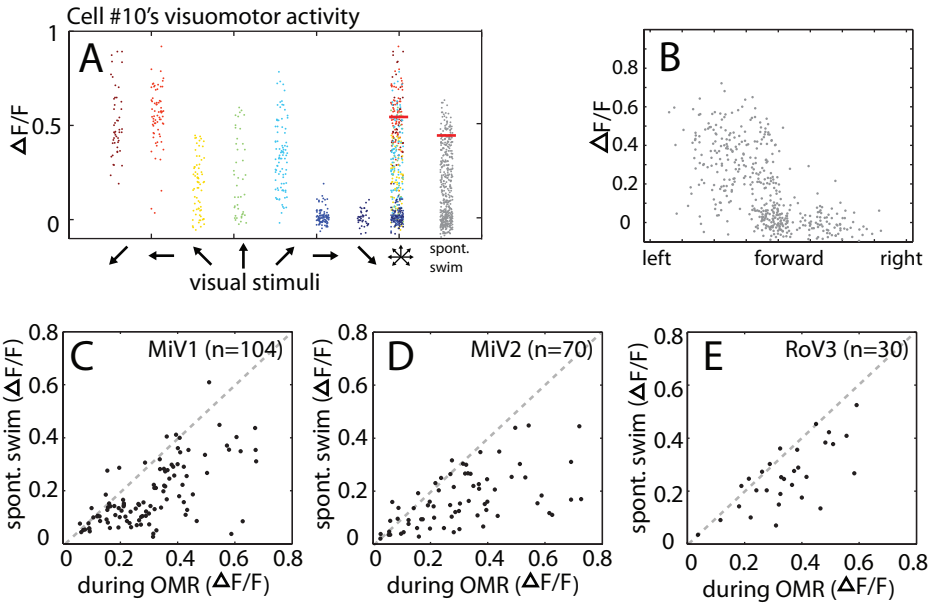
Cell #10's visuomotor activity
A
ΔF/F
1
0.5
0
visual stimuli
spont. swim
B
0.8
0.6
0.4
0.2
0
left
forward
right
C
MiV1 (n=104)
D
MiV2 (n=70)
E
RoV3 (n=30)
spont. swim (ΔF/F)
during OMR (ΔF/F)
0
0.2
0.4
0.6
0.8

2.8 Discussion

There have been relatively few studies that demonstrate how identified spinal projection neurons control behaviors in vertebrates[14–16], partly due to the complexity of supraspinal descending systems in most vertebrates. On the basis that hindbrain spinal projection neurons RoV3, MiV1 and MiV2 in larval zebrafish are necessary for controlling OMR turns, I extended this investigation to other visuomotor behaviors as well as spontaneous swims, and demonstrated exactly how these spinal projection neurons control tail movement during turns.

In principle, these spinal projection neurons can generate turns in one of two following ways: either (a) generate a complete, biased, undulating sequence of tail movements, or else (b) work with another descending system which generates symmetric tail movements such that the combined output is a biased tail movement. The experiments I presented here suggest that scenario (b) is implemented in the larval zebrafish, and this conclusion is supported by three observations.

First, using detailed kinematic analysis of tail movement, it is found that turns and forward swims differ in the first cycle of tail undulations. During turns, the initial tail bend and the cycle period are significantly increased. However, the marked difference disappears in the second undulation cycle. In later cycles, tail undulations between turns and forward swims are visually identical. This partial overlap in the undulation pattern suggests the possibility that turns could arise from forward swims by modulating the first cycle of tail movement.

Second, unilateral laser ablation of hindbrain RoV3, MiV1 and MiV2 neurons specifically affects tail movement in the first undulation cycle. Fish with the ablation are unable to perform, in the first undulation cycle, the prolonged cycle period and increased tail bend amplitude in response to turn-inducing visual stimuli. Instead, they express symmetric tail

undulations throughout the swim. This indicates that the descending pathways that generate turns are composed of two components: one that generates symmetric tail undulations, and another, mediated by RoV3, MiV1 and MiV2, that briefly modulates the rhythm and amplitude of tail movement.

Third, if turns arise from forward swims by transforming symmetric tail movements to biased tail motion, then ablation of the turn-controlling spinal projection neurons should not only abolish turns, but also increase the occurrence of forwards swims. Indeed, the percentage of forward swims (change of heading direction <10°) in a turn inducing visual environment increases from 20% to 95% after unilateral ablation of RoV3, MiV1 and MiV2. Since the overall frequency of swim events is largely unchanged after the ablation (1.2 swims/sec to 1 swim/sec), the data suggest that the increased occurrence of forward swims results from the inability to transform symmetric tail undulation into turns in the absence of the spinal projection neurons.

Together, these results suggest that hindbrain RoV3, MiV1 and MiV2 neurons modulate the first cycle of symmetric tail movement in order to generate turns. During turns, the ventromedial spinal projection neurons provide a brief and biased command that increases the cycle period and initial tail bend amplitude to create a slow, biased tail undulation.

This study also reveals that larval zebrafish without the ventromedial spinal projection neurons are unable to perform turns during three visuomotor behaviors, namely phototaxis, optomotor and dark flash response. These three behaviors require the detection of illumination contrast, visual motion, and a temporal change in luminosity, respectively; thus they may be mediated by separate neuronal types in the retina. Indeed, functional imaging in larval zebrafish has revealed the segregation of retinal arborization fields that are responsive to visual motion and to dark flashes (Naumann, unpublished data). This suggests that divergent visual pathways

converge at the level of spinal projection neurons in controlling turning behaviors. The fact that spontaneous turns are also impaired after the ablation of RoV3, MiV1 and MiV2 neurons further supports the notion that these cells have a universal role in controlling turning behaviors. I did not test turns elicited by other sensory modalities such as touch, temperature and olfaction. Nevertheless, it's interesting to note that while the Mauthner cells and their homologs, MiD2cm and MiD3cm, have been demonstrated to be involved in touch-elicited escape turns [9,17,18], ablation of these neurons only increases the response latency, but a full spectrum of turning angles is spared[19,20]. Thus a Mauthner cell-independent descending pathway appears to exist to control the amplitude of touch-elicited escape turns. On the basis that hindbrain RoV3, MiV1 and MiV2 control visually induced turns and spontaneous turns, these neurons may potentially have a broader role and control turns elicited by other sensory modalities[21].

The last part of this chapter uses two-photon calcium imaging to reveal two functional types of RoV3, MiV1, MiV2 neurons. A subset of MiV1 neurons is active during most swim directions, but is more active during weak ipsilateral turns. It is still unclear whether and how they have a critical role in controlling turning behaviors. They may, for example, deliver descending drive to increase the stiffness of the tail during swims. On the other hand, almost all RoV3, MiV2, and most of the MiV1 neurons respond only during ipsilateral turns, and their activities elevate as the swim bias increases. These cells thus express a rectifying or sigmoid activation profile in relation to the swim bias.

The current study shows that the majority of the RoV3, MiV1 and MiV2 neurons express highly lateralized responses; they are inactive during contralateral turns, weakly active during small ipsilateral turns, and strongly active during large ipsilateral turns. This is different from the previous finding that most RoV3, MiV1 and MiV2 neurons show a strong forward-motion

preference (Orger et al.[2], Figure 3). The difference should result from the method used to estimate swim directions in paralyzed fish. While Orger et al. assumed the paralyzed fish would swim in the grating direction, this study uses the motor nerve signal recorded bilaterally to calculate the directional bias of fictive swim. A surprising finding is that forward lateral gratings induce fictive swims turning away from the grating direction. For example, when a forward left grating was presented to a fish, not only the motor nerve activity on the right side of the tail became stronger, but the initial burst also occurred on the right. Freely swimming fish, without exception, perform right turns by first bending their tails toward right. Thus an initial burst of motor nerve activity on the right unambiguously indicates that the fish intended to either turn right or swim forward, but not to turn left. This finding may explain why the previous study found that most RoV3, MiV1 and MiV2 neurons show a strong forward-motion preference. For example, while left RoV3 neurons are highly active in response to backward left gratings (which induce strong left turns), they are also active during forward right gratings (which induce weak left turns). The average response vector will thus shift toward the forward direction, instead of being strongly biased toward left. This demonstrates the advantage of monitoring behaviors during neuronal recordings. In addition, neuronal activity during spontaneous behavior can only be studied by simultaneously monitoring motor outputs, since there is no external stimulus to provide the time reference for collecting data.

As a final remark, the current study along with previous findings appears to reveal a modular design of descending motor system. In this design, each descending pathway has its own role, and the addition or removal of one of the pathways does not affect the operation of other pathways. Consistent with this idea, removal of the Mauthner cells in goldfish specifically increases the response delay during touch-elicited escape turns, but did not affect the full

spectrum of turning angles[19]. Even when the functional homologs, namely MiD2cm and MiD3cm, are ablated along with the Mauthner cell, larval zebrafish are still able to perform large angle turns during touch-elicited escapes[20]. In this study, I showed that ablation of RoV3, MiV1 and MiV2 impairs turns but spares forward swims. The examples of the Mauthner cell in controlling the response delay, RoV3, MiV1 and MiV2 in controlling turning angles, and an independent pathway that controls symmetric tail undulations suggest a modular structure of supraspinal descending motor system in larval zebrafish.

2.9 Methods

Fish

6-7 day-old zebrafish from WIK strains in all experiments. *mitfa-/-* (nacre) fish[22] were used for the imaging, ablation and behavior studies, as they lack pigment in the skin, but retain normal eye pigmentation. Their behavior is indistinguishable from wild-type siblings in the assays.

The overall procedure of the ablation experiment

36 hrs before the experiment, 3% (w/v) solution of dextran-conjugated Texas red (Invitrogen) was injected into the spinal cord of tricaine-anesthetized fish. On the day of the experiment, the phototaxis behavior, the optomotor response, the dark flash response, and spontaneous swims of an individual fish were tested. The behavior of the injected fish was indistinguishable from non-injected siblings. The fish was then embedded in 2% low-melting temperature agarose, and the spinal projection neurons were ablated one by one using two photon laser. Most of the time, the fish could swim immediately after been released from the agarose, and the three visuomotor

behaviors and spontaneous swims were tested. In rare cases where fish lost balance or could not swim, the animal was not included in the post ablation analysis.

The overall procedure of the calcium imaging experiment

36 hrs before the experiment, 25% (w/v) solution of dextran-conjugated calcium green (Invitrogen) was injected into the spinal cord of tricaine-anesthetized fish. On the day of the experiment, the fish was embedded in 2% low-melting temperature agarose, and paralyzed by injecting 1mg/ml bungarotoxin solution (Sigma-Aldrich) in tail muscles. After removing the agarose caudal to the swim bladder, the electrodes were placed on intersegmental boundaries around the 10^{th} myotome, which is rostral to the injection site of the bungarotoxin. The calcium response of the spinal projection neurons and the motor nerve activity were recorded simultaneously while the visual stimulus was presented to the fish from beneath.

Behavioral assays

Zebrafish larvae swam freely in a 10-cm diameter petri dish. Fish were illuminated by an array of infrared light-emitting diodes and their swimming behavior was recorded at 500 Hz using an infrared-sensitive, high-speed CMOS camera (Mikrotron). Visual stimuli were projected directly onto a screen 5 mm below the fish using a DLP projector (Optoma). Custom image-processing software (Labview) extracted the position and orientation of the fish at the acquisition frame rate. This information was used to update the visual stimuli during the OMR and the phototaxis assay such that the illumination contrast and the grating direction were stabilized in relation to the fish.

During the phototaxis, the OMR and the dark flash response assays, the visual stimulus was presented for 12 sec followed by a homogenous illumination for at least 10 sec. The next

trial was only initiated when the fish was 2cm away from the wall in order to prevent biased turns caused by the physical barrier. To record the spontaneous swimming behavior, fish was allowed to swim in a homogenously illuminated arena for at least 10 min, and was video recorded for 5min.

During each experiment, the fish's location, orientation, and a 80-by-80 pixel image, which is enough to contain the full body of the fish, were stored in hard drives at the acquisition frame rate (500Hz). The tail movement was analyzed offline by a custom image-processing software (MATLAB).

Two-photon laser ablation

The spinal projection neurons were ablated using two-photon laser as previously described[2]. Briefly, targeted cells were identified and a central subregion was selected from a full frame scan. The power of a mode-locked laser (880 nm) was linearly increased while the beam was scanned in a spiral pattern throughout the targeted region. Scanning was immediately terminated on the detection of brief flashes of saturating intensity. This procedure always results in destruction of the cell despite immediately adjacent cells and neurites appearing unaffected.

Fictive swim recordings and analysis

The recording setup and detection algorithm of fictive swims used in this study were developed recently in the Engert lab (Ahrens et al. in press). After the larval zebrafish is embedded and paralyzed, two electrodes were placed on intersegmental boundaries around the 10^{th} myotome under guidance of the camera (integrated into the two-photon microscope and using near-infrared illumination), and gentle suction was applied. Typically, electrical signals became apparent ten

minutes after the placement of the electrodes. The fictive swims recording software was written in C# (Microsoft) and formed part of the custom written interface that controlled the two-photon microscope, the visual display and the electrophysiology acquisition (Ahrens et al. in press). The electrical signals representing fictive swims resembled large amplitude noise bursts. The main characteristic setting apart these signals from the recording noise was the increase in local variance, or power, of the signal. The signal is processed by taking a windowed standard deviation, so that if s(t) is the electrical signal and $\bar{s}(t)$ the processed signal, then $\bar{s}(t) = SD(s(t-\tau/2)...s(t+\tau/2))$, with τ = 10ms. In this way, the signal was transformed into a much cleaner signal, of high `signal-to-noise'. For offline analysis, as in Figure 2.9C & 2.9D (red traces), a Gaussian-weighted standard deviation was used instead of a square window, but the effect was similar. To detect fictive swims in the processed signal, a threshold was set automatically (Ahrens et al. in press). The method of thresholding proved to be very robust, as it detected fictive swims reliably and led to very few false positives.

To calculate the directional bias of the fictive swims, I compared the following properties recorded from the left and right electrodes: the width of the first burst, the average firing rate of the first burst, and the power of the first burst; these three parameters correspond to the width, the height and the area of the processed signal (Figure 2.9C & 2.9D, red traces) during the first burst. These parameters gave similar results in segregating swims induced by forward, backward right and backward left gratings. In this study, I used the power difference between the two channels during the first 50 ms of fictive swims, which covered the first cycle of the motor nerve activity during forward grating-induced swims. I didn't normalize the swim bias by the sum of the signal power, because weak swims tended to generate a large swim bias. Instead, swim bias was normalized by two SDs of the overall swim bias performed by the fish in response to all

grating directions. Since the recording quality varied during the experiment, every 30 min the weight of the left and right signals was calibrated. The calibration involved equalizing the power of the motor nerve activity of the two channels during swims induced by forward gratings.

Two-photon calcium imaging

While the motor nerve activity of the larval zebrafish was recorded by the two electrodes at the tail, the calcium response of the spinal projection neurons in the hindbrain were imaged simultaneously with a custom two-photon microscope (pulsed Ti-sapphire laser tuned to 920 nm, Spectra Physics). The visual stimulus was projected from below with a projector (3M) and passed through a red long-pass filter, which allowed simultaneous visual stimulation and fluorescence detection. On each imaging plane, binary gratings of seven different directions were presented in random orders; each presentation lasted 10 seconds and each grating direction was presented 10 times before changing to the next imaging plane. In each experiment, frames were acquired at 1.7 Hz. Due to the fact that neuron in the RoV3, MiV1 and MiV3 nuclei are tightly clustered, the image was analyzed by manually selecting regions of interests. The calcium time series of each cell (Figure 2.9B, green trace) was deconvolved (Figure 2.9B, blue trace) by a decaying exponential to remove the slow dynamic of the calcium indicator[23]. The exponential has a time constant of 1.2 sec, which was measured from the decaying calcium time series after a response-evoking stimulus is turned off. A cell's activity during a fictive swim was the deconvolved calcium signal at the time when the swim occurred.

2.10 References

1. Metcalfe, W. K., Mendelson, B. & Kimmel, C. B. Segmental homologies among reticulospinal neurons in the hindbrain of the zebrafish larva. *J. Comp. Neurol.* **251**, 147–159 (1986).
2. Orger, M. B., Kampff, A. R., Severi, K. E., Bollmann, J. H. & Engert, F. Control of visually guided behavior by distinct populations of spinal projection neurons. *Nat. Neurosci.* **11**, 327–333 (2008).
3. Burgess, H. A. & Granato, M. Modulation of locomotor activity in larval zebrafish during light adaptation. *J. Exp. Biol.* **210**, 2526–2539 (2007).
4. McLean, D. L., Masino, M. A., Koh, I. Y. Y., Lindquist, W. B. & Fetcho, J. R. Continuous shifts in the active set of spinal interneurons during changes in locomotor speed. *Nat. Neurosci.* **11**, 1419–1429 (2008).
5. Budick, S. A. & O'Malley, D. M. Locomotor repertoire of the larval zebrafish: swimming, turning and prey capture. *J. Exp. Biol.* **203**, 2565–2579 (2000).
6. Burgess, H. A., Schoch, H. & Granato, M. Distinct retinal pathways drive spatial orientation behaviors in zebrafish navigation. *Curr. Biol.* **20**, 381–386 (2010).
7. Berg, H. C. & Brown, D. A. Chemotaxis in Escherichia coli analysed by three-dimensional tracking. *Nature* **239**, 500–504 (1972).
8. Lockery, S. R. The computational worm: spatial orientation and its neuronal basis in C. elegans. *Curr. Opin. Neurobiol.* **21**, 782–790 (2011).
9. O'Malley, D. M., Kao, Y. H. & Fetcho, J. R. Imaging the functional organization of zebrafish hindbrain segments during escape behaviors. *Neuron* **17**, 1145–1155 (1996).

10. HENNEMAN, E., SOMJEN, G. & CARPENTER, D. O. FUNCTIONAL SIGNIFICANCE OF CELL SIZE IN SPINAL MOTONEURONS. *J. Neurophysiol.* **28**, 560–580 (1965).
11. Bhatt, D. H., McLean, D. L., Hale, M. E. & Fetcho, J. R. Grading movement strength by changes in firing intensity versus recruitment of spinal interneurons. *Neuron* **53**, 91–102 (2007).
12. McLean, D. L., Fan, J., Higashijima, S., Hale, M. E. & Fetcho, J. R. A topographic map of recruitment in spinal cord. *Nature* **446**, 71–75 (2007).
13. Masino, M. A. & Fetcho, J. R. Fictive swimming motor patterns in wild type and mutant larval zebrafish. *J. Neurophysiol.* **93**, 3177–3188 (2005).
14. Eaton, R. C., DiDomenico, R. & Nissanov, J. Role of the Mauthner cell in sensorimotor integration by the brain stem escape network. *Brain Behav. Evol.* **37**, 272–285 (1991).
15. Fetcho, J. R., Higashijima, S. & McLean, D. L. Zebrafish and motor control over the last decade. *Brain Res Rev* **57**, 86–93 (2008).
16. Roberts, A., Li, W.-C. & Soffe, S. R. Roles for inhibition: studies on networks controlling swimming in young frog tadpoles. *J. Comp. Physiol. A Neuroethol. Sens. Neural. Behav. Physiol.* **194**, 185–193 (2008).
17. Nissanov, J., Eaton, R. C. & DiDomenico, R. The motor output of the Mauthner cell, a reticulospinal command neuron. *Brain Res.* **517**, 88–98 (1990).
18. Zottoli, S. J. Correlation of the startle reflex and Mauthner cell auditory responses in unrestrained goldfish. *J. Exp. Biol.* **66**, 243–254 (1977).
19. DiDomenico, R., Nissanov, J. & Eaton, R. C. Lateralization and adaptation of a continuously variable behavior following lesions of a reticulospinal command neuron. *Brain Res.* **473**, 15–28 (1988).

20. Liu, K. S. & Fetcho, J. R. Laser ablations reveal functional relationships of segmental hindbrain neurons in zebrafish. *Neuron* **23**, 325–335 (1999).

21. Gahtan, E., Sankrithi, N., Campos, J. B. & O'Malley, D. M. Evidence for a widespread brain stem escape network in larval zebrafish. *J. Neurophysiol.* **87**, 608–614 (2002).

22. Lister, J. A., Robertson, C. P., Lepage, T., Johnson, S. L. & Raible, D. W. nacre encodes a zebrafish microphthalmia-related protein that regulates neural-crest-derived pigment cell fate. *Development* **126**, 3757–3767 (1999).

23. Miri, A. *et al.* Spatial gradients and multidimensional dynamics in a neural integrator circuit. *Nat. Neurosci.* **14**, 1150–1159 (2011).

CHAPTER 3

Descending control of network rhythms in the spinal cord – a modeling study

3.1 Introduction

The result from Chapter 2 shows that the RoV3, MiV1 and MiV2 neurons increase the cycle period of tail movement during the first undulation cycle of turning behaviors. What could be the mechanism by which the spinal projection neurons control the rhythm of network oscillation in the spinal cord? Specifically, what neuronal types in the spinal cord do these hindbrain neurons innervate in order to control the rhythm during turning behaviors?

In adult lampreys, hindbrain spinal projection neurons have been shown to form glutamatergic synapses on all types of spinal interneurons, namely EINs, CINs, LINs and motor neurons[1]. Among them, the activation of LINs, the ipsilateral inhibitory neurons, have been shown experimentally[2] and computationally[3] to reduce the bursting duration and the cycle period of the ventral root activity during locomotion. Given their roles in terminating bursts and shortening the oscillation period, it is less likely that they mediate the prolonged cycle period during turns. On the other hand, descending innervations exclusively to motor neurons could increase the firing rate and perhaps increase the bursting duration of motor neurons, but are unable to explain the prolonged suppression of the ventral root activity on the contralateral side. In order to implement this contralateral suppression of motor activity, commissural inhibitory neurons (CINs), have to be activated either directly or indirectly by spinal projection neurons. In addition, mutual inhibition mediated by CINs has also been suggested to slow down the network oscillation of the spinal cord[4,5]. For these two reasons, CINs could potentially be the synaptic

target of turn-controlling spinal projection neurons. Finally, ipsilateral excitatory interneurons (EINs) have been shown to directly innervated CINs in lampreys[6]. Thus, ventromedial spinal projection neurons could potentially innervate EINs and indirectly activate CINs in order to control the rhythm of tail movement.

The effect of descending innervation on network oscillations in the spinal cord has been studied using modeling approaches in lamprey[3] and zebrafish[7,8]. In the lamprey study, while the spinal network modeled by Ekeberg et al. remarkably explains many experimental findings[9,10], it does not appear to support the fundamental observation that each half of the spinal cord is sufficient to generate oscillations[5]. The fact that each hemicord can oscillate in the absence of commissural innervation suggests the presence of pacemaking units on each side of the spinal cord.

This chapter aims to incorporate intrinsic pacemakers into a spinal network – a different way to construct spinal central pattern generators (CPGs), and examine the potential mechanisms by which descending motor commands modulate the network's rhythm. To this end, I first construct a model of a pacemaking neuron whose voltage-dependent currents are described by an I-V curve containing a negative resistance component. Other currents considered are a calcium dependent potassium current ($I_{K(Ca)}$), a voltage dependent calcium current ($I_{Ca(V)}$), a calcium extrusion current, and a passive leak current. Similar to real pacemaking neurons, the membrane potential of the modeled neuron expresses robust oscillations with four phases of activities, namely a slow depolarization, a fast depolarization, a plateau potential with slow decay and a fast repolarization. The cycle period of the oscillation can be lengthened by at least four-fold by decreasing the calcium dependence of $I_{K(Ca)}$ and the voltage dependence of $I_{Ca(V)}$. Increasing

the membrane capacitance has a moderate effect on lengthening the cycle period. The calcium extrusion rate, in contrast, minimally modulates the rhythm of oscillations.

Pacemaking neurons are then integrated into the spinal CPG as EINs[11]. Since CINs have not been found to be intrinsically rhythmic in vertebrates, this neuronal type is modeled as a non-pacemaker using a linear I-V curve. Using these two cell types, a single-segment model of a spinal CPG containing one EIN and one CIN on each side of the spinal cord is built. This four-cell network expresses robust oscillations with left-right alternations and can quickly reach the alternating stage by providing a weak bias in the initial conditions.

RoV3, MiV1 and MiV2 neurons project ipsilateral axons to the spinal cord (Metcalfe 1986) and are likely to be glutamatergic[12] (also Koyama et al. unpublished data). The effect of descending innervation by these ventromedial neurons on the spinal network is modeled by increasing the conductance of non-selective cation channels in the EIN or the CIN on the ipsilateral side. The result shows that unilateral excitation to the EIN actually shortens the network's cycle period. In contrast, unilateral excitation to the CIN is sufficient to generate a two-fold increase in the cycle period, which could explain the dynamic range of the rhythm performed by larval zebrafish during turns. These observations suggest that hindbrain RoV3, MiV1 and MiV2 neurons could innervate spinal CINs, potentially $CoBL_{gly}$ or CoLo neurons in larval zebrafish, to control the rhythm of tail movement during turns.

3.2 A model of the pacemaking neuron that expresses rhythmic activity

Pacemaking neurons exhibit membrane potential oscillations that are typically divided into four phases: a rapid depolarization, a long-lasting plateau, a fast repolarization, and a slow

depolarization (Figure 3.1B). Here I model a pacemaking neuron by considering the following two experimental observations. First, it has been shown that a negative resistance characteristic of the cell's I-V curve is essential for establishing oscillations[13]. Second, a calcium-dependent potassium current is found to be critical for terminating the long-lasting plateau of the membrane potential during oscillations[14]. On these bases, I describe the dynamics of the neuron's membrane potential and intracellular calcium concentration with two differential equations. The voltage dynamic is described by a capacitance current, an overall voltage-dependent current, a calcium dependent current, and a leak current (Eqn. 1). The overall voltage-dependent current is determined by the I-V curve measured from pacemaking cells[13]. This measured curve is approximated by a cubic function (Eqn. 3) in this modeling study. The dynamics of calcium concentration is described by a calcium extrusion current and a voltage dependent calcium current (Eqn. 2). To keep the model tractable, the calcium dependent potassium current and the voltage dependent calcium current are assumed to be proportional to the calcium concentration and the membrane potential, respectively.

Table 3.1: A pacemaker model

The pacemaking neuron	**Variables**
$C \cdot \frac{dv}{dt} = -I(v) - \alpha \cdot u + i$ (Eqn. 1) $\frac{du}{dt} = \frac{-u}{\tau} + \beta \cdot v$ (Eqn. 2)	Membrane potential (v), Intracellular calcium concentration (u)
The cubic I-V curve	**Parameters**
$I(v) = \frac{1}{660} \cdot v^3 - v - 9$ (Eqn. 3)	Membrane capacitance (C), Calcium dependence of potassium current (α), Time constant of calcium extrusion (τ) Voltage dependence of calcium current (β) Leak current (i)

At any point in the *u*-*v* space, the velocity $(\frac{dv}{dt}, \frac{du}{dt})$ can be calculated from Eqn. 1 and 2. Thus, given an initial condition (u_0, v_0), the evolution of *u* and *v* can be plotted as a trajectory in the phase plane. To analyze the behavior of a dynamical system, it's useful to find the position of the nullclines, where the speed in one of the directions is zero. In this system, the location with zero velocity in the *v* direction is described by a cubic nullcline,

$$u = \frac{-1}{\alpha}\left(I(v) - i\right), \qquad \text{(from Eqn.1, given } \frac{dv}{dt} = 0\text{)}$$

and the location with zero velocity in the *u* direction is described by a linear nullcline

$$u = \tau \cdot \beta \cdot v, \qquad \text{(from Eqn.2, given } \frac{du}{dt} = 0\text{)}$$

In most cases, the system will end up at a stable point in the phase plane and stop moving. However, when two conditions are met, the trajectory starting from any initial condition will enter a closed loop in the phase plane. First, the linear nullcline has to intersect the cubic nullcline in the cubic nullcline's negative resistance region. Second, the slope of the linear nullcline must be larger than that of the cubic nullcline at the intersecting point. The two conditions are described as the following:

Conditions for oscillation

(*i*) $i \approx -9$

(*ii*) $\beta \cdot \tau > \frac{1}{\alpha}$

The first condition ensures that the linear nullcline intersects the cubic nullcline around the cubic nullcline's inflection point, or the midpoint of the negative resistance region. This requires an intermediate leak current i of the cell. The second condition ensures that the slope of the linear

nullcline is larger than the cubic nullcline at the intersections. This requires a large calcium dependence (β) for $I_{K(Ca)}$, a large calcium extrusion time constant τ , and a large and voltage dependence (α) for $I_{Ca(V)}$. An example trajectory of this oscillating process is shown in the phase plane (Figure 3.1A). The movement of the trajectory can be divided into four steps:

(1) The trajectory starts at a low voltage and low calcium state (point **s**), and quickly moves to a high voltage state until it reaches the cubic nullcline (point **s'**).

(2) Since there is zero velocity in the *v* direction at the cubic nullcline, the trajectory moves upward in the *u* direction. However, it is quickly drawn back to the cubic nullcline since the velocity in the *v* direction is much larger than the *u* direction outside the cubic nullcline. The trajectory slowly moves along the cubic nullcline until it reaches point **b**.

(3) The trajectory then quickly moves leftward and reaches the other end of the cubic nullcline (point **c**).

(4) The trajectory again moves slowly along the cubic nullcline and reaches point **d**. From there the process of traveling through points **a**, **b**, **c** and **d** repeats itself.

In this cyclic process, the membrane potential oscillates in four phases: a rapid depolarization, a long-lasting plateau, a fast repolarization, and a slow depolarization (Figure 3.1C). This process nicely recapitulates the slow oscillation of the membrane potential in real pacemaking neurons (Figure 3.1B). The pacemaker model suggests that for a cell to express slow oscillations, two conditions are necessary and three conditions are supportive. The necessary conditions are (1) the I-V curve of the cell contains a region of negative resistance, and (2) an intermediate leak current. The supportive conditions are (1) a strong $I_{K(Ca)}$, (2) a strong $I_{Ca(V)}$, and (3) a slow calcium extrusion rate.

Figure 3.1: A model of a pacemaking neuron

A, Phase portrait shows that the modeled neuron starting from a low calcium and low voltage state "**s**" will travel through the state **s'** and enter the cyclic process of repeating the states **a**, **b**, **c**, **d**. The green asterisks demonstrating the trajectory of neuronal states are equally spaced in time. This shows that the trajectory moves faster from **b** to **c**, and from **d** to **a** in the cyclic process. The velocity on the phase plane is indicated by the arrows (blue and red). For visualization, the *u* component of the velocity vector is magnified 200 times. The location of zero velocity in each *u*-*v* direction is indicated by the two nullclines (red). The membrane potential of the modeled neuron oscillates with four distinct phases (**C**), recapitulating the slow oscillations of real spinal neurons (**B**, modified from Wallen and Grillner 1987). Simulations suggest that calcium dependence of potassium current and voltage dependence of calcium current have a strong effect in changing the pacemaker's rhythm (**D** & **E**). Membrane capacitance has a moderate effect (**F**), and calcium extrusion time constant has virtually no effect (**G**) in changing the pacemaker's rhythm.

Figure 3.1

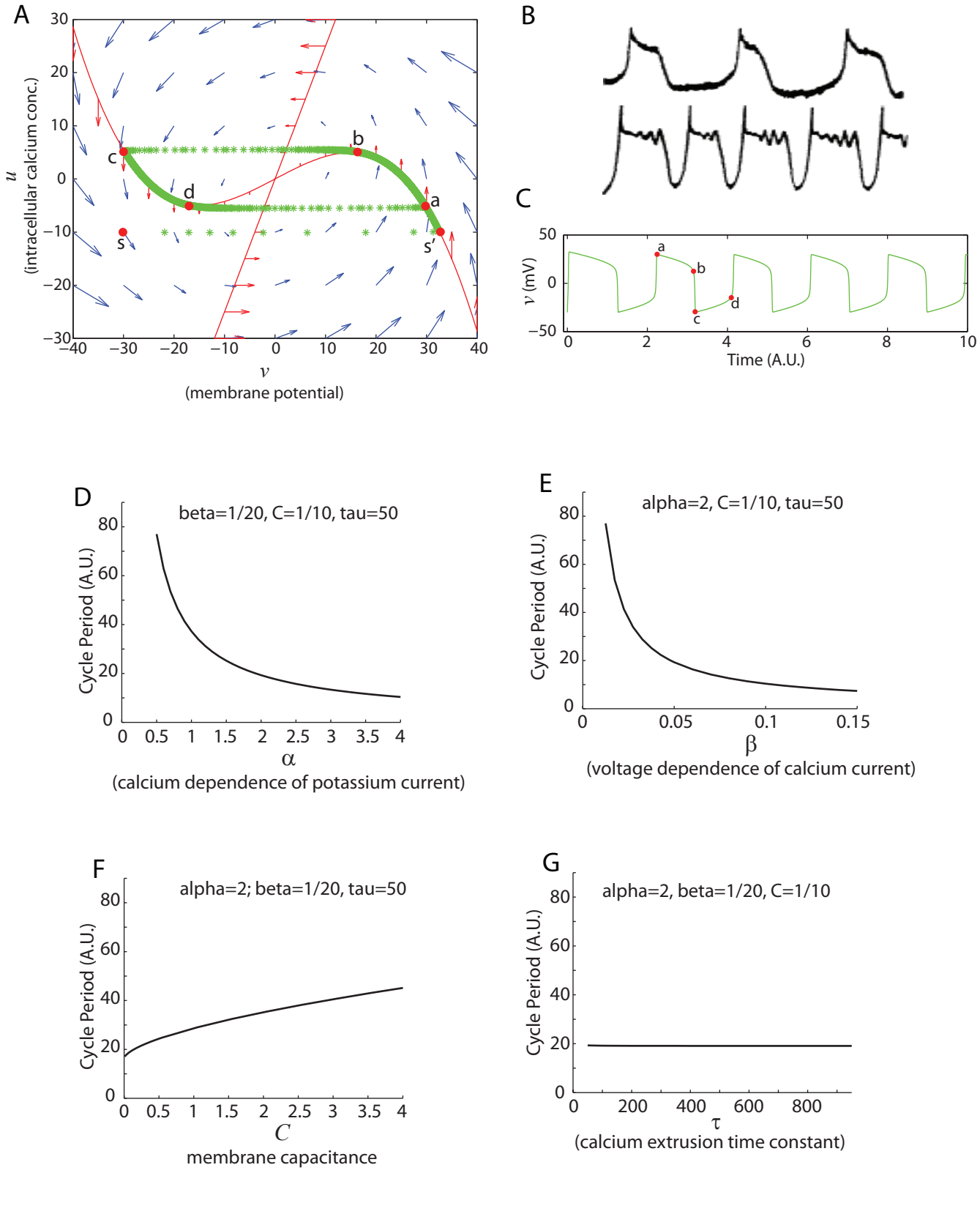
A
B
C
D
E
F
G
u
(intracellular calcium conc.)
v
(membrane potential)
a
b
c
d
s
s'
v (mV)
Time (A.U.)
beta=1/20, C=1/10, tau=50
Cycle Period (A.U.)
α
(calcium dependence of potassium current)
alpha=2, C=1/10, tau=50
β
(voltage dependence of calcium current)
alpha=2; beta=1/20, tau=50
C
membrane capacitance
alpha=2, beta=1/20, C=1/10
τ
(calcium extrusion time constant)

3.3 Modulating the rhythm of the pacemaking neuron

The modeled pacemaking neuron in this study contains five parameters: the membrane capacitance (C), the calcium dependence of $I_{K(Ca)}$ (α), the voltage dependence of $I_{Ca(V)}$ (β), the calcium extrusion time constant (τ), and a leak current (i). As shown in chapter 2, the cycle period of the tail movement during turns in larval zebrafish ranges from 40ms to 75ms. Thus the analysis here focuses on mechanisms that can increase the cycle period by at least two-fold. Simulations show that decreasing the calcium dependence of $I_{K(Ca)}$ (α) and voltage dependence of $I_{Ca(V)}$ (β) supralinearly increase the cycle period of the oscillation; at least a four-fold increase in the cycle period can be generated by modulating these two parameters (Figure 3.1D & 3.1E). On the other hand, increasing the membrane conductance (C) can also increase the cycle period by more than two-fold (Figure 3.1F). However, the calcium extrusion time constant (τ) has a very weak effect on the pacemaker's rhythm (Figure 3.1G). The effects of each parameter in modulating the cycle period and the stiffness of the oscillation are summarized in Table 3.2.

Table 3.2: Effects of model parameters on the pacemaker's oscillation rhythm and stiffness

	Calcium dependence of $I_{K(Ca)}$ (α)	**Voltage dependence of $I_{Ca(V)}$ (β)**	**Calcium extrusion time constant (τ)**	**Membrane capacitance (C)**
To increase cycle period	decrease α	decrease β	decrease τ	increase C
Efficiency in increasing cycle period	high	high	low	Medium
Effect on stiffness	almost no effect	decrease β enhances stiffness	decrease τ reduces stiffness	increase C reduces stiffness
Note: oscillation condition $\beta \cdot \tau > \frac{1}{\alpha}$	Decreasing α may lose oscillation.	Decreasing β may lose oscillation.	Decreasing τ may lose oscillation.	

Among these parameters, the calcium dependence of $I_{K(Ca)}$ (α) is of particular interest. The neurotransmitter serotonin (5-HT) is known to suppress the calcium dependent potassium current by directly decreasing potassium channel conductance[15,16]. In the presence of 5-HT, the reduced potassium current results in a suppressed afterhyperpolarization (AHP) and a prolonged plateau potential in spinal cord neurons. As a result, an isolated spinal cord exhibits a higher spiking frequency, a prolonged burst period, and a longer cycle period in the presence of 5-HT or 5-HT reuptake blockers[14,17,18]. This model mimics the action of 5-HT by using a small α to decrease $I_{K(Ca)}$. In line with experimental findings, this modulation results in a marked increase in the cycle period.

Despite $I_{K(Ca)}$ being an ideal target for modulating the pacemaker's rhythm, it has been shown in lamprey that 5-HT positive spinal projection neurons have no synaptic structures [17,19,20]. It appears that 5-HT is released in a paracrine fashion to adjacent neurons[18]. Thus 5-HT may play a role in regulating the rhythm of spinal networks at a time scale of tens of seconds, but is unlikely to regulate the cycle period during turns, where each cycle lasts tens of milliseconds.

Together, this simple model nicely captures the four phases of membrane potential activity during pacemaker-like oscillation, i.e. a rapid depolarization, a long-lasting plateau, a fast repolarization, and a slow depolarization. It explains the experimental finding that a negative resistance is necessary for the expression of oscillations[13]. Its behavior is also in line with the role of 5-HT in increasing the oscillation period[17,18]. This model, however, cannot explain the experimental finding that a constant depolarizing current reduces the cycle period of rhythmic neurons[21,22]. Nevertheless, as will be shown in Section 3.5, a synaptic excitation modeled by

increasing the conductance of non-selective cation channels is able to decrease the pacemaker's cycle period.

3.4 A model of the spinal network that generates left-right alternations

To examine the putative mechanisms by which descending excitations increase the cycle period of network oscillations during turns, I constructed a single-segment model of the spinal network that consists of one ipsilateral excitatory interneuron (EIN) and one commissural inhibitory interneuron (CIN) on each side of the spinal cord. The model is constructed on the basis that intrinsically rhythmic neurons, or pacemakers, exist on each side of the spinal cord. This assumption is supported by two experimental findings. First, lesion along the midline of the spinal cord spares the rhythmic activity in each hemicord[5], suggesting that commissural innervations are not necessary for establishing spinal oscillations. Second, the existence of pacemaking EINs has been identified in mice, where a subset of EINs that express homeogenes Hb9 shows rhythmic activity in the absence of synaptic inputs. Here the pacemaker constructed in the previous section serves as EINs. The EIN on each side of the spinal cord innervates the ipsilateral CIN, and the CIN in turn inhibits the contralateral EIN (Figure 3.2A). So far there is no evidence suggesting that CINs are intrinsically rhythmic, therefore a linear I-V curve is assigned to the CIN such that the neuron does not oscillate by itself.

Table 3.3: A spinal CPG model containing EINs and CINs

Cell type	*Voltage and calcium dynamics of the cell*	*Note*
Right EIN	$C \cdot \frac{dv_E}{dt} = -\tilde{I}(v_E) - \alpha \cdot u_E - \gamma_{CIN} \cdot v_{C^*}$ $\frac{du_E}{dt} = \frac{-u_E}{\tau} + \beta \cdot v_E$	v_E : voltage of right EIN u_E : intracellular $[Ca^{+2}]$ of right EIN v_C : voltage of right CIN v_{E^*} : voltage of left EIN u_{E^*} : intracellular $[Ca^{+2}]$ of left EIN v_{C^*} : voltage of left CIN $\tilde{I}(v) = \frac{1}{660} \cdot v^3 - v - 9$ (cubic I-V curve) $I(v) = v$ (linear I-V curve) γ_{CIN} : synaptic strength of CIN to contra. EIN γ_{EIN} : synaptic strength of EIN to ipsi. CIN α : calcium dependence of I_K β : voltage dependence of I_{Ca} C : membrane capacitance τ : time constant of calcium extrusion
Right CIN	$C \cdot \frac{dv_C}{dt} = -I(v_C) + \gamma_{EIN} \cdot v_E$	
Left EIN	$C \cdot \frac{dv_{E^*}}{dt} = -\tilde{I}(v_{E^*}) - \alpha \cdot u_{E^*} - \gamma_{CIN} \cdot v_C$ $\frac{du_{E^*}}{dt} = \frac{-u_{E^*}}{\tau} + \beta \cdot v_{E^*}$	
Left CIN	$C \cdot \frac{dv_{C^*}}{dt} = -I(v_{C^*}) + \gamma_{EIN} \cdot v_{E^*}$	

As shown in Figure 3.2B, by providing a bias in the initial condition, the modeled network expresses a pattern of left-right alternation after a short delay. A difference of 0.1mV between the left and right EINs leads to a pattern of left-right alternation after 34% of the cycle period (Figure 3.2B). A larger bias of the membrane potential in the two EINs can further reduce the delay to near 27 % of the cycle period (Figure 3.2D). A large bias in the initial EIN intracellular concentration can further reduce the delay to less than 10% of the cycle period (Figure 3.2C & 3.2D). These observations suggest that a balanced descending motor command may not be advantageous for initiating turns and forward swims, since it may take longer for the spinal network to generate left-right alternations. For instance, this increase in the response delay would prevent larval zebrafish from swimming away from danger.

To further characterize the properties of the network, I examined how network rhythm is affected by the CIN's inhibitory synapses and the EIN's intrinsic rhythm. A previous study showed that a lesion along the midline of the spinal cord resulted in a faster oscillation in each half of the spinal cord[5]. This suggests that commissural innervations slow down the rhythm of each hemicord. Consistent with this idea, an enhanced commissural inhibition mimicked by increasing the CIN's axonal synaptic strength (γ_{CIN}) strongly increases the cycle period of the network's oscillation; more than a five-fold increase in the cycle period is observed by increasing the γ_{CIN} in both CINs (Figure 3.2G). Interestingly, bilateral modulation of γ_{CIN} is necessary for modulating the network's rhythm; changing the γ_{CIN} of one CIN has no effect on the cycle period (Figure 3.2G).

Since pacemaking EINs provide the source of rhythmicity in this modeled CPG network, it makes sense that slowing down the pacemaker's rhythm will increase the network's cycle period. Here I decrease the EIN's rhythm by reducing its calcium dependent potassium current, and find that the network's rhythm is significantly decreased only when both EINs are modulated (Figure 3.2F). While a bilateral modulation of the EINs can generate a 3.5 fold increase in the network's cycle period, unilateral modulation only increases the cycle period by 10%. Together with the ineffectiveness of unilateral modulation of γ_{CIN} in changing network's rhythm, it appears to be a general property that unilateral modulations of spinal networks have a weak effect on network rhythm.

Figure 3.2: A model of the spinal CPG

A, Wiring diagram of the modeled CPG. **B**, An example of membrane potential oscillation in the left and right EINs. When the membrane potential of the left EIN is 0.1 mV higher than the right EIN, the network takes around 1/3 of the cycle period to generate the first left-right alternation (black asterisk). (**C** & **D**) The model suggests that a calcium bias between the two EINs has a strong effect in reducing the delay of expressing left-right alternation. **F**, Pacemaking EIN rhythm can effectively change the CPG's rhythm when both EINs are modulated. Here the EIN's rhythm is slowed down by decreasing its calcium dependence of potassium current. **G**, CIN axonal synaptic strength can change the CPG's rhythm when both CINs are modulated. It appears that the CPG model requires bilateral modulation to effectively modulate the network's rhythm.

Figure 3.2

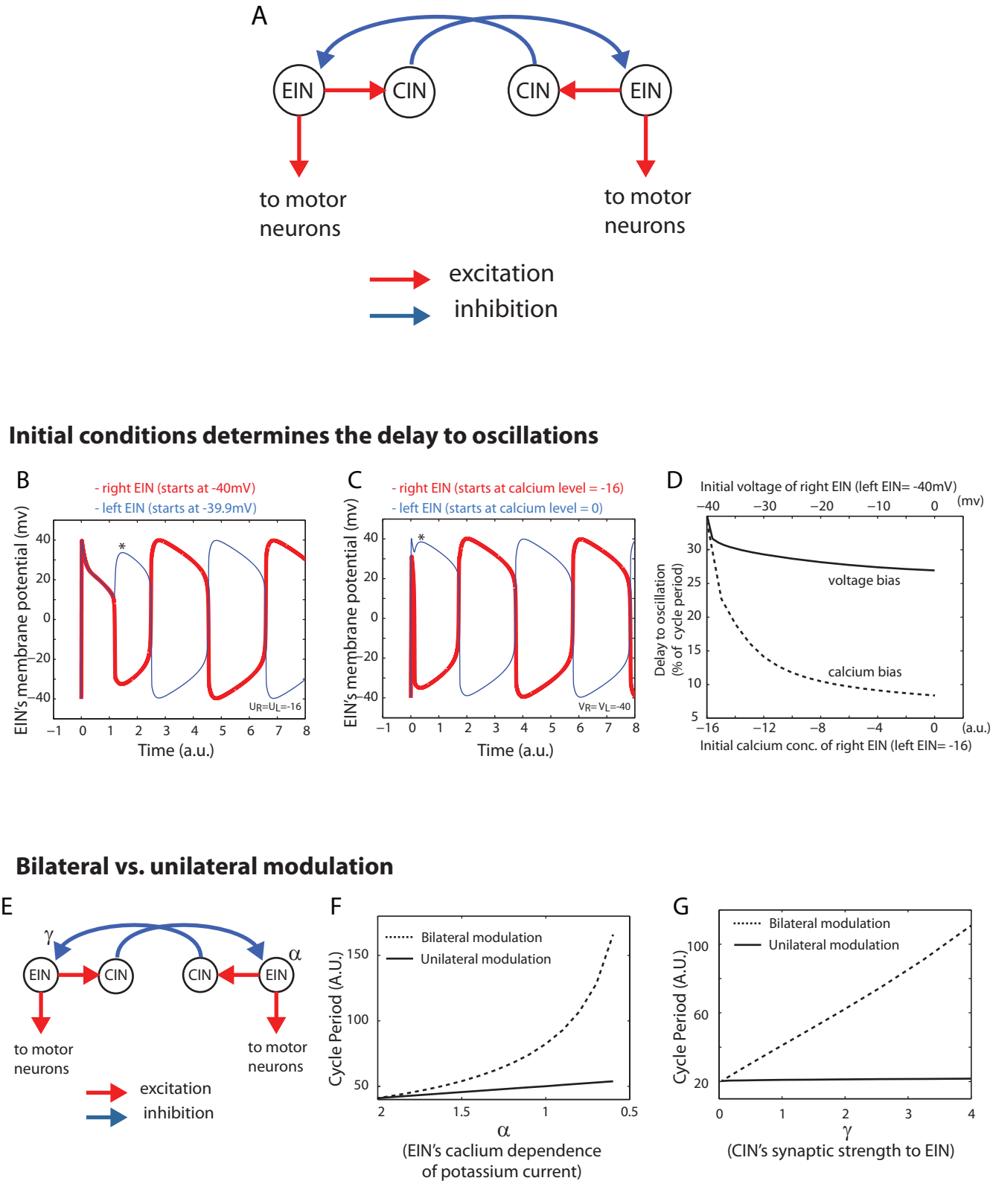
A
EIN
CIN
CIN
EIN
to motor neurons
to motor neurons
excitation
inhibition
Initial conditions determines the delay to oscillations
B
- right EIN (starts at -40mV)
- left EIN (starts at -39.9mV)
EIN's membrane potential (mv)
Time (a.u.)
C
- right EIN (starts at calcium level = -16)
- left EIN (starts at calcium level = 0)
EIN's membrane potential (mv)
Time (a.u.)
D
Initial voltage of right EIN (left EIN= -40mV)
(mv)
voltage bias
calcium bias
Delay to oscillation (% of cycle period)
Initial calcium conc. of right EIN (left EIN= -16)
(a.u.)
Bilateral vs. unilateral modulation
E
γ
α
EIN
CIN
CIN
EIN
to motor neurons
to motor neurons
excitation
inhibition
F
Bilateral modulation
Unilateral modulation
Cycle Period (A.U.)
α
(EIN's caclium dependence of potassium current)
G
Bilateral modulation
Unilateral modulation
Cycle Period (A.U.)
γ
(CIN's synaptic strength to EIN)

3.5 Descending modulation of the spinal network's rhythm

As shown in chapter 2, hindbrain RoV3, MiV1 and MiV2 neurons are necessary for increasing the initial cycle period of tail undulations during turns. What types of spinal neurons do RoV3, MiV1 and MiV2 innervate in order to slow down the undulation? As described in the introduction section, descending innervation to ipsilateral inhibitory LINs or exclusively to motor neurons is unlikely to generate the observed tail undulation properties during turns. A potential mechanism for increasing the network's cycle period is to innervate the commissural inhibitory CINs, either directly by the spinal projection neurons or indirectly through the action of ipsilateral excitatory EINs. Here I examine how descending innervations to EINs and CINs in the spinal CPG model would affect the network's cycle period.

The neurotransmitter types of RoV3, MiV1 and MiV2 have not been characterized conclusively. However in larval zebrafish, RoV3, MiV1 and MiV2 neurons are labeled in the *alx*-GFP transgenic line where only glutamatergic neurons with ipsilateral descending axons are labeled[12]. Thus, these spinal projection neurons are very likely to be glutamatergic. In addition, double patch recordings of MiV1 and motor neurons also show that MiV1 form monosynaptic excitatory synapses onto motor neurons (Koyama et al., unpublished data). To model the unilateral descending excitation provided by the spinal projection neurons, I introduced a synaptic current, $g_{glut} \cdot (v - v_{glut})$, to the ipsilateral EIN or CIN. The parameter g_{glut} is the conductance of glutamate-gated non-selective cation channels, v is the membrane potential of the EIN or CIN, and v_{glut} is the reversal potential of the cation channel, which is set to 0 in this simulation. The descending excitation serves to increase the channel conductance g_{glut}. The voltage dynamic of the EIN and CIN is described by the following equations.

EIN $$C \cdot \frac{dv_E}{dt} = -\tilde{I}(v_E) - \alpha \cdot u_E - \gamma_{CIN} \cdot v_{C^*} - g_{glu} \cdot v_E \quad \text{(Eqn. 4)}$$

CIN $$C \cdot \frac{dv_C}{dt} = -I(v_C) + \gamma_{EIN} \cdot v_E - g_{glu} \cdot v_C \quad \text{(Eqn. 5)}$$

The negative sign of the term $g_{glu} \cdot v$ indicates that as the membrane potential of the cell becomes negative, there is an inward current that provides a positive influence on $\frac{dv}{dt}$.

The effect of the descending excitation on the network's cycle period is shown in Figure 3.3B. Unilateral excitation to an EIN actually results in a decrease in the network's cycle period. The modulation is weak; setting g_{glut} to the maximal value only decreases the cycle period by 10%. A further increase in g_{glut} abolishes the negative resistance characteristic of the pacemaker and results in the loss of oscillations. Bilateral excitation to EINs also decreases the network's cycle period, and the extent of the decrease is larger (26%). On the other hand, unilateral excitation delivered to a CIN results in a marked increase in the cycle period (Figure 3.3 D). The same manipulation of g_{glut} in the CIN can generate a two-fold increase in the cycle period of the network. Finally, consistent with the idea that bilateral modulations of spinal networks is more effective in changing network rhythm than unilateral modulations, a drastic increase in the cycle period can be produced by innervating CINs on both sides of the network (Figure 3.3D).

To explain the two-fold increase in the cycle period of tail movement during turns in larval zebrafish, the simulation study suggests that CINs are the most likely neuronal type to be innervated by hindbrain RoV3, MiV1 and MiV2 neurons. Although not simulated in this study, RoV3, MiV1 and MiV2 neurons should also innervate motor neurons in order to generate the increased tail bend during turns.

Figure 3.3

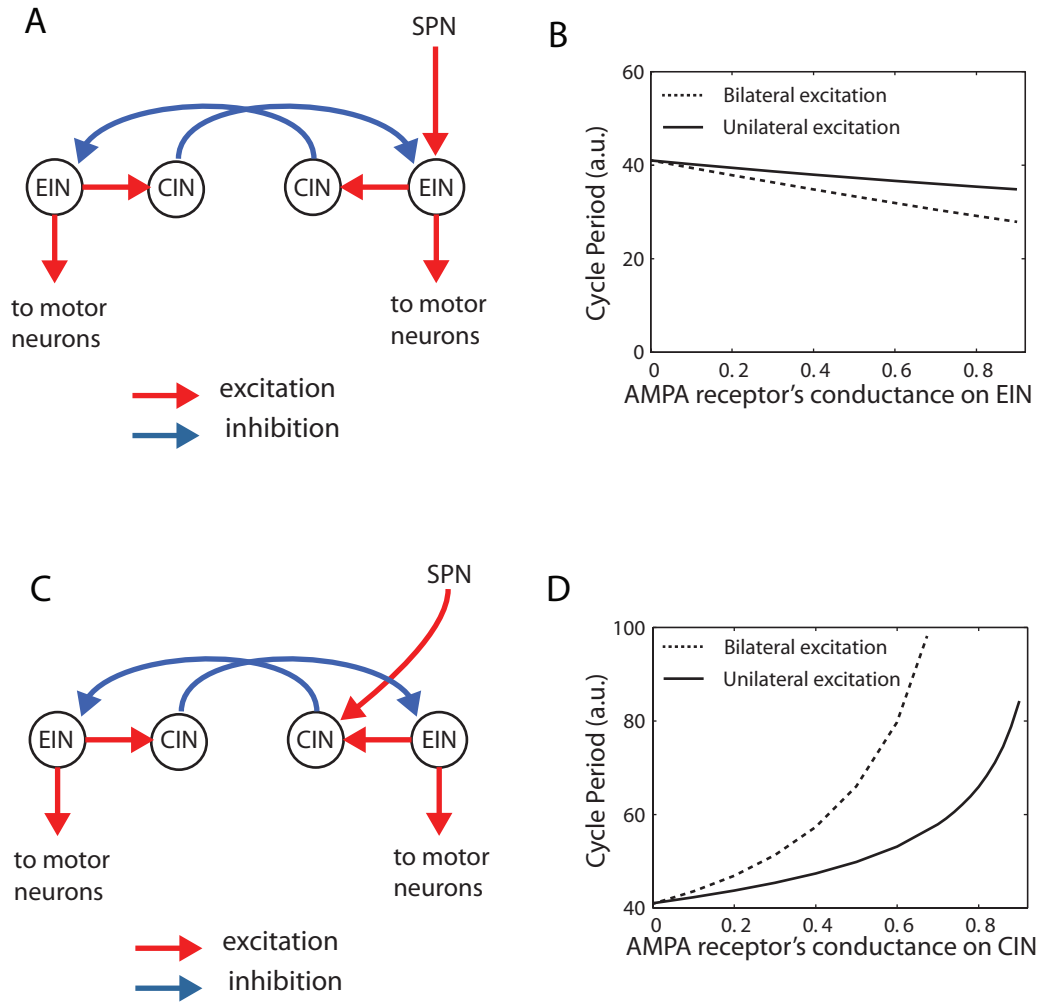

Descending modulation of the CPG's rhythm
Unilateral excitatory descending innervation to an EIN (A) results in a weak decrease in the CPG's cycle period (B). Bilateral excitation to both EINs has a stronger effect in decreasing the CPG's cycle period (B). Unilateral excitatory descending innervation to a CIN (C) can increase the CPG's cycle period more than two-fold (D). Bilateral excitation to both CINs has a drastic effect on increasing the CPG's cycle period.

3.6 Candidate spinal interneurons that mediate turning in larval zebrafish

Commissural inhibitory interneurons in larva zebrafish spinal cord include $CoBL_{gly}$, CoLo, CoLA and $CoSA_{gly}$. Among them, the morphology of $CoBL_{gly}$ is similar to the *Xenopus* tadpole cIN neuron that has been shown to be involved in reciprocal inhibition during locomotion[23–25]. In addition, $CoBL_{gly}$ dendrites are located in the same region as the dendrites of motor neurons; thus, the two groups of neurons may receive similar inputs and respond accordingly. In fact, electrophysiological recordings shows that $CoBL_{gly}$ is rhythmically active during locomotion[26–28], indicating its role in central pattern generation. On the basis of these findings, one potential mechanism by which hindbrain RoV3, MiV1 and MiV2 neurons increase the cycle period of tail movement during turns is to directly innervate $CoBL_{gly}$ interneurons.

CoLo interneurons are not rhythmically active during locomotion. However, they receive electrotonic transmission from hindbrain Mauthner cells and are transiently active during escape turns[29]. The turning behaviors examined in this study, namely phototaxic turns, OMR turns, dark-flash induced turns and spontaneous turns, all share the feature that the cycle period is increased in the first undulation cycle. This transient modulation in the behaviors is consistent with CoLo's response of a brief activation during escape turns. Thus in addition to $CoBL_{gly}$, CoLo is another candidate that could be innervated by RoV3, MiV1 and MiV2 for mediating turning behaviors. The interneurons CoLA and $CoSA_{gly}$ project long ascending axons and may serve mainly as sensory interneurons.

Figure 3.4

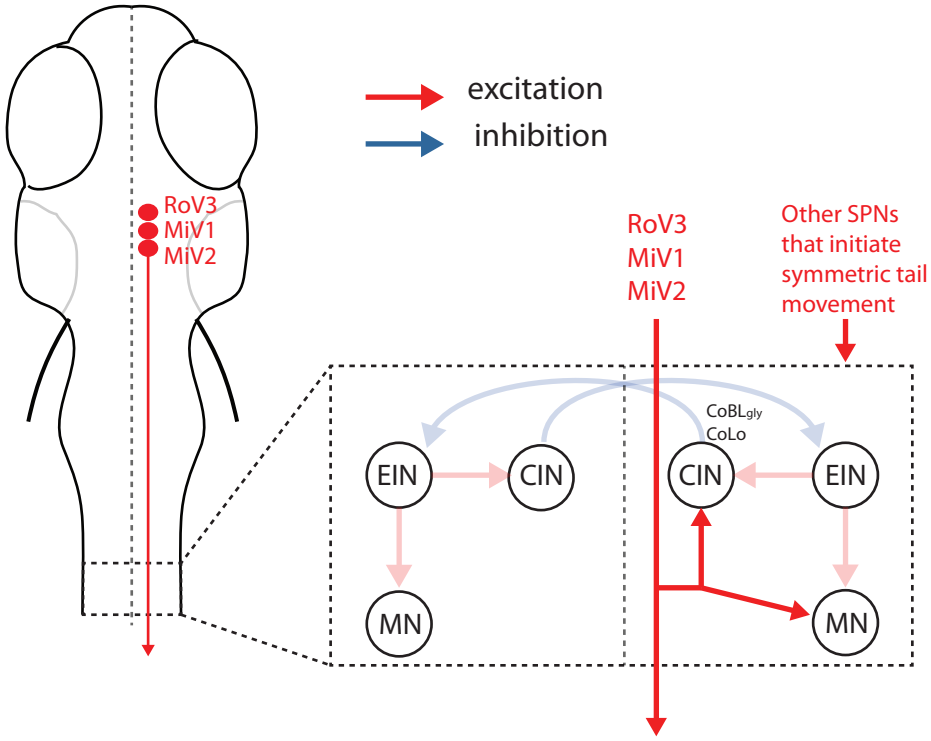

Proposed synaptic targets of RoV3, MiV1 and MiV2 neurons
RoV3, MiV1 and MiV2 neurons provide ipsilateral glutamatergic excitation to the spinal cord. Based on the simulation study in this chapter, they are proposed to innervate commissural inhibitory neurons, most likely $CoBL_{gly}$ and CoLo neurons, to increase the cycle period of tail undulations as well as to inhibit the contralateral spinal network during the prolonged tail bend. In addition, RoV3, MiV1 and MiV2 neurons should innervate motor neurons in order to increase the tail bend angle during turns.

3.7 Discussion

The results from Chapter 2 indicate that the spinal projection neurons, namely RoV3, MiV1 and MiV2, control turns by increasing the tail bend angle and the cycle period during the first undulation of tail movement. In this chapter, I investigated the mechanisms by which spinal projection neurons could increase the cycle period of network oscillations in the spinal cord using a modeling approach. The results show that unilateral innervations of the spinal network are generally unlikely to cause a large change in the cycle period, but unilateral excitation to CINs in the spinal network is sufficient to generate a two-fold increase in the cycle period. This suggests that one of the mechanisms by which RoV3, MiV1 and MiV2 neurons increase the cycle period during turns is to directly innervate CINs in the spinal cord. Specifically, glycinergic commissural spinal interneurons, namely $CoBL_{gly}$ and CoLo, are the most promising synaptic targets of hindbrain RoV3, MiV1 and MiV2 neurons in larval zebrafish. This hypothesis is based on the following observations.

First, an intuitive way to increase the network cycle period is to slow down the intrinsic rhythm of the pacemaker. The spinal CPG model constructed in this chapter differs from the previous models[4,9,10,30] in that it contains a pacemaker on each side of the spinal cord, providing direct access for this type of modulation. I find that by down-regulating the calcium dependence of $I_{K(Ca)}$, the cycle period of an isolated pacemaker can increase by at least four-fold. However, when the pacemaker is integrated into a spinal network, unilateral modulation of the pacemaker's rhythm is ineffective in changing the network's rhythm. For example, a four-fold increase in the pacemaker's intrinsic cycle period only increases the network's cycle period by 20%. In contrast, bilateral modulation of the pacemaker's rhythm is effective in changing the network's rhythm; a

four-fold increase in the cycle period of both pacemakers results in a 3.5-fold increase in the network's cycle period.

Second, consistent with the experimental finding that a surgical lesion of commissural axons in the spinal cord results in a decrease in the cycle period[5], an enhancement of mutual inhibition in this CPG model causes a marked increase in the cycle period. This enhancement of mutual inhibition is simulated either by enhancing the CIN's inhibitory synapses, or by providing descending excitations to enhance CIN's activity. In line with the idea that unilateral manipulation is ineffective in changing the network's rhythm, enhancing the inhibitory synapse of just one CIN in this four-cell model results in virtually no change in the network's cycle period. In this context, it is surprising to find that unilateral excitation to CIN can increase the network's cycle period by at least two-fold. This increase can cover the range of the cycle period, from 40ms to 75ms, observed during turns in larval zebrafish.

$CoBL_{gly}$, CoLo, $CoSA_{gly}$, CoLA are the four types of commissural inhibitory interneurons characterized in larval zebrafish. $CoSA_{gly}$ and CoLA neurons project ascending axons and probably serve as sensory interneurons. $CoBL_{gly}$ is rhythmically active during swims[26–28] and its dendrites overlap with those of motor neurons[31]. For these reasons, $CoBL_{gly}$ may serve as the CIN in the canonical CPG model. On the other hand, CoLo is not rhythmically actively during swims, but has been found to be transiently active during touch-elicited escape turns[29]. It receives eletrotonic inputs from hindbrain Mauthner cells, and is proposed to silence the motor neurons on the contralateral side of the tail during escape turns. Given that CIN is important for slowing down locomotion rhythm, as well as suppressing the motor activity on the contralateral side during turns, it is likely that hindbrain RoV3, MiV1 and MiV2 neurons form synapses to

spinal interneurons $CoBL_{gly}$ and CoLo in order to control the rhythm of tail movement during turns.

Third, as CINs receive direct excitatory inputs from ipsilateral EINs[6], it appears reasonable that unilateral excitation to EIN can indirectly excite CIN and consequently increase the network's cycle period. Nevertheless, I find that both bilateral and unilateral excitation to EINs actually results in a small decrease in the cycle period of network oscillations. This finding is consistent with previous modeling studies using different spinal CPG models[3,30]. In larval zebrafish, a type of ipsilateral excitatory spinal interneuron, namely CiD, has been found to be rhythmically active during locomotion, and is considered an important cell type in the spinal CPG[26–28]. However, the result from this modeling study suggest that hindbrain RoV3, MiV1 and MiV2 neurons are less likely to innervate CiDs in order to increase the cycle period of tail movement during turns.

In summary, this modeling study suggests that one of the mechanisms by which RoV3, MiV1 and MiV2 neurons can increase the cycle period during turns is to innervate CINs in the spinal cord. In larval zebrafish, these CINs could be motor related spinal interneurons $CoBL_{gly}$ and CoLo. In addition to controlling the rhythm of tail movement, RoV3, MiV1 and MiV2 neurons also increase the tail bend during turns. Although not simulated in this modeling study, this is most likely achieved by descending excitation to ipsilateral motor neurons. In agreement with this idea, excitatory synaptic connections between MiV1 neurons and spinal motor neurons have recently been identified (Koyama et al., unpublished data).

A missing component of the abovementioned modeling studies is the role of commissural excitatory interneurons. In walking animals, commissural excitatory interneurons have been

proposed to coordinate the synchronous firing between the flexor and the extensor on the contralateral limbs[32]. In swimming animals such as lamprey and larval zebrafish, the role of commissural excitatory interneurons is unclear. However, evidence shows that a type of commissural excitatory spinal interneuron, namely MCoD, in larval zebrafish is rhythmically active during locomotion, and is necessary for the expression of slow swims[27,28]. The clear involvement of MCoD neurons in the central pattern generation is further supported by a recent finding that hindbrain MiV1 neurons form glutamatergic synapses to MCoD neurons (Koyama et al., unpublished data). As suggested by the modeling study in this thesis, bilateral modulations are much more efficient than unilateral modulations in controlling the cycle period of network oscillation. Thus a potential role of MCoD neurons may be to relay the unilateral descending command from RoV3, MiV1 and MiV2 to the contralateral side of the spinal cord, potentially to the contralateral CINs. In this way, the unilateral descending command from hindbrain RoV3, MiV1 and MiV2 neurons activates ipsilateral motor neurons to increase the tail bend angle, while MCoD neurons mediate bilateral modulation of CINs providing a robust mechanism to slow down the rhythm of network oscillations during turns.

3.8 References

1. Ohta, Y. & Grillner, S. Monosynaptic excitatory amino acid transmission from the posterior rhombencephalic reticular nucleus to spinal neurons involved in the control of locomotion in lamprey. *J. Neurophysiol.* **62**, 1079–1089 (1989).
2. Gosgnach, S. *et al.* V1 spinal neurons regulate the speed of vertebrate locomotor outputs. *Nature* **440**, 215–219 (2006).
3. Kozlov, A. K. *et al.* Mechanisms for lateral turns in lamprey in response to descending unilateral commands: a modeling study. *Biol Cybern* **86**, 1–14 (2002).
4. Hagevik, A. & McClellan, A. D. Coupling of spinal locomotor networks in larval lamprey revealed by receptor blockers for inhibitory amino acids: neurophysiology and computer modeling. *J. Neurophysiol.* **72**, 1810–1829 (1994).
5. Cangiano, L. & Grillner, S. Fast and slow locomotor burst generation in the hemispinal cord of the lamprey. *J. Neurophysiol.* **89**, 2931–2942 (2003).
6. Buchanan, J. T. & Grillner, S. Newly identified 'glutamate interneurons' and their role in locomotion in the lamprey spinal cord. *Science* **236**, 312–314 (1987).
7. Hill, S. A., Liu, X. P., Borla, M. A., Jose, J. V. & O'Malley, D. M. Neurokinematic modeling of complex swimming patterns of the larval zebrafish. *Neurocomputing* **65-66**, 61–68 (2005).
8. Knudsen, D. P., Arsenault, J. T., Hill, S. A., O'Malley, D. M. & Jose, J. V. Locomotor network modeling based on identified zebrafish neurons. *Neurocomputing* **69**, 1169–1174 (2006).
9. Ekeberg, O. *et al.* A computer based model for realistic simulations of neural networks. I. The single neuron and synaptic interaction. *Biol Cybern* **65**, 81–90 (1991).

10. Brodin, L. *et al.* Computer simulations of N-methyl-D-aspartate receptor-induced membrane properties in a neuron model. *J. Neurophysiol.* **66**, 473–484 (1991).
11. Wilson, J. M., Cowan, A. I. & Brownstone, R. M. Heterogeneous electrotonic coupling and synchronization of rhythmic bursting activity in mouse Hb9 interneurons. *J. Neurophysiol.* **98**, 2370–2381 (2007).
12. Kimura, Y., Okamura, Y. & Higashijima, S. alx, a zebrafish homolog of Chx10, marks ipsilateral descending excitatory interneurons that participate in the regulation of spinal locomotor circuits. *J. Neurosci.* **26**, 5684–5697 (2006).
13. Wilson, W. A. & Wachtel, H. Negative resistance characteristic essential for the maintenance of slow oscillations in bursting neurons. *Science* **186**, 932–934 (1974).
14. el Manira, A., Tegnér, J. & Grillner, S. Calcium-dependent potassium channels play a critical role for burst termination in the locomotor network in lamprey. *J. Neurophysiol.* **72**, 1852–1861 (1994).
15. Wallén, P. *et al.* Effects of 5-hydroxytryptamine on the afterhyperpolarization, spike frequency regulation, and oscillatory membrane properties in lamprey spinal cord neurons. *J. Neurophysiol.* **61**, 759–768 (1989).
16. Wallén, P. *et al.* Mechanisms underlying the serotonergic modulation of the spinal circuitry for locomotion in lamprey. *Prog. Brain Res.* **80**, 321–327; discussion 315–319 (1989).
17. Harris-Warrick, R. M. & Cohen, A. H. Serotonin modulates the central pattern generator for locomotion in the isolated lamprey spinal cord. *J. Exp. Biol.* **116**, 27–46 (1985).
18. Christenson, J., Franck, J. & Grillner, S. Increase in endogenous 5-hydroxytryptamine levels modulates the central network underlying locomotion in the lamprey spinal cord. *Neurosci. Lett.* **100**, 188–192 (1989).

19. Van Dongen, P. A. *et al.* Immunohistochemical demonstration of some putative neurotransmitters in the lamprey spinal cord and spinal ganglia: 5-hydroxytryptamine-, tachykinin-, and neuropeptide-Y-immunoreactive neurons and fibers. *J. Comp. Neurol.* **234**, 501–522 (1985).
20. Brodin, L., Buchanan, J. T., Hökfelt, T., Grillner, S. & Verhofstad, A. A. A spinal projection of 5-hydroxytryptamine neurons in the lamprey brainstem; evidence from combined retrograde tracing and immunohistochemistry. *Neurosci. Lett.* **67**, 53–57 (1986).
21. Wallén, P. & Grillner, S. The effect of current passage on N-methyl-D-aspartate-induced, tetrodotoxin-resistant membrane potential oscillations in lamprey neurons active during locomotion. *Neurosci. Lett.* **56**, 87–93 (1985).
22. Wallén, P. & Grillner, S. N-methyl-D-aspartate receptor-induced, inherent oscillatory activity in neurons active during fictive locomotion in the lamprey. *J. Neurosci.* **7**, 2745–2755 (1987).
23. Roberts, A. & Clarke, J. D. The neuroanatomy of an amphibian embryo spinal cord. *Philos. Trans. R. Soc. Lond., B, Biol. Sci.* **296**, 195–212 (1982).
24. Dale, N., Ottersen, O. P., Roberts, A. & Storm-Mathisen, J. Inhibitory neurones of a motor pattern generator in Xenopus revealed by antibodies to glycine. *Nature* **324**, 255–257 (1986).
25. Yoshida, M., Roberts, A. & Soffe, S. R. Axon projections of reciprocal inhibitory interneurons in the spinal cord of young Xenopus tadpoles and implications for the pattern of inhibition during swimming and struggling. *J. Comp. Neurol.* **400**, 504–518 (1998).
26. Liao, J. C. & Fetcho, J. R. Shared versus specialized glycinergic spinal interneurons in axial motor circuits of larval zebrafish. *J. Neurosci.* **28**, 12982–12992 (2008).

27. McLean, D. L., Fan, J., Higashijima, S., Hale, M. E. & Fetcho, J. R. A topographic map of recruitment in spinal cord. *Nature* **446**, 71–75 (2007).

28. McLean, D. L., Masino, M. A., Koh, I. Y. Y., Lindquist, W. B. & Fetcho, J. R. Continuous shifts in the active set of spinal interneurons during changes in locomotor speed. *Nat. Neurosci.* **11**, 1419–1429 (2008).

29. Satou, C. *et al.* Functional role of a specialized class of spinal commissural inhibitory neurons during fast escapes in zebrafish. *J. Neurosci.* **29**, 6780–6793 (2009).

30. Buchanan, J. T. Neural network simulations of coupled locomotor oscillators in the lamprey spinal cord. *Biol Cybern* **66**, 367–374 (1992).

31. Higashijima, S.-I., Schaefer, M. & Fetcho, J. R. Neurotransmitter properties of spinal interneurons in embryonic and larval zebrafish. *J. Comp. Neurol.* **480**, 19–37 (2004).

32. Juvin, L., Simmers, J. & Morin, D. Propriospinal circuitry underlying interlimb coordination in mammalian quadrupedal locomotion. *J. Neurosci.* **25**, 6025–6035 (2005).

CHAPTER4

Ontogeny of Classical and Operant Learning Behaviors in Zebrafish

4.1 INTRODUCTION

The ability to associate two environmental cues, as in classical conditioning, or correlate one's behavior with its consequences, as in operant conditioning, are processes often essential for an animal's survival[1]. While there are studies that have followed the ontogeny of learning behaviors in animal model systems of classical conditioning paradigms[2–5], the ontogeny of operant learning, in particular, remains much less explored.

The ability for classical conditioning is pervasive across the animal kingdom and often interpreted as the most basic and robust form of associative learning, however, it has been shown that adding an operant component to a learning task may increase performance or show it where it was not present before[6,7].

Zebrafish is an exceptional model of vertebrate neural development and amenable both to forward genetics and genetic manipulation[8]. The transparent larvae are uniquely suited to functional imaging and have recently served to uncover fundamental mechanisms in fish locomotor control[9,10]. Behavior is the ultimate functional readout of neural activity, indeed behavior is the ultimate evolutionary reason for the existence of brains, the changes in behavior during development should reflect the changes the nervous system undergoes as the larval organism develops into the adult. While there are well-established learning paradigms for *Drosophila* and rodent experimental models, zebrafish still lacks a systematic learning characterization. We describe here an approach to implement and test such learning assay that utilizes the fact that zebrafish can see and track visual stimuli and clearly perform visually-

evoked locomotor behaviors as early as 5 days post fertilization (dpf)[11,12]. To that end we use visually-guided stimuli combined with a noxious electroshock to control learning behaviors. We characterize these assays and specifically obtain a full ontogeny of operant learning from 7 day old larvae to adult. This ontogeny will thus not only provide a full developmental picture of operant learning in a model vertebrate in itself but also provide a full functional correlate to the well described development of the nervous system in zebrafish. Moreover, it will determine how early zebrafish start to be able to not just integrate and respond to visual stimuli, but significantly change their behavior as a response to visual learning.

4.2 Classical and Operant Conditioning in Adult Zebrafish

To evaluate associative learning in zebrafish we set out to test two forms of learning robustly present in vertebrates, classical and operant conditioning. We developed tests that can easily be adapted and closely compared at different developmental stages from 7 dpf larvae, to complete adult maturation at 8 weeks. The general layout of our learning arena is described in Figure 4.1A and 4.1B. Fish swim freely in a tank cued with distinct patterns that demarcate the two halves of the arena. They are monitored continuously with a video tracking system, which registers their position online at all times.

During classical conditioning (Figure 4.1C) fish learn to associate an unconditioned stimulus (US), a small whole tank electroshock, with a visual pattern that is presented beneath the tank, the conditioned stimulus (CS). The US is preceded and overlapped with the CS as illustrated and delivered in nine consecutive pairings at 0.1 Hz (Figure 4.1C, pink region). This assay could also be interpreted as a form of differential classical conditioning in which one visual stimulus (the CS+ represented in Figure 4.1A, 4.1B and 4.1C as a prominent checkered

board) is paired with the US and another one is not (the CS-, in this case the grey panel as in Figure 4.1C)[13]. The animals can be trained as easily to either of the stimuli. Remarkably, 2 hours after a successful training session against the checkerboard the same animal could be quickly conditioned against the grey stimulus as illustrated in supplementary movies 1 and 2.

In operant conditioning (Figure 4.1D), during the 30 minutes of training, a small shock is paired with the presence of the freely moving animal in one of two visually defined halves of the tank. The distinct difference with respect to the classical conditioning assay is that here it is an aspect of the animals' own locomotor behavior, its position along the visual cues, that determines the presence of the CS and US. Training was followed by a 30 minute dark period, in which fish are deprived of all visual cues.

Both forms of learning are tested by monitoring the behavior of fish in the presence of the paired and unpaired (conditioned and neutral) visual cues (fig.1C and 1D, second half). The spatial preference of the fish is analyzed either based on their recorded position or on the number of times fish turn away from the conditioned cues. In the data shown in figure 1D and1F fish were conditioned against red. They can be equally conditioned against the white stimulus. Both positional and turning analyses clearly show that adult fish can learn these tasks extremely well (Figure 4.1E and 4.1F), avoiding to swim in the areas paired with the noxious stimuli with performance indexes (PIs) close to +1.

If visuo-spatial stimuli are reversed during testing the animals' preferred position reverses accordingly. In Figure 4.1C and 4.1D the vertical lines at 33.5min and 90min respectively indicate the time point at which the visual cues are reversed (symbolic icons above the panel).

Figure 4.1: Classical and operant conditioning in adult zebrafish.

(**A**) Experimental setup. The visual conditioned stimulus is presented on a LCD screen beneath an infrared lit fish tank. The unconditioned stimulus consists of an electric shock across the arena. (**B**) Left panel: a view of the arena from above without an infrared filter. Right panel: online analysis of fish location. (**C**) A typical example trace from a classical conditioning experiment showing the basic training protocol. Upper panel: experiments start with a baseline period (0 – 30 min), followed by a training period (30 – 31.5 min) and end with a test period (31.5 – 64 min). The visual cues presented at each of these stages are symbolized on top of the trace. Each black circle represents the animal's location recorded at 1 frame/sec. The curly bracket indicates the time window used for analyzing conditioned behavior. Lower panel: magnified trace around the training period. Two visual cues are displayed alternatively but only one is associated with electric shocks (red ellipses). The trained fish changes position when the visual cues are switched (31.5 – 36.5 min). (**D**) A typical example trace from an operant conditioning experiment. The assay starts with a baseline period (0 – 30 min), is followed by a training period (30 – 60 min), then a dark period (60 – 90 min) and ends with a test period (90 – 120 min). The electric shocks applied during training are indicated by red ellipses. The conditioned response disappears immediately after visible light is removed in the dark period, but reappeared after the visual cues are presented in the test period (see Figure 4.5). (**E**) Adult zebrafish show a significant learning response after classical conditioning as analyzed both by the animal's position or it's turning behavior. The results of the two analyses are similar. In the turning analysis, each circle represents the performance index (PI) of a fish and the area of the circle represents the turning numbers within the analysis window. This allows visualizing and taking into account animals that show little movement and thereby perform fewer turns. In the

plot animals represented by a smaller dot performed fewer turns in the tank. The size of the dots gives us a strong degree of confidence in the data. Animals were trained against either grey or checkerboard with comparable learning indices and data are pooled in the figure. (**F**) Adult zebrafish show a significant learning response after operant conditioning; analysis as in E.

Figure 4.1

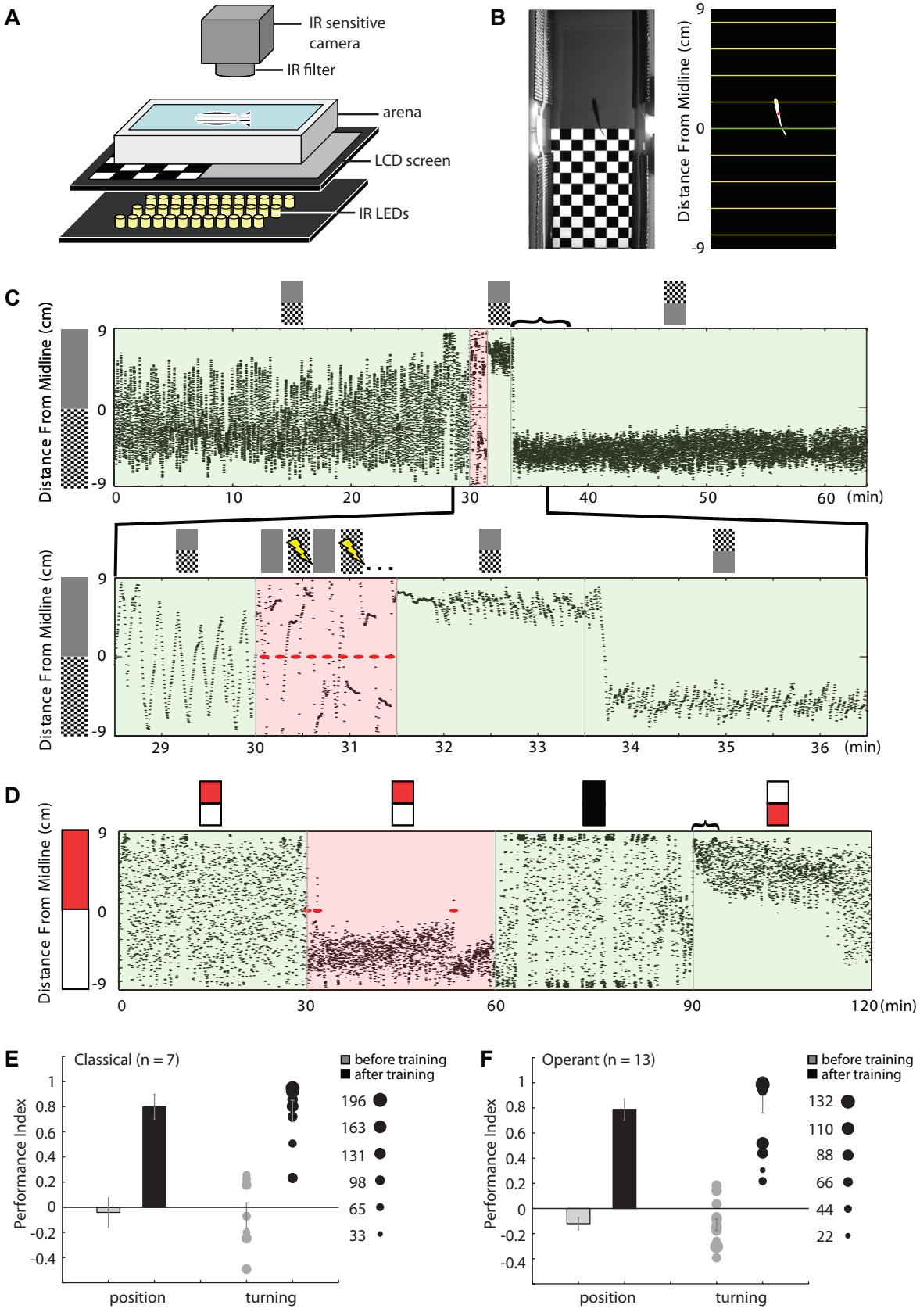
A
IR sensitive camera
IR filter
arena
LCD screen
IR LEDs
B
Distance From Midline (cm)
9
0
-9
C
Distance From Midline (cm)
0
10
20
30
40
50
60 (min)
29
30
31
32
33
34
35
36 (min)
D
0
30
60
90
120 (min)
E
Classical (n = 7)
before training
after training
Performance Index
position
turning
196
163
131
98
65
33
F
Operant (n = 13)
132
110
88
66
44
22

4.3 Ontogeny of Learning in the Classical Conditioning Assay

To assess when zebrafish first start expressing learning behaviors, we continuously tested the same group of fish in our classical conditioning assay from larval to adult stages (see Figure 4.2A through 4.2C). Tank and visual stimulus size was scaled to fish stage in order to provide similar learning conditions to all animals. Figure 4.2D depicts the performance index of an individual group of fish that underwent classical conditioning for 5 consecutive days every week, over a period of more than six weeks.

The freely swimming group of fish was briefly exposed to a visual pattern paired to precede and overlap with a whole-tank electroshock for nine consecutive pairings at 0.1 Hz (Figure 4.1C, pink region). Figure 4.2D shows the performance index of the animals after training as they mature to adults. It is apparent that fish start learning significantly at week 4 and reach close to the maximum PI by week 6. As seen in figure 1, this is maintained in older adults. While the data gathered with this assay are striking and informative there are several caveats with this experiment. Firstly, fish are trained in groups, which may lead to interference effects between animals. Secondly, the repeated training sessions, which have been chosen for maximum impact, also contain inherently repeated extinction trials, which make the results harder to interpret. These compromising factors might serve as an explanation why fish apparently start learning only at an age greater than 25 days. Finally, as mentioned in the introduction, adding an operant component is known to increase the performance and the experiment shown here relies mostly on a classical assay. Therefore we subsequently tested individual animals in an operant assay to investigate the ontogeny of learning.

Figure 4.2

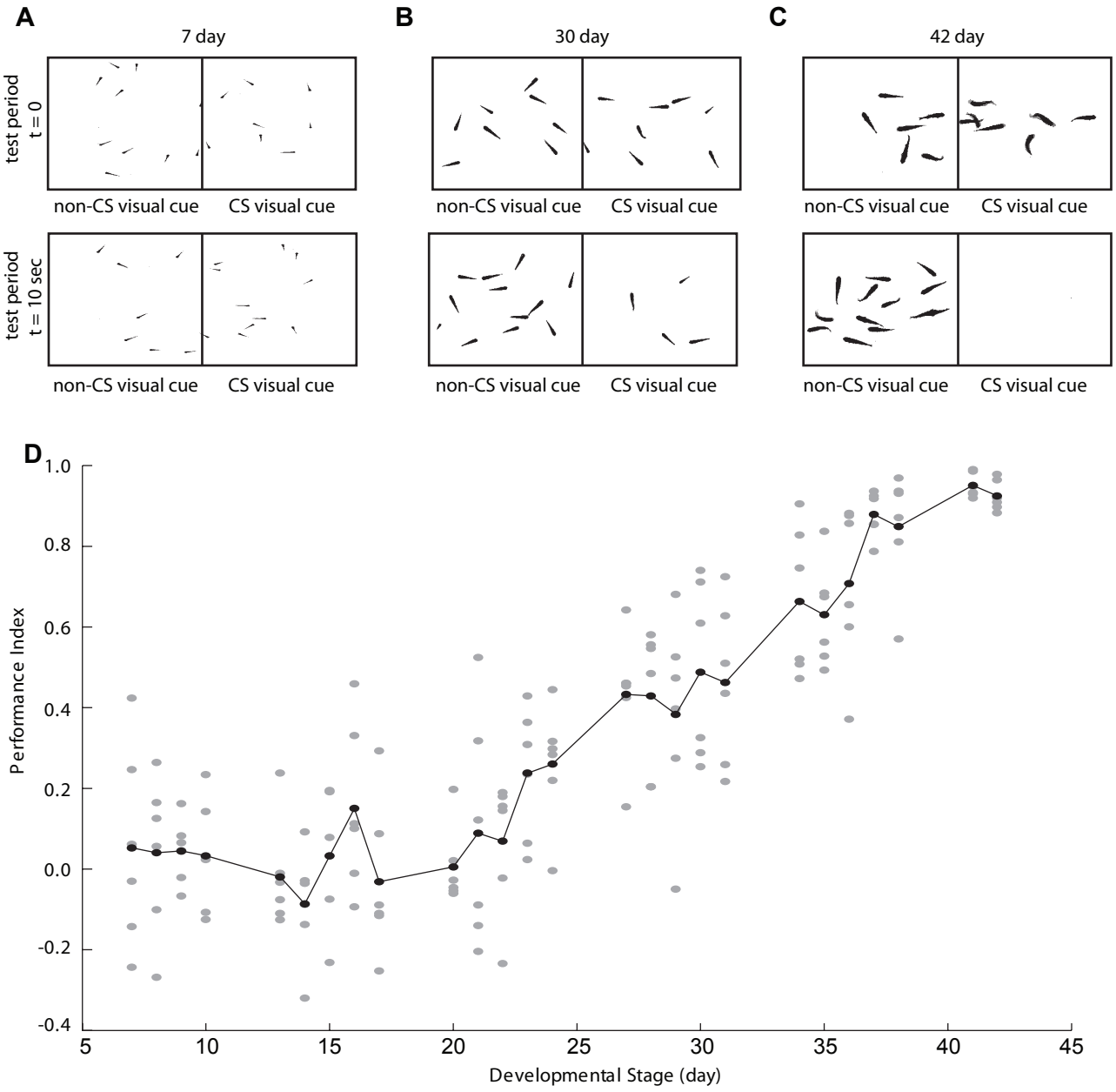

Ontogeny of learning in the classical conditioning assay.
(A - C) Typical example responses of 7-, 30- and 42-day old fish to the presence of visual CS. As fish mature, they progressively show a clear response, distributing themselves to avoid the CS during testing. (D) In our classical conditioning assay, learning is significant at week 4 and reaches adult performance level at week 6. The animals are trained and tested 6 times per day and their performance is quantified based on their position in the arena.

4.4 Ontogeny of Learning in the Operant Conditioning Assay

We analyzed operant conditioning over the course of development assaying different individual fish, each taken naively at different stages, from larva to adult. We observed that the capacity to learn, in this assay, begins at week 3 and reaches the maximum PI of +1 for almost all individuals tested by week 6, which is maintained in adult performance (Figure 4.3D). Even though we established a common training period of 30 minutes, it is evident that the number of shocks fish expose themselves to decrease as they develop, that is, they take progressively fewer shocks to learn to avoid the paired stimulus (Figure 4.3E). Even between weeks 7 and 8 when their performance level appears indistinguishable, there is a significant decrease in the number of shocks fish expose themselves to during training. This number decreases to less than half, from an average of 19 to 7 shocks (t test, $p=0.0272$) per training session.

There is substantial individual variability in results before week 3, indicating that some larvae could be able to perform these tasks. Although there is a progressive decrease in the number of shocks individuals expose themselves to, the decrease only becomes significant between week 2 and 3 when the performance index also becomes significantly higher (t-test, $p=0.0492$).

Figure 4.3: Ontogeny of learning in the operant conditioning assay.

(**A - C**) example traces of operant conditioning assay at different developmental stages. The baseline period (0 – 30 min) is followed by a training period (30 – 60 min) and ended with a test period (60 – 120 min). The visual cues are indicated on the left and maintained throughout the experiments. Striped visual cues are used for fish younger than 4 weeks to increase their chance of encountering the borderlines. The red dots indicate the shock events in the training period. The curly bracket indicates the time window for analysis. (**D**) Upper panel, conditioned behavior at different developmental stages. Each circle represents the performance index (PI) of a fish. The area of the circle is proportional to the turning events during the analysis window. Arrows indicate the PI of the fish demonstrated in (**A - C**). A consistent learning behavior in zebrafish emerges in week 3 and reaches adult performance during the juvenile stage and specifically week 6. The animals are trained and tested individually, and naive animals are used at each developmental stage. Lower panel, zebrafish show no innate preference for the visual stimuli at all developmental stages. (**E**) Number of shocks received during the training period (30-60 minutes) at each developmental stage assayed. The number of shocks decreases throughout development, even after week 4 when the PI is already close to 1. The number of shocks fish expose themselves to shows significant decrease between weeks 2 to 3, 4 to 5 and 7 to 8 (t-test, $p=0.0492$; $p=0.0004$ and $p=0.0272$, respectively).

Figure 4.3

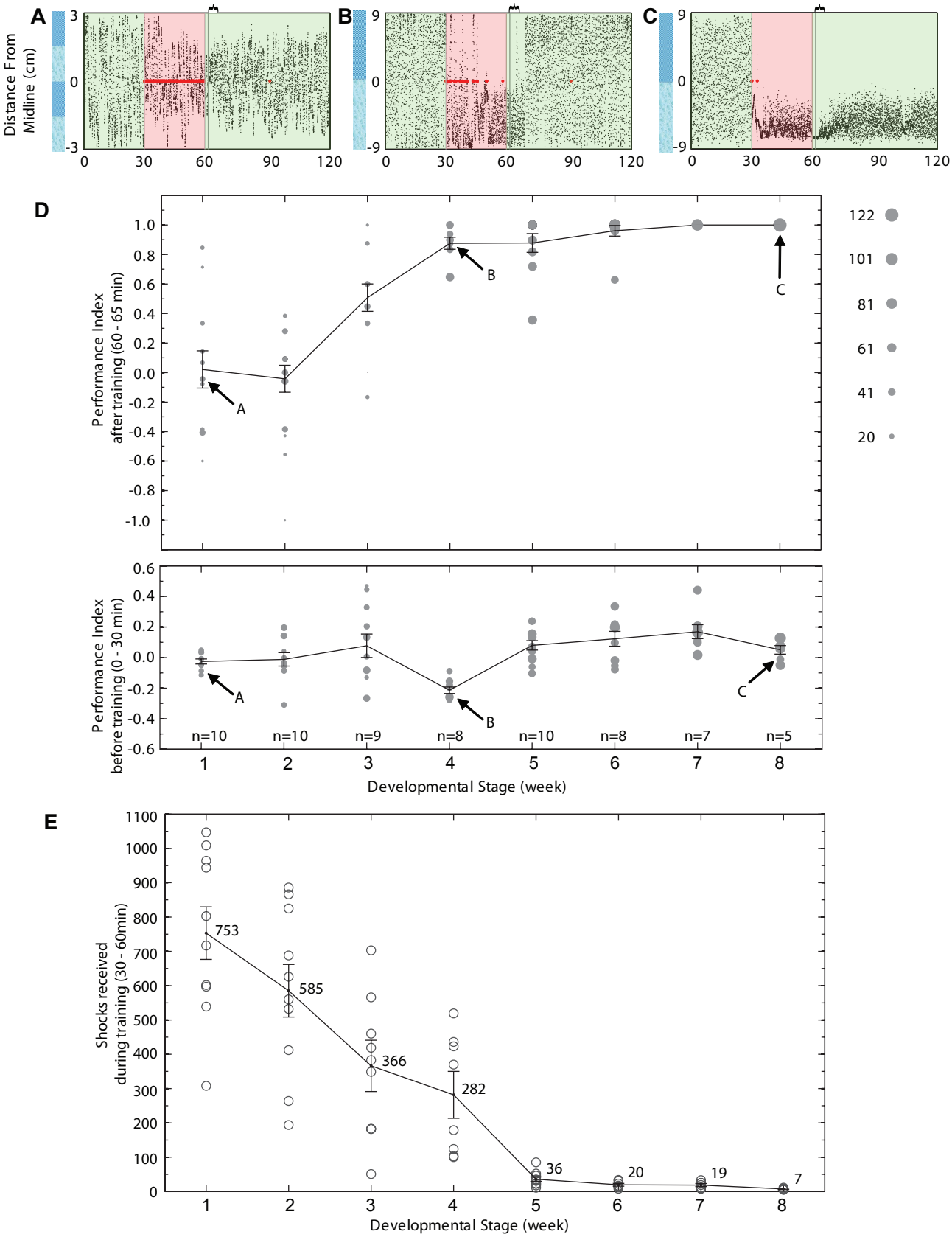
A
B
C
Distance From Midline (cm)
3
0
-3
9
0
-9
0
30
60
90
120
D
Performance Index after training (60 - 65 min)
1.0
0.8
0.6
0.4
0.2
0.0
-0.2
-0.4
-0.6
-0.8
-1.0
A
B
C
122
101
81
61
41
20
Performance Index before training (0 - 30 min)
0.6
0.4
0.2
0.0
-0.2
-0.4
-0.6
n=10
n=10
n=9
n=8
n=10
n=8
n=7
n=5
1
2
3
4
5
6
7
8
Developmental Stage (week)
E
Shocks received during training (30 - 60min)
1100
1000
900
800
700
600
500
400
300
200
100
0
753
585
366
282
36
20
19
7
Developmental Stage (week)

4.5 Persistence of Memory in Behavior of Adult Zebrafish

To assess the persistence of the learned behavior in adults we tested for the presence of conditioned behavior in response to the visual cues after an increasing length of time in the absence of visual stimuli after operant training.

Visual stimuli with reversed orientation were introduced after a period of no light in the tank to assure that the conditioned behavior is based on the presented visual stimuli, rather than other non-visual or distal visual cues (Figure 4.4A, example trace at 90 min). We found that the conditioned response disappears immediately after the removal of light, indicating that the behavior was purely visually-mediated (figs. 1D and 4A, 60-90 min, dark icon).

To test for the permanence of the memory in behavior, the length of the period with no light was gradually increased before reintroduction of the visual cues. Figure 4B plots the performance index observed for increasing periods in the absence of light. Figure 4A serves as an example typical raw trace where the positional distribution of the animal after the reintroduction of the stimulus is clearly biased towards the unpaired visual stimulus in spite of the reversal of orientation of the stimuli presented (Figure 4.4A, t>90 min).

In this assay the memory is shown to control the fish's behavior, showing a PI significantly different from zero, for at least 6 hours (Figure 4.4B). By 12 hours fish have on average apparently lost the conditioned behavior (although high variability is seen here).

The apparent decrease in average PI to zero observed after 12 h in the absence of light (figure 4B) could mean that most animals have by this time positively lost the memory conditioned, that they are less responsive to stimulus reintroduction as this comes during the night time of their light-dark cycle or, alternatively, that this memory is still represented in the nervous system though no longer dominating the animals behavior in response to the conditioned

visual stimulus. In order to test for the ability to effectively recall this memory we provided a shock 30 minutes after testing (red dot at 120 min in figure 4A). It is clear that in most animals a brief electric shock can reinstate the behavior even after a 12-hour lag. We performed an additional experiment with 24hrs in the absence of light to test whether reintroduction of the visual cues during the Dark phase of their cycle could be showing an effect of sleep in the 12h time point and observed a similar result, the animals do not show significant conditioned behavior. However after a reinstatement shock, 4 of the 8 individuals tested show a learning performance index, indicating that even if there is high variability the memory may still be present in many individuals after this time.

Figure 4.4: Persistence of memory in adult zebrafish.

Persistence of conditioned response after an increasing length of dark period. Fish are trained and tested individually and a new fish is used in each condition. Turning performance analysis calculated unless otherwise indicated. (**A**) An example trace of an operant conditioning experiment involving a 30-min dark period (60 – 90 min) between the training (30 - 60) and test period (90 – 120 min). Each dot represents the animal's location in the arena. The red ellipse in the training period represents the shock event. This animal expresses a robust conditioned response 30 minutes after learning. (**B**) *Left panel*, Naïve adult zebrafish show no innate preference to the visual stimuli. *Middle panel*, the conditioned response is largely intact 30 minutes after learning and gradually decreases until a residual response at 6 hr after training. *Right panel,* Seven fish serve as a yoke experiment receiving the electroshocks applied to the paired training group (2-min dark period) These shocks were uncorrelated to the fishes' own location and the animals show no significant learning behavior. (**C**) A whole tank electric shock leads to re-expression of conditioned memory in behavior. After thirty minutes of test in the presence of visual cues after different lengths of time in the dark (90-120 min as example in fig. 4A) fish are given a single electroshock in the middle of a 20 sec period with light removed (to hinder direct association with visual stimuli). Fish that had apparently lost the expression of memory from behavior after 12 hours in the absence of light show a recovered performance index.

Figure 4.4

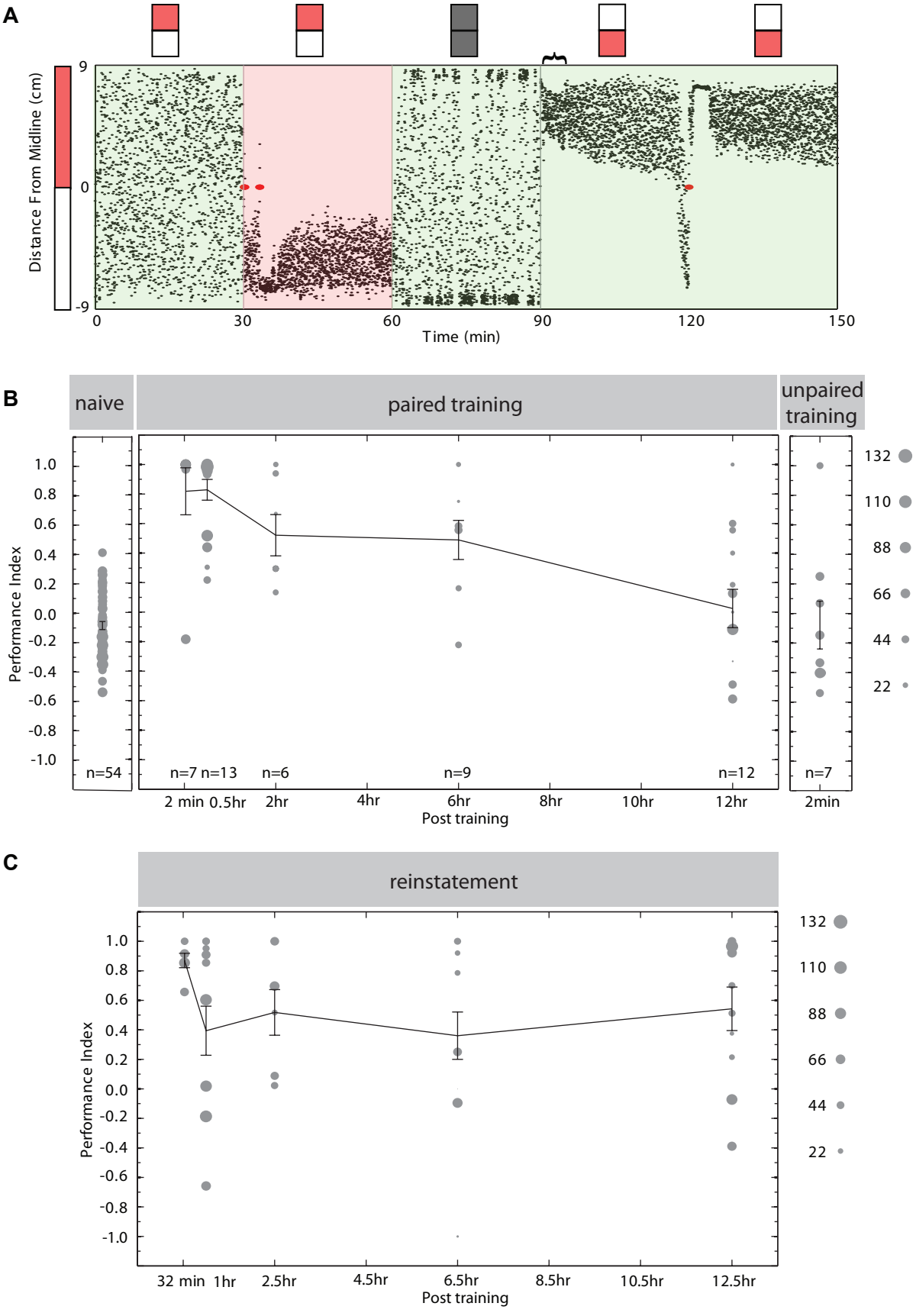
A
Distance From Midline (cm)
9
0
-9
0
30
60
90
120
150
Time (min)
B
naive
paired training
unpaired training
Performance Index
1.0
0.8
0.6
0.4
0.2
0.0
-0.2
-0.4
-0.6
-0.8
-1.0
n=54
n=7 n=13
n=6
n=9
n=12
n=7
2 min 0.5hr
2hr
4hr
6hr
8hr
10hr
12hr
2min
Post training
132
110
88
66
44
22
C
reinstatement
Performance Index
32 min
1hr
2.5hr
4.5hr
6.5hr
8.5hr
10.5hr
12.5hr
Post training

4.6 Vision is the Sensory Modality Governing the Expression of the Learned Behavior

The learned spatial avoidance is expressed solely in the presence of visual cues and disappears completely when these are removed (Figure 4.5A). Locomotion is maintained or increased in the absence of visual cues and thus a decrease in PI is not confounded by fish ceasing activity (Figure 4.5B). Particularly, when the visual cues are reintroduced to fish kept in the dark, animals almost immediately return to their learned performance (Figure 4.5C) while maintaining their average locomotor activity in the tank (Figure 4.5D). The presence of other sensory modalities such as audition and lateral line sensing thus do not contribute or are insufficient for the expression of the learned behavior.

Figure 4.5

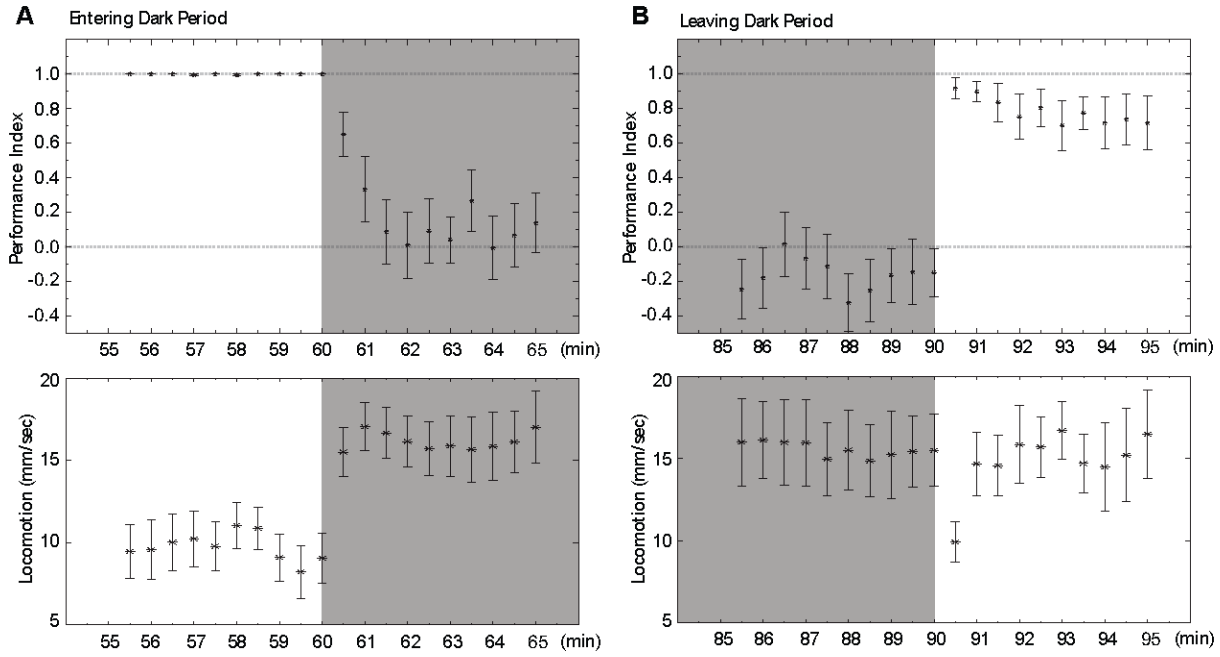

Figure 4.5: Vision is the sensory modality governing the expression of the learned behavior. (**A**) Performance index of fish 5 minutes before and after removal of light. Animals used in operant conditioning experiment in fig. 1F. When the dark period is instated fish quickly redistribute their movement to the whole tank as can be seen by the decrease in the performance index. (**B**) Locomotion of fish during the same period registered in A. At the end of the training period animals are moving constantly while expressing the learned behavior and this transition to the dark period results in increased swimming. (**C**) Performance index of fish 5 minutes before and after visual stimuli are reintroduced. Reintroducing the visual cues results in the memory being re-expressed as can be seen by the increase in the performance index. (**D**) The change observed upon light reintroduction in C is achieved while retaining the same mobility in the tank.

4.7 DISCUSSION

Here, we provide a close analysis of the development of both classical and operant learning behaviors in zebrafish. We characterized the complete ontogeny of a learning behavior in a vertebrate model system from the time larvae first exhibit controlled visually elicited behaviors to full adult maturation. Results from our assays show that the ability to learn is first expressed in a window of time from 3 weeks post fertilization.

Ontogenies of classical conditioning in model systems have been intensely studied[3,4] and more recently, with advances in molecular and developmental neurobiology, these ontogenies have taken an important role in serving as functional readouts for the underlying neural circuitry as it develops and progressively assembles components required for behavior and plasticity. The possibility of real time *in vivo* imaging of neural development and activity in zebrafish makes this particular model system especially attractive[14].

Our results show remarkable similarity to those observed in mammals: rats and mice also show a defined window of time in which conditioning can first be induced. This window (generally occurring between two and three weeks after birth) is common for many different paradigms, such as different forms of Pavlovian fear conditioning and eyeblink conditioning[2–5]. Moreover, studies of Pavlovian fear conditioning in infant hooded rats have found a dissociation in time between the ability to first detect visual events and to use these for associative learning[3].

To date there are no studies focusing on the initial development and maturation of learning behaviors in zebrafish. Studies have shown that adult zebrafish are good learners both using food as appetitive reward[15,16] and noxious electroshock stimuli[17–20], some of these uncovering potential anatomical pharmacological and neurochemical components of the system where learning occurs[18,20–23]. We have developed computer-based automated behavioral assays

which we can easily control and comprehensively analyze. In our assays, adult zebrafish are clearly shown to be excellent learners as in both assays animals create a robust memory after only brief exposure to the unconditioned stimulus-conditioned stimulus (US-CS) pairing. Training and testing can be done without removing the animal from the water during the post-training period and the assay can easily be upgraded to monitor large numbers of animals at the same time for high throughput analyses.

We have used two different classical and operant conditioning freely-swimming behavioral assays. Despite the differences between these assays, both show a similar time-window for learning onset in development. Even though most zebrafish larvae performed poorly in both assays, the systems involved in visual detection and locomotor response are known to be fully functional at 7 dpf. Larval zebrafish at 5 dpf already express robust visually-induced behaviors including the optokinetic response (OKR)[10,11,24], phototaxis[25], the optomotor response (OMR)[26,27] and prey capture[12,28,29]. In several of these studies the locomotor behavior of larval zebrafish was characterized in detail and included multiple swimming and turning components which can be assembled together to generate very fine motor control as observed for example during prey capture. Larval zebrafish can perform visual tracking and fine optomotor responses even when immobilized in agar and in such experimental preparation also failed to show classical conditioning. Nonetheless it is possible that the visual system of larval zebrafish is not mature enough to distinguish between the different stimuli in our assay. We deliberately avoided the use of stimuli that elicit any innate preference or aversion as these make the interpretation of the assay inherently difficult. Together, this indicates that larval zebrafish between week 1 and week 2 already have a functional visual system and control of locomotion, but that these sensorimotor capabilities may have not yet have matured sufficiently to reliably support learning

in our conditioning assays. Some of the larvae tested did show high learning performance indices (fig.3D) and recent data suggests that larval zebrafish are able to associate visual cues and tactile noxious stimuli[30].

4.8 METHODS

Animals and Apparatus

In all experiments, where sexual dimorphism was clear, only female zebrafish were used to avoid any possible sexual bias in behavior[31]. Zebrafish of strain AB swam freely in a custom-built acrylic tank with opaque walls and transparent bottom. The tank's size is 6cm x 6cm x 2.5cm with water 1-cm deep for animals younger than 3 weeks[29], and 18cm x 6cm x 12cm with water 3-cm deep for older fish. Visual stimuli are presented on a LCD screen immediately below the tank (Samsung, SyncMaster, 15inch, 1024 X 768 Pixels). Swimming behavior is recorded at one frame per second using an infrared-sensitive CCD camera positioned above the tank. A 15 volt Infrared LED array was custom built within the LCD screen to illuminate the arena from below. An infrared filter is positioned in front of the camera to block visible light. This facilitates online analysis of fish position via a custom-written LabView program (National Instruments). A small fan is used to dissipate the heat generated by IR-LEDs. Electric shocks (70ms, 9V/6cm) are delivered via four pieces of steel mesh, two on each side of the arena. Shock delivery at each side of the arena is controlled independently. Dose response curves to strength of electric stimuli were obtained (data not shown) and we chose stimulus values around 9V, which were placed in the range of values that elicits a response in all stages with 100% reliability and no detectable short or long-term damage to the animal. Experiments were undertaken at daytime in the animals

14-10 h light-dark cycle (L-9am-11pm, D-11pm-9am). In experiments in fig.4 memory retention after 12 hours was assayed at nighttime.

Training protocols

All behavioral experiments are divided into baseline, training and test periods. Fish are introduced to the arena 30 minutes before starting experiments with the LCD screen on with the cues to be used for conditioning.

During classical conditioning, in the baseline and test periods, the two distinct visual cues are presented below the tank and no electric shocks are delivered. During training, the conditioned visual stimulus (CS) is presented for 1.5 sec followed by the non-conditioned visual stimulus (non-CS) for 8.5 sec, 9 times, for 1.5 minutes. An electric shock (70ms, 9V/6cm) serves as unconditioned stimulus (US), which overlaps and ends simultaneously with the CS visual cue. For the experiments described in figure 1C and 1E, individual naive 1-year old fish were used. For the experiments described in figure 2, 17 fish were trained and tested as a group starting at 7dpf. This group was used repetitively throughout the experiment up to 42dpf. In this experiment fish were trained as in the protocol above, but 6 consecutive times, with test periods of 90 seconds between them.

During operant conditioning experiments, the design for the baseline and test periods is the same as in the classical conditioning assay. During operant training, the two visual cues are presented simultaneously below the tank, and electric shocks are delivered at frame acquisition rate (1Hz) only whenever the animal enters the area demarcated by the conditioned visual cue. This is followed by a dark period of variable length and subsequent reverse cue introduction. Cues are always reintroduced for testing when the animal is swimming over the area

corresponding to non-CS. For the experiments described in figure 1D and 1F, individual naïve 1-year old fish were used. For those described in figure 3, individual naïve fish were trained and tested at each developmental stage. Training was performed for both different cues used in each experiment to control for any innate preference. In addition, cues of similar luminance were used for larvae and juveniles to prevent bias from the strong phototaxis response present in larvae.

In the experiments that test the *persistence of memory*, a period during which all visible lights are turned off is introduced between training and test periods. A whole-tank reinstatement shock is provided after 30 minutes of test, this shock is presented in the middle of a twenty second period of no light in the tank so as to avoid pairing with any particular visual cue.

Analysis

The swimming behavior along the tank is quantified based on either the animal's position or its turning behavior. In *positional analysis*, the animal receives a score of -1 or +1 in each image frame if its center of mass is in the conditioned or non-conditioned visual area of the tank, respectively. The performance index (PI) is the average of the scores in the first 5 minutes of the test period. An animal that only swims in the non-CS area during the time window shows a PI of +1, a fish that swims evenly between the two zones shows a PI of zero and conversely a fish that would only swim in the conditioned area would have a PI of -1.

In *turning behavior analysis*, an animal receives a score of +1 if it turns away from the CS visual cue and receives -1 if it turns away from the non-CS visual cue. The animal receives a score of 0 if it turns at the two ends of the tank. The PI is the sum of scores divided by the half number of all turning events during the analysis window. Thus an animal that always turns away from the CS visual cue receives a PI of +1. A fish that only turns at the end of the tank, a

behavior that is often observed in naïve animals, receives a score of 0. The PI of a fish in the figures is represented by a circle. The center represents the value of the PI and the area is proportional to the overall number of turning events. The analysis of turning behavior therefore weighs the performance of fish according to their total locomotion.

In *Locomotion analysis* we analyzed the movement of the fish at a 5 Hz frame rate. We calculated speed from the difference in position every second and plot the average for every 30 second on figure 5. T-tests are performed where necessary, always assuming unequal variance.

4.9 Reference

1. Skinner, B. F. The evolution of behavior. *J Exp Anal Behav* **41**, 217–221 (1984).
2. Campbell, B. A. & Ampuero, M. X. Dissociation of autonomic and behavioral components of conditioned fear during development in the rat. *Behav. Neurosci.* **99**, 1089–1102 (1985).
3. Moye, T. B. & Rudy, J. W. Ontogenesis of learning: VI. Learned and unlearned responses to visual stimulation in the infant hooded rat. *Dev Psychobiol* **18**, 395–409 (1985).
4. Paczkowski, C., Ivkovich, D. & Stanton, M. E. Ontogeny of eyeblink conditioning using a visual conditional stimulus. *Dev Psychobiol* **35**, 253–263 (1999).
5. Raineki, C., Shionoya, K., Sander, K. & Sullivan, R. M. Ontogeny of odor-LiCl vs. odor-shock learning: similar behaviors but divergent ages of functional amygdala emergence. *Learn. Mem.* **16**, 114–121 (2009).
6. Heisenberg, M., Wolf, R. & Brembs, B. Flexibility in a single behavioral variable of Drosophila. *Learn. Mem.* **8**, 1–10 (2001).
7. Moore, B. R. The evolution of learning. *Biol Rev Camb Philos Soc* **79**, 301–335 (2004).

8. Neuhauss, S. C. F. Behavioral genetic approaches to visual system development and function in zebrafish. *J. Neurobiol.* **54**, 148–160 (2003).
9. Orger, M. B., Kampff, A. R., Severi, K. E., Bollmann, J. H. & Engert, F. Control of visually guided behavior by distinct populations of spinal projection neurons. *Nat. Neurosci.* **11**, 327–333 (2008).
10. Portugues, R. & Engert, F. The neural basis of visual behaviors in the larval zebrafish. *Curr. Opin. Neurobiol.* **19**, 644–647 (2009).
11. Easter, S. S., Jr & Nicola, G. N. The development of vision in the zebrafish (Danio rerio). *Dev. Biol.* **180**, 646–663 (1996).
12. Budick, S. A. & O'Malley, D. M. Locomotor repertoire of the larval zebrafish: swimming, turning and prey capture. *J. Exp. Biol.* **203**, 2565–2579 (2000).
13. Jami, S. A., Wright, W. G. & Glanzman, D. L. Differential classical conditioning of the gill-withdrawal reflex in Aplysia recruits both NMDA receptor-dependent enhancement and NMDA receptor-dependent depression of the reflex. *J. Neurosci.* **27**, 3064–3068 (2007).
14. Niell, C. M., Meyer, M. P. & Smith, S. J. In vivo imaging of synapse formation on a growing dendritic arbor. *Nat. Neurosci.* **7**, 254–260 (2004).
15. Williams, F. E., White, D. & Messer, W. S. A simple spatial alternation task for assessing memory function in zebrafish. *Behav. Processes* **58**, 125–132 (2002).
16. Colwill, R. M., Raymond, M. P., Ferreira, L. & Escudero, H. Visual discrimination learning in zebrafish (Danio rerio). *Behav. Processes* **70**, 19–31 (2005).
17. Pradel, G., Schachner, M. & Schmidt, R. Inhibition of memory consolidation by antibodies against cell adhesion molecules after active avoidance conditioning in zebrafish. *J. Neurobiol.* **39**, 197–206 (1999).

18. Xu, X., Scott-Scheiern, T., Kempker, L. & Simons, K. Active avoidance conditioning in zebrafish (Danio rerio). *Neurobiol Learn Mem* **87**, 72–77 (2007).
19. Rawashdeh, O., de Borsetti, N. H., Roman, G. & Cahill, G. M. Melatonin suppresses nighttime memory formation in zebrafish. *Science* **318**, 1144–1146 (2007).
20. Blank, M., Guerim, L. D., Cordeiro, R. F. & Vianna, M. R. M. A one-trial inhibitory avoidance task to zebrafish: rapid acquisition of an NMDA-dependent long-term memory. *Neurobiol Learn Mem* **92**, 529–534 (2009).
21. Pradel, G., Schmidt, R. & Schachner, M. Involvement of L1.1 in memory consolidation after active avoidance conditioning in zebrafish. *J. Neurobiol.* **43**, 389–403 (2000).
22. Jesuthasan, S. Fear, anxiety, and control in the zebrafish. *Dev Neurobiol* **72**, 395–403 (2012).
23. Okamoto, H., Agetsuma, M. & Aizawa, H. Genetic dissection of the zebrafish habenula, a possible switching board for selection of behavioral strategy to cope with fear and anxiety. *Developmental Neurobiology* (2011).doi:10.1002/dneu.20913
24. Brockerhoff, S. E. *et al.* A behavioral screen for isolating zebrafish mutants with visual system defects. *Proc. Natl. Acad. Sci. U.S.A.* **92**, 10545–10549 (1995).
25. Burgess, H. A. & Granato, M. Modulation of locomotor activity in larval zebrafish during light adaptation. *J. Exp. Biol.* **210**, 2526–2539 (2007).
26. Clark, D. T. Visual responses in developing zebrafish. Thesis. Univ. of Oregon (1981).
27. Orger, M. B., Smear, M. C., Anstis, S. M. & Baier, H. Perception of Fourier and non-Fourier motion by larval zebrafish. *Nat. Neurosci.* **3**, 1128–1133 (2000).
28. Borla, M. A., Palecek, B., Budick, S. & O'Malley, D. M. Prey capture by larval zebrafish: evidence for fine axial motor control. *Brain Behav. Evol.* **60**, 207–229 (2002).

29. Gahtan, E., Tanger, P. & Baier, H. Visual prey capture in larval zebrafish is controlled by identified reticulospinal neurons downstream of the tectum. *J. Neurosci.* **25**, 9294–9303 (2005).

30. Aizenberg, M. & Schuman, E. M. Cerebellar-dependent learning in larval zebrafish. *J. Neurosci.* **31**, 8708–8712 (2011).

31. Dalla, C. & Shors, T. J. Sex differences in learning processes of classical and operant conditioning. *Physiol. Behav.* **97**, 229–238 (2009).

CHAPTER 5

General discussion and future directions

The data presented in the preceding chapters demonstrates the behavioral role and functional organization of three small groups of spinal projection neurons, namely RoV3, MiV1 and MiV2 neurons, in controlling turning behaviors of larval zebrafish. This is one of the very few examples[1–4] where the behavioral role of spinal projection neurons is explicitly characterized in vertebrates.

The behavioral setup developed in this thesis is able to (a) automatically record the swimming behavior of larval zebrafish at 500 frames per second while updating four types of visual stimuli in real time, and (b) automatically extract detailed kinematics of tail movements. The ability to examine tail motion in detail allows characterizing the behavioral role of small sets of spinal projection neurons. Using the experimental setup, I show that:

1. Hindbrain RoV3, MiV1 and MiV2 neurons modulate the first undulation cycle of tail movement during turns by increasing the tail bend angle and the cycle period.
2. Forward swims remain intact after the removal of these ventromedial neurons, suggesting the presence of an independent descending pathway that controls symmetric tail movements.
3. The occurrence of forward swims drastically increases after ablating RoV3, MiV1 and MiV2 neurons, suggesting that the ventromedial neurons generate turns by modulating the basic motor pattern of forward swims. This is in contrast to the scenario where RoV3, MiV1 and MiV2 neurons generate turns by creating a complete, biased waveform of tail movement.

4. Turning strength is most likely to be mediated by an activity-dependent mechanism at the level of spinal projection neurons, rather than a recruitment mechanism.

On the basis that RoV3, MiV1 and MiV2 neurons increase the tail bend angle and the cycle period of tail movements, I propose the following connection patterns between the ventromedial spinal projection neurons and the neurons in the spinal cord: (a) they innervate motor neurons in order to increase the tail bend angle, and (b) they innervate commissural inhibitory spinal interneurons, most likely $CoBL_{gly}$ and CoLo neurons, to increase the cycle period as well as to indirectly suppress the spinal network on the non-turning side. More work will be required to completely detail the descending motor control of turning behaviors. Specifically, double patch recordings of neurons in the hindbrain and the spinal cord are required to confirm the proposed synaptic connections. Second, the behavioral role of spinal interneurons such as $CoBL_{gly}$ and CoLo neurons during turns should be tested by using laser ablation technique. Finally, the axonal arborization of RoV3, MiV1 and MiV2 neurons should be examined by using single-cell electroporation of dyes; this should provide critical insights on how these three pairs of nuclei differ in their anatomy and how they work together.

The results from this thesis along with previous findings[3,5] also suggest a modular design of descending motor control in the larval zebrafish. In this design, each component of the descending motor system has its unique function; removing one component does not affect the operation of others. In addition, combining the action of multiple components can generate new functions. This thesis demonstrates that RoV3, MiV1 and MiV2 neurons control turning angles but are not necessary for generating symmetric tail oscillations. A previous study[3] showed that the Mauthner neuron and its segmental homologs, namely MiD2cm and MiD3cm neurons, control the response delay of escape turns but are not necessary for generating the wide spectrum

of turning angles. These results suggest that descending pathways mediated by the ventromedial neurons, the Mauthner neuron and its homologs, and an independent subset of spinal projection neurons (likely nMLF neurons) control the turning angle, the response delay, and symmetric tail undulations, respectively. In line with a modular design, turns and forward swims appear to share a common descending pathway that generates symmetric tail undulations, but turns require the additional action of RoV3, MiV1 and MiV2 neurons to elicit the increased tail bend angle and the cycle period during the first undulation cycle. There are roughly 200 spinal projection neurons in larval zebrafish, and the abovementioned ventromedial and Mauthner neurons only constitute ~46 of them. Other spinal projection neurons must control other aspects of locomotor behaviors. For example, the "J shaped" tail bend during prey capture[6] could result from the combined action of the spinal projection neurons that generate the visually induced turns and the additional neurons that stiffen bilateral muscles on the rostral portion of the tail[7]. In this way, the undulation at the rostral portion of the tail is suppressed, and only the caudal end of the tail undulates.

The purpose of the brain is often considered to generate higher order functions such as learning, memory, consciousness and emotion. These functions are all important, but they are only important because they influence how animals behave. It is through behaviors that these brain processes can interact with the external world and have evolutionary relevance. In chapter 4 of my thesis, I showed that the adult zebrafish is able to perform robust learning behaviors. The learning behavior requires the brain to distinguish different visual stimuli, associate the visual stimulus with aversive shocks, and remember the association for hours; the emotion of fear may also be established. These sensory, memory and cognitive processes are only relevant to the animal's well being because they modulate the turning behavior of the fish to avoid

electroshocks. Due to its optical and genetic accessibility as well as the simple descending motor system, the larval zebrafish has become an ideal vertebrate model to characterize the network connection between the brain and the spinal cord. A thorough understanding of how the brain controls body movement in a vertebrate animal model may soon be achieved.

Reference

1. Faber, D. S., Fetcho, J. R. & Korn, H. Neuronal networks underlying the escape response in goldfish. General implications for motor control. *Ann. N. Y. Acad. Sci.* **563**, 11–33 (1989).
2. Dale, N., Ottersen, O. P., Roberts, A. & Storm-Mathisen, J. Inhibitory neurones of a motor pattern generator in Xenopus revealed by antibodies to glycine. *Nature* **324**, 255–257 (1986).
3. Liu, K. S. & Fetcho, J. R. Laser ablations reveal functional relationships of segmental hindbrain neurons in zebrafish. *Neuron* **23**, 325–335 (1999).
4. O'Malley, D. M., Kao, Y. H. & Fetcho, J. R. Imaging the functional organization of zebrafish hindbrain segments during escape behaviors. *Neuron* **17**, 1145–1155 (1996).
5. DiDomenico, R., Nissanov, J. & Eaton, R. C. Lateralization and adaptation of a continuously variable behavior following lesions of a reticulospinal command neuron. *Brain Res.* **473**, 15–28 (1988).
6. Budick, S. A. & O'Malley, D. M. Locomotor repertoire of the larval zebrafish: swimming, turning and prey capture. *J. Exp. Biol.* **203**, 2565–2579 (2000).
7. Hill, S. A., Liu, X. P., Borla, M. A., Jose, J. V. & O'Malley, D. M. Neurokinematic modeling of complex swimming patterns of the larval zebrafish. *Neurocomputing* **65-66**, 61–68 (2005).